ELECTRICAL PROPERTIES OF AU_{55} CLUSTER SYSTEMS

Inauguraldissertation

zur Erlangung des Grades eines

Doktors der Naturwissenschaften

(Dr. rer. nat.)

vorgelegt dem Fachbereich Chemie

der Universität Essen

von

Viktória Torma

aus Ungarn

Essen Januar 2002

Hiermit bestätige ich, die Arbeit nur mit den angegebenen Hilfsmitteln ohne fremde Hilfe angefertidt zu haben

Viktoria Torma

Vorsitzender: Prof. Dr. Frank-Gerrit Klärner

1. Gutachter: Prof. Dr. Gunter Schmid

2. Gutachter: Prof. Dr. Ulrich Simon

Tag der mündlichen Prüfung:

To my best friend and husband, Zoli

Acknowledgment

The present Ph.D. thesis has been completed between September 1998 and November 2001 in the Institute of Inorganic Chemistry, University of Essen.

First I would like to thank to my scientific supervisor,

Prof. Dr. Günter Schmid

for the interesting research topics and his continuous motivation, for the numerous stimulating discussions and the freedom in the work as well. His help in the most complicated problems was indispensable for the success of this study.

I am indebted also to Prof. Dr. Ulrich Simon for the valuable discussions on the physical aspects. He introduced me in the amazing field of nanoelectronics from the very first moment, helped me in the measurements and finally took over the role of the second referee to my thesis.

I thank to Prof. Dr. Frank-Gerrit Klärner for his participation by defending my doctoral thesis.

Olivia Vidoni was my immediate tutor in the organic synthetic work. She helped also with some of the electrical conductivity measurements. I thank her kindly cooperation these important stages of my research.

Torsten Reuter is thanked for valuable discussions. I thank to Steffen Franzka the AFM measurements and his critical comments. Ursula Giebel is thanked for the synthesis of $Au_{55}(PPh_3)_{12}Cl_6$.

I am indebted to the whole research group for the support and the good atmosphere.

I thank to Matthias Schumann und Prof. Dr. C. Radehaus (University of Chemnitz) for the external cooperation and for the probes fabricated by electron beam lithography.

Finally I thank to Mária Mörtl (Eötvös University, Budapest) for the synthesis of *N*,*N*-dimethyl-*O*-(3-chloropropyl-dimethylsilyl)-carbamate.

Index

1 Abstract

A very interesting topic of nanotechnology today is the investigation of clusters exhibiting electrical quantum size effects, with the future aim of fabricating single-electron devices. One of the most suitable model compound is Au_{55} cluster [1], protected with various ligand shells of phosphorous- and sulfur organic molecules. In this work two main themes will be addressed: the effect of the covalent cross-link on the charge transfer mechanism of these nanoparticle systems and the conductive properties of the dense-packed cluster-monolayers.

The current literature opinion, whether the chemical nature of the ligands bridging two clusters influence the charge-transfer mechanism or not, is non-equivocate. Reifenberger et. al. [69] assume that the chemical nature of the ligands, especially their end-groups have an impact on the conductance of a certain sample. Simon [114] found that the activation energy of nanoparticle systems does not depend on the chemical nature of the ligands, but on the distance between the nanoparticles.

To clarify this apparent contradiction, the electrical properties of two-, quasi-two and three-dimensional systems were investigated. The measurements indicate that Simon's model is valid for physically cross-linked systems only. For covalently (chemically) cross-linked nanoparticle systems the activation energy is, however, smaller than expected from this and depend strongly on the chemical nature of the cross-linker ligand. The activation energy exhibits no trends as the function of the inter particle distance in this case.

In the last part of this work the electrical properties of cluster monolayers are presented. For the measurements Si substrates were used, equipped with tungsten contact structures by electron beam lithography. In order to get an electrically insulating layer under the electrical contacts, the top of the sample was oxidized to SiO_2. It could be shown that a nanoparticle system on this substrate can be activated by an exposition to a low energy electron beam. We explain this phenomenon with trapping of excess electrons in the SiO_2 layer, which induce image charges of opposite charge in the cluster layer. This effect causes changes in the electron-configuration and perhaps also in the structure of the arrangement. Asymmetrical spatial exposition of the layer leads to asymmetrical *I-V* charac-

teristics. This phenomenon can be explained similar to the rectifying behavior of the semiconductor diode: the arising image charges acts as electron holes in the layer.

2 Introduction and literature overview

The fabrication of the first transistor by Shockley, Brattain and Bardeen about 50 years ago is arguably the most important technological development of the 20th century [2]. There is almost no area of our life, on which transistors do not have significant impact. They are medical and chemical sensors, parts of countless medicinal equipments, but they are also parts of our mobile phones, CD players, or television. The greatest triumph of the transistor is the personal computer, which now possesses more memory in the space of a small brief-case, than computers that once filled large rooms. The above examples were made possible because the transistor has shrunk incredibly in dimensions over the past 50 years (Fig. 2.1). The size of the transistor has decreased by a factor two every 18 months. This trend was pointed out by Gordon Moore in the 1960s (Moore's Law), and one that continues to-day[3]. Nowadays, electronic devices employed in state-of-the-art integrated circuitry have dimensions of the order of 300 nm.

Nowadays the big challenge of the computer technology is to be able to continue this trend.

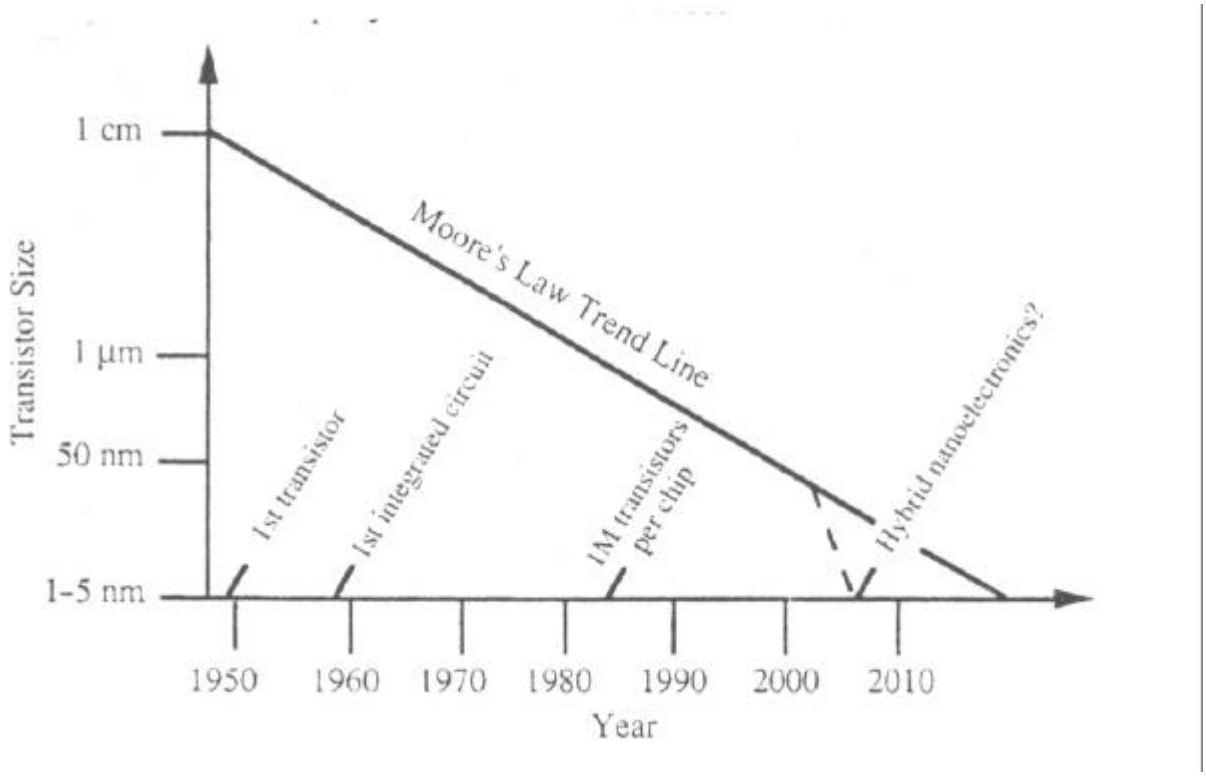

Fig. 2.1: "Moore's Law" plot of transistor size *vs*. year: The trend line illustrates the fact that the transistor size has decreased by factor of 2 every 18 months since 1950. Picture from [4]

2.1 The great challenge of the computer technology

How can Moore's Law (Fig. 2.1) be continued? If the resolution of the surface patterning techniques such as electron beam lithography improves, conventional transistors could simply be made even smaller. The properties of the solid matter, and the solid-solid interfaces change dramatically, if the size falls into the nanometer range. That means that radical changes in the way transistors are fabricated and operated will be necessary. What will these changes exactly be? Which materials will the futuristic transistor made from? How will they be assembled? How will they operate? The challenge of future electronics industry is to find out answers to these questions.

Many schemes for building nanometer-scale computer components have been proposed [5]. These include logic based on single molecules [6], molecular shuttles, resonant tunneling diodes and atomic relays. Of all the designs, proposed for the use in future integrated circuitry, the one receiving the most attention is perhaps the single electron transistor (SET).

2.2 Single electron tunneling (SET) effect, and the single electron transistor (SET)*

The first signs to the SET were observed by C. J. Gorter in 1951 [7]. He investigated the hopping conductivity in granular films. The activation energy extracted from the temperature-dependence of the conductivity was associated with the charging of individual grains composing the film. The first clear demonstration was made by Giaver and Zeller [8], [9]. They studied the vertical tunneling through a layer of Sn grains, coated by a thin insulator film, and sandwiched between Al electrodes. The *I-V* characteristics of the junction both with and without magnetic field were measured. That allowed to exclude superconductivity as a source of nonlinearity, and to associate the observed finite-bias offset in the *I-V* curve with the effect of the charging. The authors [8], [9] have realized, that at low temperatures

* Both the single electron tunneling effect, and the single electron transistor will be denoted with the same abbreviation: SET in the text. In the non-definite cases the whole name will be written.

electrons must tunnel through a grain one by one. A single additional electron localized on the grain in the course of tunneling, raises the potential of the grain. This prevents other electrons from hopping onto the grain, before that electron has finished its path between the leads, and the grain is discharged.

A single electron transistor consists of two electrodes (source and drain) and between these a small metal or semiconductor island, which is isolated from the electrodes by some insulator. The system must obey very small capacitance (typically. 10^{-18} F). The central island is capacitively coupled with a third electrode, the gate electrode, which helps to change the potential of the small island, and with this, influence the tunneling probability. In Fig. 2.2 C_1 and C_2 are very small, C_g is so large, that there is no current flowing through the gate.

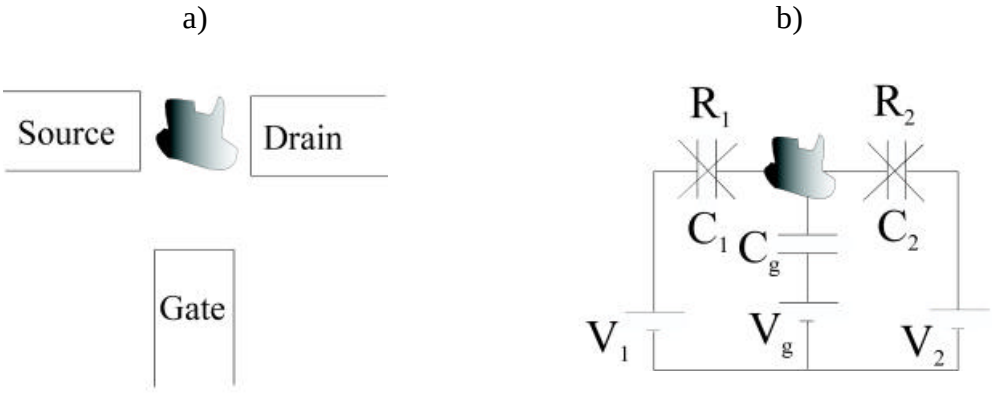

Fig. 2.2**:** *a*: SET arrangement. The gate is only capacitively coupled to the central island so that it is farther than the source and the drain. *b*: an equivalent circuit for the SET. C_1,R_1 and V_1 is the capacitance and the resistance between the source and the central island and the potential of the source respectively. C_2, is the capacitance and the resistance between the drain and the central island and the potential of the drain respectively, C_g and V_g are the capacitances between the gate and the central island, and the potential of the gate.

There are two limiting parameters for the observation of single electronic phenomena. First, the tunneling barrier has to be high enough, that the electrons can be localized on the central island, and just a weak overlap of their wave functions occur outside the island. Using the tunneling resistance (R_T) as a characteristic parameter of the tunneling barrier, it can be pronounced that R_T has to exceed the quantum resistance (R_Q) [10] (Eq. 2.1).

$$R_T >> R_Q = h/e^2 \qquad 2.1$$

where h is the Planck constant, and e is the charge of the electron.

An other limiting parameter is the characteristic thermal energy: it should not be higher than the energy required for the capacitive charging of the island. In the other case the thermal exciting of the electron is enough to charge the central island:

$$E_C = e^2/2C >> k_B T \qquad 2.2$$

where k_B is the Boltzman constant, and T is the temperature.

One possible solution to reach these conditions is the use of small metal or semiconductor islands. For a small metallic particle the capacitance can be approximated by

$$C = 2\pi \varepsilon_0 \varepsilon d \qquad 2.3$$

where d is the diameter of the cluster, ε is the dielectric constant of the insulating medium between the islands.

The second limiting condition is realizable with decreasing either the temperature or the size of the clusters. For the investigation of the room temperature SET, particles smaller than 2 nm are needed.

2.3 Arrangements of different metal clusters

The need for room temperature SET and other applications means the need of new materials. The appearance of several types of nanoparticles showed that they have a wide range use like electronic circuit elements, gas sensors, light emitting diodes [11], and catalysis.
In the literature nanoparticles mean usually metal or semiconductor particles in the range of 1-100 nm. In this work the word nanoparticle will be used mainly for metal particles smaller than 20 nm, since for electrical applications particles smaller then 10 nm are the most interesting. The word “cluster” usually means a smaller particle, than “colloid”. Another difference between cluster and colloid refer to their size: clusters always are written with a strict stoichiometry, as for instance $Au_{55}(PPh_3)_{12}Cl_6$ whereas colloids exhibit a size distribution. In this work, clusters and colloids will be used more or less as synonyms.

2.3.1 Synthesis of clusters, and colloids

There are five general chemical synthetic methods to prepare clusters in the size range of 1-100 nm. These are: 1. transition metal salt reduction, 2. thermal decomposition and photochemical methods, 3. ligand reduction and displacement from organometallics, 4. metal vapor synthesis, and 5. the use of electrochemical methods. The first, third and fifth method are proven to give isolated transition metal clusters. It is also possible to prepare colloids in constrained environments, like micelles, or inside porous materials, like zeolites. Of course, there are also some physical methods for preparing nanoparticles. Gas phase syntheses of metal clusters are used to generate so-called naked clusters (clusters without a ligand shell). As they are highly reactive and tend to aggregate if they have a physical contact, they can be studied in gas phase, or on a substrate, (see for example [12], [13], [14] and [15]). The main strategies for gas-phase preparations are: homogeneous nucleation in the gas phase, laser ablation of solids and the use of electrospray systems [11]. In the following sections all these methods will be described in detail.

2.3.1.1 Chemical methods

a) Transition metal salt reduction

The reduction of transition metal salts in solution is the most widely applied method of generating nanoparticles of metals. For this type of synthesis four different chemicals are needed, for four different functions. These are:

1) a transition metal salt as a precursor,
2) a suitable solvent as a reaction medium,
3) a reducing agent to generate the colloids from the metals salts,
4) a stabilizing molecule to form a protecting ligand shell around the metal core.

The same molecule can play one or two of the above functions

The function of the four entities mentioned before will be exemplified on the synthesis of $Pd_{\sim 561}(phenantroline)_{\sim 60}(OAc)_{\sim 180}$. This cluster is formed in two steps. The first one is the reduction of palladium(II) acetate (component 1) by hydrogen (component 3) in acetic acid (component 2), in the presence of 1,10 phenantroline (Phen, component 4.). The workup of

this cluster in air leads to the uptake of O_2 in 20 min with formation of air stable particles in a good yield.

The most common particles for the investigations of SET devices are made of gold. Among the many reasons for this, one of the most important is that they are easy to synthesize to characterize and air stable. Several well-elaborated methods are currently in use. Faraday [18] was the first to synthesize nanoparticles of gold during the 18th century by reduction of an aqueous solution of $[AuCl_4]^-$ with phosphorus vapor. Later Turkevitch and co-workers reproduced this and many other syntheses [20] for the preparation of gold nanoparticles. The 20 nm gold sol, prepared by the reduction of $[AuCl_4]^-$ with sodium citrate has become standard for histological staining applications. This reaction involves two steps and the rate determining is the first one (eq 2.5).

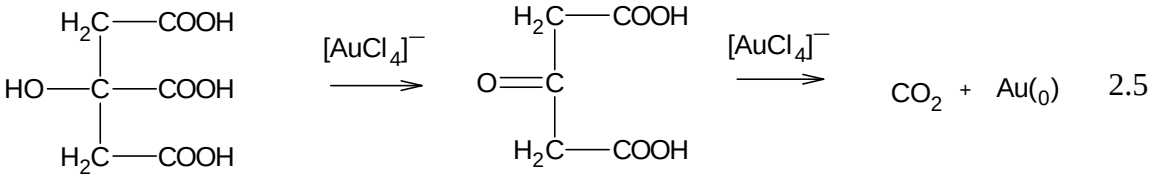

2.5

This preparation can also be used for the synthesis of other metal colloids, like platinum [21], [22], [23]. Different reducing agents like formiate, acetone-dicarboxylate, and various pH values were also used and they have given good control on the particle size [24].

Many other techniques are used to prepare size selective colloids from metal salts. One of the most famous is the synthesis of thiol capped gold colloids realized by Brust [25][26].

For size selective nanoparticles, a two-phase method is used. Hydrogen tetrachloroaurate was dissolved in water, and tetraoctylammonium bromide in toluene. The two-phase mixture was vigorously stirred until the tetrachloroaurate was transferred into the organic layer. After the full phase transfer reaction, dodecanethiol was added to the organic phase, and the aqueous solution was changed to an aqueous solution of sodium borohydride. The electron source is the aqueous solution of the $NaBH_4$ (see e.g. [27]).

b) Thermal decomposition and photochemical methods

Some organometallic compounds of the transition metals thermally decompose to their respective metals under relatively mild conditions, hence providing a rich source of colloidal metal precursors [28] [29].

The organometallic precursor can be also destroyed photochemically. Two methods can be used: photolysis of photolabile metal complex, or reduction of the metal salts by radiolytically produced reducing agents, like solvated electrons and free radicals. The photolysis of photographic images from silver halide emulsions have an extensive literature, and great practical relevance. Lately a wide range of other colloidal metals has also been prepared by this method [1].

Radiolytic methods differ in the type of reducing species, formed under irradiation, as function of solvent and any added solute. The radiolysis of aqueous solutions of metal ions produces solvated electrons which may either react with the dissolved metal ions directly, or with other solutes to produce secondary radicals, which then reduce the metal cations [30], [31].

c) Ligand reduction and displacement from organometallics

Reduction to metal can be carried out prior to colloid preparation whereby a zerovalent metal complex is the immediate colloid precursor. Thermolysis of metal carbonyls in cluster synthesis is an example for this approach. Further, the ligands can be changed to these, which produce weak complexes, and during the nanoparticle preparation they can be removed through sonication or ligand reduction [32], [33], [34],[35].

d) Metal vapor synthesis

Conceptually, but not practically, the simplest method to prepare colloidal metals is the co-condesation of atomic metal vapor into a dispersing medium. Since the activation energy for agglomeration of metal atoms is very low, the possibility for competing molecular

complex formation processes which have higher activation energies can be minimized by operating at low temperatures

The first successful nanoparticles synthesis using this method was elaborated by Roginsky and Schalnikoff in 1927 [36]. Fig. 2.3 shows the schematic drawing of the apparatus. The metal is evaporated from the metal reservoir, and let cocondense on the cold finger (cooled by liquid air) with the organic vapors coming from the liquid reservoir. The organosols were prepared at reduced pressure by evaporation of relatively volatile metals like cadmium or lead, and a subsequent cocondesation of these metal vapors with the vapors of organic diluents, like benzene or toluene, on the cold finger. After a complete cocondesation, warming up the frozen matrix and collecting the liquid gives a colloidal suspension of the metal. New publications report also from the synthesis of particles as small as 1-2 nm size [37].

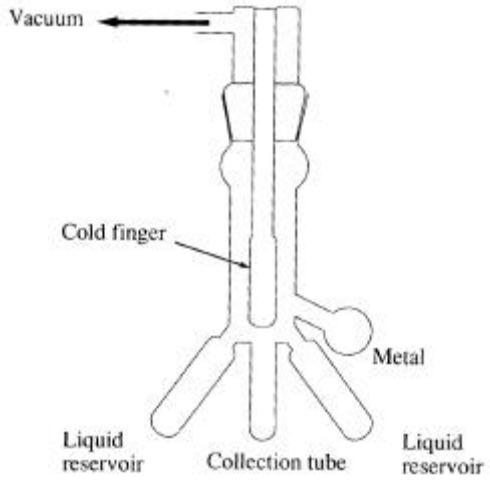

Fig. 2.3: The first reactor for metal vapor synthesis. The metal is evaporated from the metal reservoir, and let cocondense on the cold finger with the organic vapors coming from the liquid reservoir. The cold finger is cooled by liquid air. The picture is adapted from [36]

e) Electrochemical synthesis

A quite new method for synthesizing nanoparticles was developed by Reetz in 1994 [38]. He prepared quite small clusters using an electrochemical cell. The synthesis turned out to be a large-scale and size selective method, and the products are redissolvable in organic solvents.

2.3.1.2 Preparations of colloidal metals in constrained environment

a) Micelles and Vesicles

The reduction of physically constrained metal precursors offers the potential for restricting the growth of the metal particles either by limiting the amount of metal particle precursor accessible to a growing nucleus, or by restricting the motion of the precursor species and the growing nuclei, thus diminishing the rate of productive collisions. Using this approach, colloidal metals have been prepared in micelles or vesicles, which act as microreactors for the preparations, and also stabilize the growing colloid.

For example, aqueous suspensions of surfactant micelles were shown to be effective in stabilizing colloidal platinum, produced either photochemically or chemically (by reduction of H_2PtCl_6 with H_2 [39]).

b) Porous materials

Nanoparticles can also be prepared and stabilized in the confinement of porous solids with well-defined pore or channel structures. Both semiconductor (PbS, CdS, CdSe) and metals (Pt, Pd, Ag) can be synthesized with this method, inside molecular sieves like zeolites [40]. The clusters can grow due an ion-exchange reaction, or with the use of organometallic precursors, like metal carbonyls, as it is written in chapter 2.3.1.1b).

The first method uses the ion-exchange property of the zeolite. That means, that mobile Na^+ ions can be changed to mono or multivalent metal cations and afterwards reduced by reducing agents like hydrogen to give zero valent metal colloids (Fig. 2.4).

By the second method the pores of the zeolites are filled with organometallic precursors (coming from gas phase or from solution). After that, the so-prepared zeolite is heated up, to produce the nanoparticles.

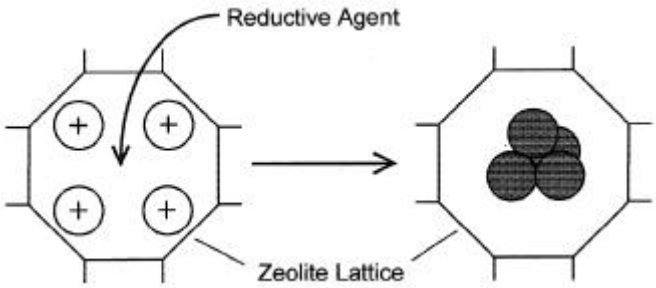

Fig. 2.4: Formation of nanoparticles in a zeolite matrix by the reduction of transition metal ions with suitable reductive agents. Figure is adopted from [41]

2.3.1.3 Physical methods

a) Homogeneous nucleation in the gas phase

This title includes every method, which generates nanoparticles from the vapor phase. For this the establishment of supersaturation is required. To reach this goal several physical and chemical methods and reactors can be used [11], like *Furnace flow reactors, Laser reactors, Laser vaporization of solids, Flame reactors, Plasma reactors, Spark source and exploding wire, Sputtering, Inert gas condensation, and Expansion-cooling*.

b) Laser ablation of solids

Laser ablation is a technique in which a pulsed laser rapidly heats a very thin layer of the substrate material, resulting in the formation of an energetic plasma above the substrate. The pulse duration and energy determines the relative amounts of ablated atoms and particles. The non-equilibrium nature of the short-pulse (10-50 ns) laser heating enables the synthesis of nanoparticles of materials, which normally would decompose when vaporized directly, such as most semiconductors and multicomponent oxides do.

c) Electrospray systems

A simple way to produce nanoparticles is to evaporate micron-sized droplets of a dilute solution. By choosing the appropriate solute concentration, nanosized particles consisting of the solid residue can be obtained. For instance, drying a 1 µm droplet containing a ppm solution of NaCl, theoretically will yield a 10 nm NaCl particle.

2.3.2 Ligand exchange reactions

In the last chapter, different strategies have been presented for the cluster preparation. One of the most important difference between clusters chemically and physically synthesized concerned the presence or not of the ligand shell. Physically synthesized, clusters generally have no ligand shell, thus the determined properties characterize the particles without any disturbance. On the other hand, without molecules around them, nanoparticles cannot make stable crystals or closed monolayers. They are air sensitive, cannot be stored and finally their shape is changing even if they are adsorbed to surfaces. They could not be isolated, so the most of the chemical properties cannot be determined. The clusters prepared with chemical methods are surrounded therefore with protecting ligands. Of course the existence of non-colloidal molecules disturbs the "purity" of the system, on the other hand the particles synthesized with this method can be isolated and investigated with chemical methods. The diversity of the ligands, which can be used in the synthesis, is relatively poor, for example in the case of gold particles citrate, one can use phenantroline derivatives, phosphine derivatives, thiols and polymers. Multidentate molecules, for instance, cannot be used, especially if both function groups have an affinity to the material of the nanoparticle. The chemical properties of the nanoparticles depend on the chemical nature of the ligands, and in certain cases a change of the ligand shell involves the formation of materials with completely different properties.

2.3.2.1 How to add a ligand shell

In the literature, some methods to cover clusters synthesized with physical methods are described. Most of them start with the deposition of the cluster onto a substrate and after dipping the cluster into a solution, containing the protecting molecule. This technique is used mostly for multilayer synthesis on various substrates.

An interesting method for synthesizing thiol capped gold nanoparticles is a mixed physico-chemical method [42] [43] [44]. The gold atoms are evaporated in a carbon crucible, in a resistively heated carbon tube (Fig. 2.5), are entrained in He and induced to condense into nanoclusters by mixing the hot flow from the oven with a room temperature stream of He

(see 2.3.1.3 a) oven methods). Controlling the conditions of the oven and the flow downstream in (1) from the oven, controls the mean cluster size. In order to assure that the clusters are single crystals, they pass through a one meter long tube, where they first are heated above they melting point in (2) and cooled down in (3)(see Fig. 2.5). This guarantees that the nanoparticles are transformed into single face centered-cubic crystals. To pack the clusters into ligand shells, the aerosol of the bare metal clusters was passed through a spray chamber in which they come in contact with a fine spray of organic solvent and surfactants. The key to the successful operation of this technique is a surfactant that rapidly adsorbs onto the surface of the clusters and prevents aggregation. Plenty of molecules were tried out, including fatty acids, alkyl thiols, alkyl disulfides, alkyl nitriles, and alkyl isonitriles. More or less they were all effective, but the best result was reached with alkyl thiols with a chain length of between 8-12 carbon atoms [44]. The aerosol was then finally collected in a collecting tube (4).

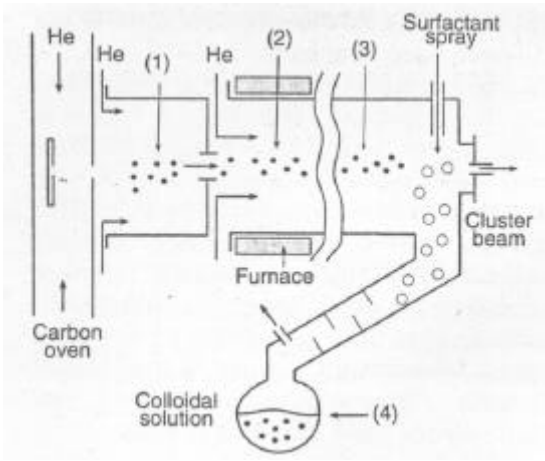

Fig. 2.5: Schematic of process for synthesizing a stable colloidal suspension of crystalline gold clusters. Picture is adopted from [44].

2.3.2.2 Ligand exchange reactions in solution

The clusters can be protected with many types of ligands. As already mentioned, only a few of them can be used directly in the synthesis. These can be, however, later exchanged to other ones. Certain ligand phosphines or the most polymers make a weak bond with the metal core, while others make strong bonds, like the thiol-gold bond, or the thiol-CdS core bond.

The ligand exchange reaction in solution is usually equilibrium one, similar to classical metal-ligand equilibria in aqueous solutions (E.g. Zn^{2+} + EDTA). Eq. 2.8a shows this reaction applied to the case of ligand stabilized metal clusters and colloids. This reaction holds an equilibrium-constant, called the ligand exchange constant (K_x, eq. 2.8b).

$$ML_y + k\,P \quad ML_{y-k}P_k + k\,L \tag{2.8a}$$

$$K_x = \frac{[ML_{y-k}P_k]\cdot[L]^k}{[ML_y]\cdot[P]^k} \tag{2.8b}$$

where M's are the metal cores, L's are the ligands, P's are the new molecules, and squared brackets denote concentrations. The same reaction and reaction constant can be defined to the ligand exchange reactions, which take place with the solvent molecules, but the other ligand, competing for the place next to the metal core, are the solvent molecules.

Since for an equilibrium reaction

$$\sum n_i m_i = 0 \tag{2.9}$$

where the n_i-s are the stoichiometric numbers and the m_i-s are the chemical potentials of the entities and

$$m_i = m_i^0 + RT \ln a_i \tag{2.10}$$

where m_i^0-s are the standard values of the chemical potentials, R is the gas constant, T is the temperature and a_i-s are the activity of the molecules, which are in the case of diluted solutions (which is the case in almost every synthesis with this clusters), and for not charged molecules are equal to concentrations, K_x can be written as:

$$K_x = \exp\left(\frac{m_{ML_y}{}^0 + k m_L{}^0 - m_{ML_{y-k}P_k}{}^0 - k m_P{}^0}{RT}\right) \tag{2.11}$$

Since

$$\Delta m_r = \Delta G_r \qquad (p, T = const.) \tag{2.12}$$

where p is the pressure,

$$K_d = \exp\left(\frac{m_{ML_y}{}^0 + k m_L{}^0 - m_{ML_{y-k}P_k}{}^0 - k m_P{}^0}{RT}\right) = \exp\left(\frac{\Delta G_r{}^0}{RT}\right) \tag{2.13}$$

where ΔG_r^0 is the free enthalpy exchange of the whole reaction. ΔG_r^0 is the difference of the Gibbs-energies of the destroyed and the developed bonds. Entropy changes can usually be neglected, because there are the same number of molecules on the two sides of the two sides of the reaction equation.

$$\Delta G_r^0 = k \cdot \left(\Delta H_b^{\mathrm{P}} - \Delta H_b^{\mathrm{L}} \right) \qquad 2.14$$

where ΔH_b^{P} is the bond enthalpy between the metal core and the new molecules and ΔH_b^{L} is the bond enthalpy between the metal core and the ligands.

$$K_x = \frac{\left[\mathrm{ML}_{y\text{-}k}\mathrm{P}_k\right] \cdot \left[\mathrm{L}\right]^k}{\left[\mathrm{ML}_y\right] \cdot \left[\mathrm{P}\right]^k} = \exp\left(\frac{k \cdot \left(\Delta H_b^{\mathrm{L}} - \Delta H_b^{\mathrm{P}} \right)}{RT} \right) \qquad 2.13$$

That means that, if the metal core – ligand bond is weak, but the metal core-new molecule bond is strong, than ΔG_r^{P} has a very large and ΔG_r^{L} a smaller negative value. K_x is large, so practically all of the ligands will be exchanged to the new molecules. On the other hand, in an opposite case, the ligand-new molecule exchange practically does not take place.

There are mainly two strategies for exchanging the ligands in a homogeneous reaction. The first is to transfer the colloids from a weaker bonded ligand shell to a stronger bonded, like exchanging phosphines, polymers or citrate to thiols. These reactions are usually fast, and with yields of 80% to 100% (K_x is large). The second is based on the exchange of two types of molecules with same bond strength, like thiols to thiols, or thiols to dithiols. The yields of these slow reactions (between 40% and 60%) depend on the steric and other properties of the molecules (K_x is close to 1).

A huge number of examples for all the strategies can be found in the literature. In this section an overview of the techniques and results obtained with gold clusters will be presented.

Ligands like phosphines, citrate, or different polymers are easily removable, and substitutable by thiol ligands [46] [48] [45]. Tannic acid stabilized gold sols can be turned to thiol stabilized simply by adding thiol to the solution, and remove the free tannic acid with dialysis [45]. Citrate stabilized gold sols can be cross-linked with propanedithiol, with simply adding the new ligand, and let the nanoparticle-polymer precipitate [48]. In Ref. [46]

gold particles were transferred from an aqueous phase to the organic phase, using toluene soluble thiols.

A more spread out technique is to synthesize the clusters with thiol ligands. This is practically more advantageous, because they are more stable in solution, but they are not as much available for clear ligand exchange reactions. The non-stoichiometric exchange of the ligands sometimes causes problems, because the used material is not chemically pure. On the other hand many measurements can be imagined (and were done), to determine the exact number of the exchanged ligands. In Ref. [47] octhanethiol molecules was exchanged to *w*-ferrocenyloctanethiol molecules, to study the electrochemical properties of the as-synthesized particle. By a simple measure of the area under the voltammetric curve, the authors were able to determine the number of ligands exchanged.

It is also possible to investigate the ligand exchange reactions by kinetic measurements [63]. In the case of thiol-to-thiol exchange, Murray [63] found that the speed of the ligand exchange reactions depends on the concentration of the ligands and the nanoparticle. They also suggest a mechanism. According to this, a thiol molecule enters into the ligand shell of the molecule and protonates the bound thiolate. In the second step the protonated molecule leaves the cluster. They also assume that the molecules on the terraces of the clusters form stronger bonds with the metal core than those on the edges and corners.

2.3.2.3 Ligand exchange reactions on the surface (preparation of mono-and multilayers)

The ligand exchange reactions can also take place through a specific adsorption step. That means that first the surface is functionalised, using a functional group able to create a strong specific interaction with the metal core. After this the nanoparticles are adsorbed. During the second step, an exchange between a part of the ligand shell and the function group of the ligands on the surface takes place. This phenomenon can be supported by the solvent. This method can be used to synthesize monolayers like in [55], [57], [59], and [60], as well as multilayers [56], [58]. It is also possible to use the Langmuir-Blodgett technique in order to create two dimensional cross-linked nanoparticles assemblies [61], [62]. This strategy doesn't contain an adsorption step, the ligand exchange happening in a

homogeneous reaction on a water surface. In the following it will be focused mainly on the ligand exchange reactions of gold nanoparticles.

The easiest strategy to obtain closed monolayers of clusters is obviously to exchange a weak bonded ligand to a strong bonded function group, like phosphine to thiol[55]. Partial change of thiols to dithiols is also possible[59], [60], but the reaction is very slow and not stoichiometric.

In Ref. [55] a SET was prepared using phosphine stabilized gold colloids and a thiol functionalised surface. Gold nanoelectrodes were prepared with Electron Beam Lithography (EBL), then functionalised with hexanedithiol. Particles, bigger in diameter, than the space between the electrodes, were let to adsorb onto the surface. The particles partly loose their ligands and adsorb between the two electrodes onto the surface, making a link between the two contacts (see Fig. 2.6).

A very interesting use of the ligand exchange reactions is the light lithography with nanoparticles [58]. A light sensitive molecule is bonded to the surface, and with the use of a mask, some parts are destroyed, others not. On the destroyed part an amino-functionalised surface is gained from the original molecules. Dodecylamine stabilized gold particles are adsorbed to the surface so that their metal core anchored to the free amino groups on the surface. To get a multilayer of the clusters, the sample was dipped into a dithiol solution and back to the gold sol. These steps are repeated several times, to get a real microstructure on the surface. (For details see [58].)

The ligand exchange reaction from thiol to dithiol is a very slow reaction, so the adsorption of the thiol capped molecules with a thiol functionalised surface is very slow. The reaction time can be up to 1 week as reported in Ref. [51], [59] and [60]. To fasten the reaction it is easier to start with partially functionalised particles and to anchor them onto the gold substrate like in Ref. [59].

The ligand exchange reactions are commonly used techniques for the preparation of many types of cluster arrangements.

2.3.3 Preparation and properties of zero-, one -, two–, *quasi*-two-, and three-dimensional arrays of metal clusters

Arrangements of different particles from many kinds of metals and semiconductors are discussed in the literature. Mainly two strategies are followed in the publications which mostly differ in the strength of the bonds in the array. One type of these methods are the "physical methods", where there is just a weak bond, or no bond between the particles, the others are the "chemical methods" which build up the array with strong covalent or ionic bonds.

In the following chapters the different types of arrangements will be introduced.

2.3.3.1. Zero-dimensional "arrangements"

A zero-dimensional "array" is represented by one nanoparticle on a surface. There are essentially two methods to get information about the properties of one single cluster. The first, and the most spread out technique is the use of STM. A submonolayer of nanoparticles is deposited onto a surface, with physical or chemicals methods [66][67][68][69] and an STM tip is positioned over it. This technique is used mostly for electrical measurements, but it can be also used to determinate the size of the clusters. A very interesting aspect of this method is, that the size of the monolayer-coated particles seems to be as big as the diameter of the cluster and the ligand shell together (see e.g. [67]). This means that the effect of the covering molecules cannot be avoided by the models built up for the charge transfer mechanisms, since the electrons tunnel through the protecting molecules.

The second method for the zero-dimensional measurements is, to capture the nanoparticles between two electrodes [55][70][71][72][73]. The distance between the two-electrode systems fabricated must be smaller than the diameter of the studied cluster. To reach this goal, EBL is used to get electrode systems with distances of 20-50 nm between the metal contacts. To obtain even smaller gaps between the nanocontacts, some metal is evaporated onto the surface (Fig. 2.6). With this help electrode distances between 10 and 20 nm can be reached. The particles can be captured as well by specific chemical bonds [55][71], as with

electrophoretic effects from solutions[72], or simply moving them on the substrate with an AFM tip[70][73].

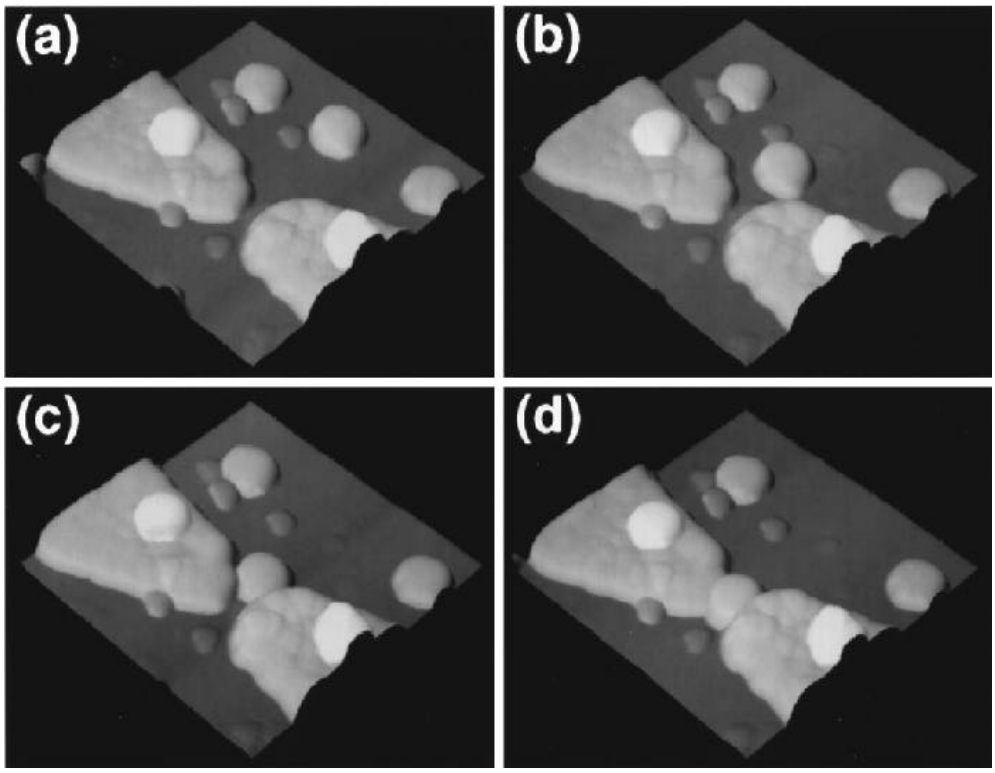

Fig. 2.6: Nanocontacts prepared by EBL. AFM measurements are made during the manipulation of 50 nm gold particles. Figure is adapted from[73].

2.3.3.2. One-dimensional arrangements

An ideal one-dimensional arrangement is a row of clusters. This structure is difficult to obtain, so in the literature mainly *quasi*-one-dimensional structures are presented. That means, that instead of one single row of clusters a thin wire is fabricated, with a width of some hundreds of nanometers.

There is no commonly used strategy to fabricate nanowires. The difficulty is; how to create chemically or physically different regions on a substrate in order to avoid a two-dimensional particles assembly on the entire surface.

The easiest way to fabricate chains of clusters is to crystallize the nanoparticles slowly on a surface, and stop the process in an early stage, when there are mainly one-dimensional structures [79].

Small chains of nanoparticles are obtainable also by stepwise chemical methods [57]. Longer chains of bigger colloids can be prepared by the reduction of metal salt onto a DNA template [78].

Quasi-one-dimensional structures can also be obtained using Langmuir-Blodgett (LB) technique [74], [75]. One possibility is to prepare a low-density LB film [74]; the other is to break the closed LB layer during the transfer to the substrate, with the use of high transfer speed. Chi and coworkers broke the LB layer of a fatty acid, using the periodic move of the meniscus at high transfer speeds, and filled the obtained channels with gold clusters [75].

Selective adsorption techniques are commonly used to fabricate nanowires. Building specific bonds between clusters and biomolecule templates is just one of the possibilities[77]. With an oxidation process, a certain part of a passive surface can be activated. So, spacer molecules can selective by adsorb onto it. Nanoparticles can adsorb to the spacers, but not on the passive part of the substrate. That means, that with the use of a conducting AFM tip, which is able to oxidize, nanowires can be fabricated [80] (Fig. 2.7).

a)

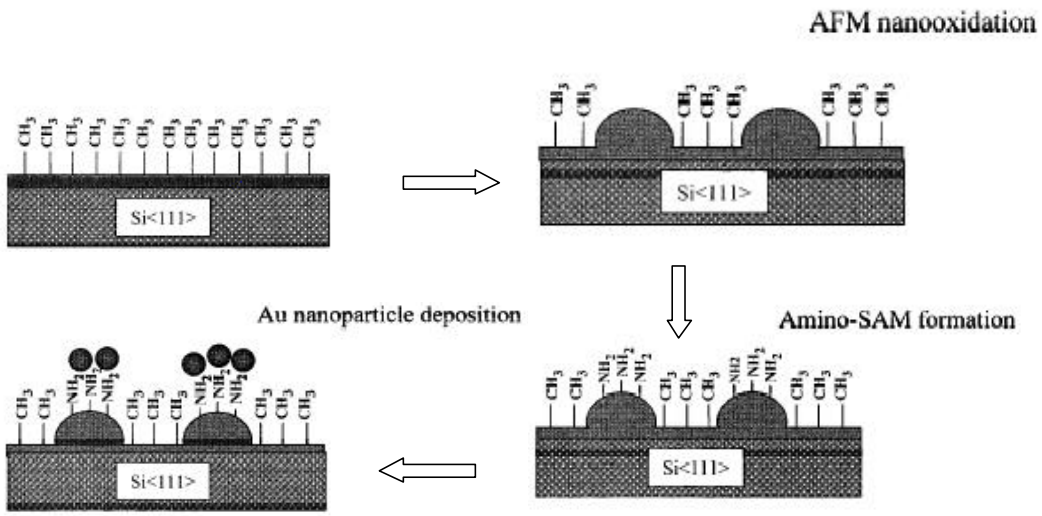

b)

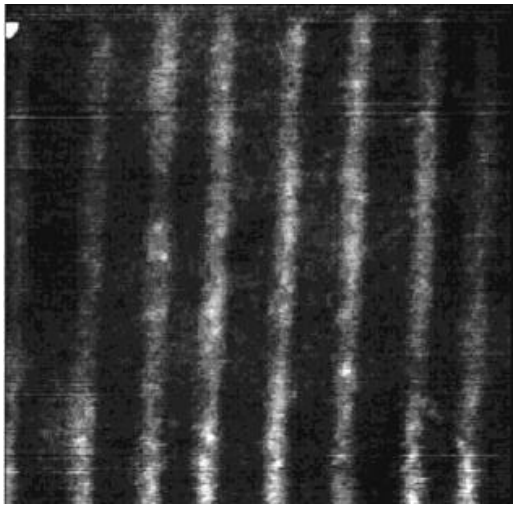

Fig. 2.7: Preparation of nanowires with nanooxidation method. Figures adapted from [80]

An interesting approach to prepare nanowires is to fill Al_2O_3 pores with the nanoparticles [65], [64],[76],[77].

2.3.3.3. Two-dimensional arrangements

The easiest method to prepare monolayers of nanoparticles is to dispose a drop of the cluster solution onto a substrate, and let the solvent evaporate[79][81][82][83][84]. This technique was used to get ordered monolayers of Ag_2S nanocrystals on various substrates [81][82]. Using this method, the nicest result was obtained on a carbon coated copper TEM grid [82] (Fig. 2.).

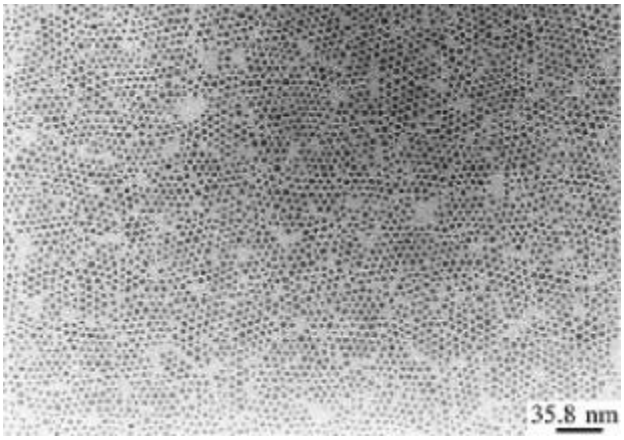

Fig. 2.8: Self-organization of Ag_2S nanocrystals by the “dropping and evaporating” method. Figure is adapted from [82].

Murray and coworkers [83] investigated how the core size influences the ordering ability of the nanoparticles. The authors dropped the solution on a TEM grid, and they let the solvent evaporate. They found that it is easier to get ordered layers from larger clusters.

Kubiak and coworkers [44] used the spin coating technique (see chapter 2.4.5.4, Fig. 5.24) to prepare ordered layers of dodecanethiol-encapsulated particles.

It is also possible to let the clusters recrystallise in a chamber, where the gas phase is saturated with the vapor of a good solvent of the particles. It induces a very slow recrystallisation, which results in highly ordered two-dimensional structures. In Ref. [79] a toluene atmosphere was used.

LB technique is a common used method for the fabrication of ordered monolayers. It is proved to result mainly in hexagonal lattices in the case of nanoparticles [61][85][86][87].

Mayya and Sastry [88] were able to immobilize a monolayer of gold clusters on the toluene-water interface. The aqueous solution of carboxytiophenol-capped particles was brought in contact with a toluene solution of octadecylamine. After vigorous stirring, the clusters were transferred to the interface and the wall of the glass container [88]. The thickness of the layer on the glass indicated that a monolayer formed.

Nanoparticle adsorption onto a modified surface, using the fact that most type of the clusters easily self-assemble, is the most spread-out technique for monolayer preparation (see E.g. [51][59][89][90][91][92]). The chemisorption happens mainly through ligand exchange reactions. Weak bonded ligands can be changed to stronger bonded ones [89][92], or in the case of equal strong bonds with slow ligand exchange reactions [51][59][90][91].

It is also possible to get two-dimensional arrays with the use of AFM [93]. In this article the authors manipulate the single particles with an AFM tip, to get structures consisting of 5-10 clusters.

An interesting strategy to get highly ordered arrangements of naked particles at large distances, is the preparation through the self-assembling of micelles [94]. The particles encapsulated in a surfactant micelle are let to adsorb to a surface. After this step trough a treatment with oxygen plasma, the walls of the micelles are burned away, so single naked clusters remaining on the substrate. The distance of the clusters about is 5 to 10 nm, approximately two times the thickness of the micelle.

2.3.3.4. Quasi-two-dimensional arrangements

Quasi-two-dimensional arrangements of nanoparticles are thin films or multilayers of clusters. They can be built up using direct or step-by-step methods.

Direct preparations are the one-step fabrications like dropping a relative concentrated cluster solution onto a substrate and let the solvent evaporate, or the spin coating of solutions (see chapter 2.4.5.4 and Fig. 5.24).

An interesting thin-film preparation method is made by Zhong [53]. He synthesized a gold cluster cross-linker polymer on a thiol-modified surface by ligand exchange reaction. This technique is the one step-cross-linking and precipitation method. The polymer precipitated from the solvent to the surface, resulting in a layer with relative high surface roughness (see Fig. 2.2).

Step by step synthesis of multilayers means that after adsorption of a cluster monolayer by a substrate a linker layer is deposited, causing once more the substrate active for the adsorption of another cluster layer. These two steps are following each other, 2 to 100 times, resulting in the formation of a thin film, with different thickness. Layers can be ionic, e.g. polymers [95][96][97], small ionisable molecules [98][99], differently coated clusters [100], or covalent.

The easiest method to prepare ionic bonded multilayers with polymer linkers is the use of positively charged clusters and negatively charged polymers [96]. In this case, the film consists of a cationic polymer coated nanoparticle system alternating with an anionic polymer linker.

A bit more complicated method was used by Mallouk and coworkers [95]. He used a gold substrate for the preparation. First, the sample was modified with cysteamine hydrochloride to immobilize positive charges on the surface. After this step, the sample was soaked alternately in aqueous solutions containing single anionic sheets of lamellar inorganic solids, like $KTiNbO_5$ and organic polyelectrolyte cations like polyallylamine hydrochloride (PAH). The thickness of the film obtained was determined by the number of cycles. When

they reached the desired junction thickness, the Au nanoparticles were introduced to the system. The scheme of the work can be seen from Fig. 2.9.

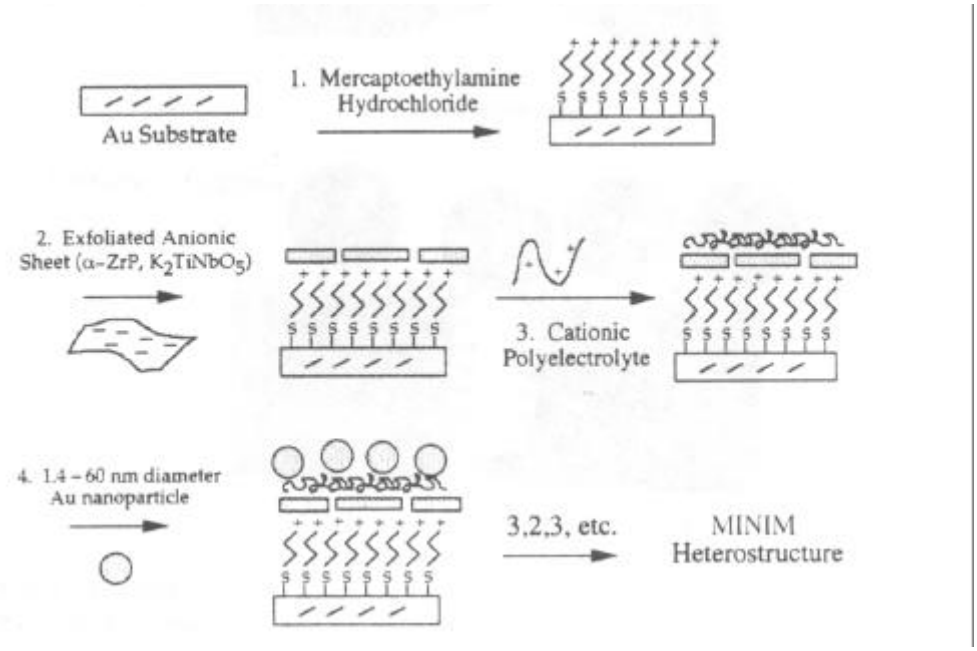

Fig. 2.9: The scheme of the multilayers synthesis, as is done by Mallouk and coworkers. Figure is adopted from [95].

The use of small ionic molecules is also possible to prepare multilayers. In this case e.g. bipyridinium cyclophanes [98] or benzamidines [99] can be used as linkers.

An interesting example of ionic self-assembly is described by Kumar [100]. In this work gold and silver particles, stabilized respectively by 4-aminothiophenol and 4-carboxythiophenol were used. Because of a possible ionic interaction between the ligand (positively charged of the amino group negatively charged of the carboxyl group), an alternative multilayer gold-silver was built.

The preparation of covalently bonded multilayers is similar to the ionic ones, except, that in this case the linker bonds covalently between the layers and also the particles inside the layer. The preparation usually happens through two-phase ligand exchange reactions. In the case of gold particles the fabrication starts with the mercapto functionalisation of the surface (except [58]), than altering rinsing in the gold cluster, and dithiol solution (except [101], where the linkers are diisocyanide molecules).

An interesting preparation is presented in Ref [102], in which a composite semiconductor-metal layer is fabricated, with altering rinsing in dithiol-CdS nanoparticle solution-dithiol-

Pt clusters. The change of the sequence was of course also possible, so different composite multilayers were also obtainable.

2.3.3.5. Three-dimensional arrangements

Three-dimensional arrangements of nanoparticles are easily obtainable by crystallization of cluster solutions. This happens actually in every synthesis of clusters, when the product is isolated.

Crystallization can also be induced by cross-linking of colloids [53][59]. Both papers report that the precipitation pf the clusters leads to a polymer, although this was not intended.

Induced crystallization of nanoparticles in toluene atmosphere is reported by Gutierrez [79]. During the very slow rearrangement of the entities in this case, relatively big single-crystals of nanoparticles can be obtained.

2.3.4 Preparation techniques of chemically cross-linked nanoparticle systems

2.3.4.1 Homogeneous reactions

The mixing of nanoparticles with different di-, or polyfunctional molecules having a strong specific bond to the metal core in a solution, after shorter or longer time ligand exchange reactions will happen (see chapter 2.3.2.2). This reaction will polymerize the system, to lead to precipitation of the clusters.

Citrate stabilized gold colloids precipitate in the course of a half an hour after mixing them with propanedithiol. The reaction is followed by UV-Vis spectroscopic measurements of the solution [48]. The color changes from blood red to violet before precipitation occurs.

If thiol stabilized gold clusters are codissolved with dithiols, and in the presence of a gold plate, as it is done in [44], [49], [50], [51], [52] and [53], it is not necessary to change all ligands against dithiols for the precipitation, but only some of them. In Ref. [44] conjugated molecules were used to interconnect particles in a monolayer and the electrical properties were measured. As it is well known for the electron transport in a layer, conducting

paths are enough (see chapter 4.5.2)[54], so for the measured current-voltage characteristics the exchange of all the ligands is not proved.

In Ref. [49] a monolayer of gold nanoparticles was prepared with codissolving the dithiols and the thiol-stabilized clusters in a solution and dipping a pure gold plate into it. If on the surface of a gold particle at least one of the thiols is changed to dithiol, it has the chance to anchor down to the gold plate. If the oxidation of the dithiols is prevented, a closed monolayer can be gained with this technique. In Ref. [50] and [51] dithiols were codissolved with gold particles. In Ref. [50] it is shown, that cross-linking clusters can take place, and the resulting polymer can precipitate from the solvent, if the solution is concentrated enough. To get thiol functions outside the entities, then it has to be worked in diluted solution [51] and the product has to be separated by liquid extraction (Fig. 2.1).

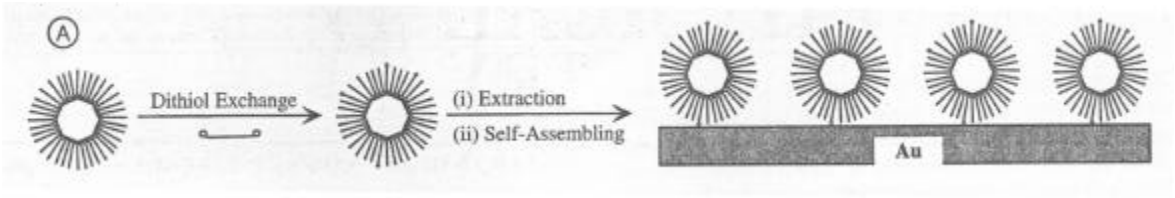

Fig. 2.1: Functionalising a gold nanoparticle with thiol groups. The strategy for preparing a monolayer with this technique is, to exchange some of the thiols by dithiols, and the so gained particle anchoring to a gold surface. The figure is adopted from [51].

In Ref. [52] and [53] ligands are exchanged to prepare cross-linked thin films of nanoparticles. The authors suggest, that this is an easy and fast technique to prepare layers of clusters (Fig. 2.2). Thiol protected clusters are codissolved with dithiols in the presence of a substrate. The cross-link is allowed and the gained polymer is precipitated from the solution onto the substrate. The thickness of the film is changing inside the layer, because the precipitation is not homogeneous. Changing the reaction time, the average thickness of the film can be controlled.

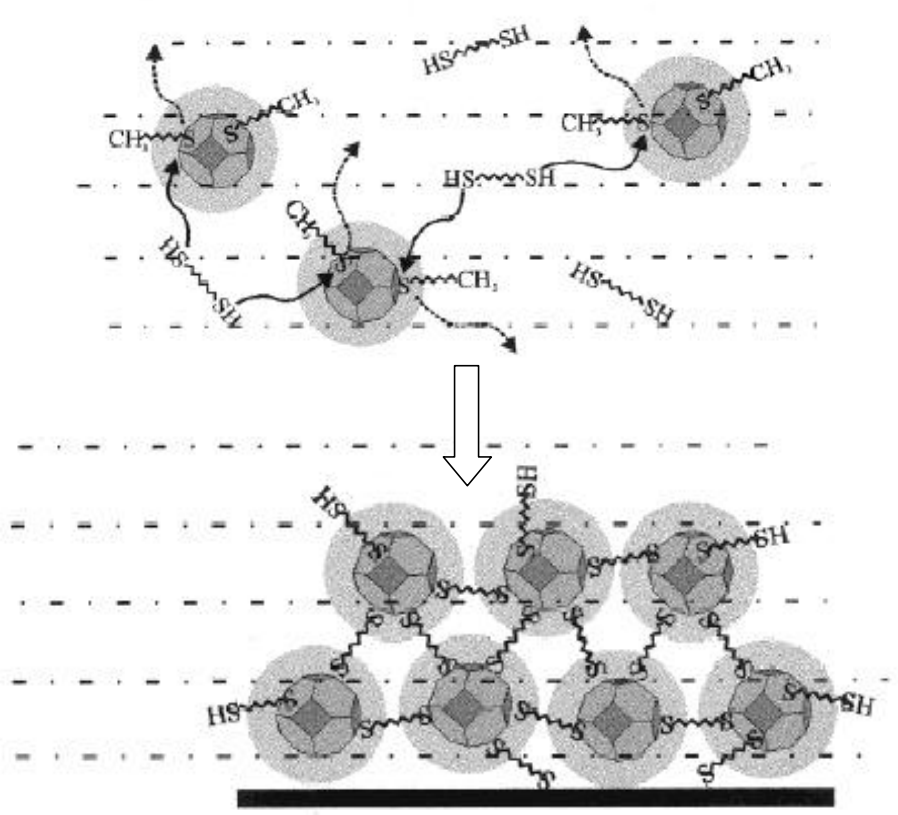

Fig. 2.2: Polymerization of nanoparticles in the presence of dithiols. Figure is adopted from [53].

In all papers dealing with dithiols, an important rule has to be pointed out. All authors work with solvents like toluene or hexane, which are not acid-base active (except [44]), and does not contain much water which can act as acid-base catalyst. When the proton of the –SH group is dissociated, the dithiols can polymerize easily. For solvents like ethanol or dichloromethane (which always contains traces of HCl as a decomposition product, and absorbs readily the humidity) nitrogen atmosphere has to be used, to avoid this process.

2.3.4.2 Langmuir-Blodgett techniques

Chen [61] experienced that chemically cross-linked samples can be prepared on a water surface using LB technique. She spread the cluster solution (hexanethiolate protected clusters in hexane solution) onto a water surface, followed by spreading of a dithiol in $CHCl_3$ solution. The molar ratio of the two components was approximately 1. It is observable, that

the solvent of the dithiol doesn't dissolve the clusters. This is very important, because otherwise microcrystals of clusters would be formed.

After spreading both component and evaporation of all solutions, the layer was compressed for a relative high surface pressure. After waiting for 6 hours, the cross-linkage was complete and the sample could transferred to the substrate. The layer proved to be a rigid and very stable one.

2.3.4.3 Heterogeneous reactions

Every multilayer preparation technique that is based on covalent bonds between the metal core and the ligands are covalently cross-linking the particles during the reaction [56], [58]. (see chapters 2.3.2.3 and 2.3.3.4)

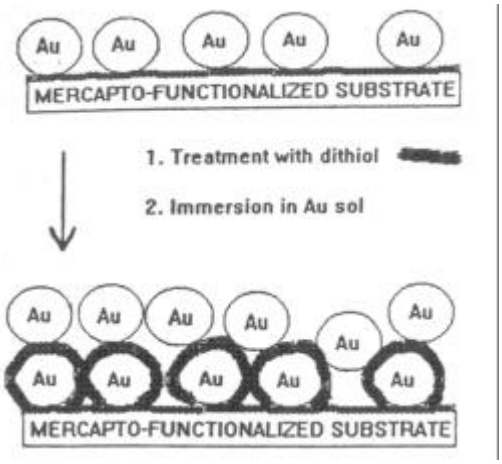

Fig. 2.3: Build up of a multilayer using tetraoctylammonium bromide stabilized gold clusters, and dithiols. Figure is adopted from [56].

In Ref. [56] a multilayer was built up with tetraoctylammonium bromide stabilized gold particles, and dithiols. A thermally grown SiO_2 layer was functionalised with thiol, using 3-(mercaptopropyl)-trimethoxysilane. After, the sample was dipped into the gold solution to get a layer of the particles. This dipping procedure, thiol solution-gold solution, was repeated in order to obtain multilayers of clusters (Fig. 2.3).

In Ref. [57] also the synthesis of cross-linked particles is reported. The first step was the immobilization of citrate stabilized particles. They adsorbed onto an amine functionalised surface. The authors did not mention, but it could be a chemically rather complicated step,

because the citrate stabilized gold clusters in water solution can adsorb to an amine surface with (electrostatic bonds), and without (covalent bond from amine to metal core) their ligand shell. After this step the substrate was dipped into an ethanol solution of very diluted hexane dithiol molecules for 24 hours. The authors claim that the dithiol exchanges the stabilizing citrate molecules and functionalises the surface of the clusters with thiol, so after immersing to the gold sol again, the particles will form small chains. The Scanning Electron Microscope image of their layer before and after dithiol immersion is depicted on Fig. 2.4. It is observable, the number of the islands on the second image is smaller than on the first one (104 particles on the first picture, and 129 on the second one). That indicates that the dithiol solution dissolved some of the deposited gold particles, but still made an interconnection between them. The bond between the surface and the entities can be covalent, but acid-base as well.

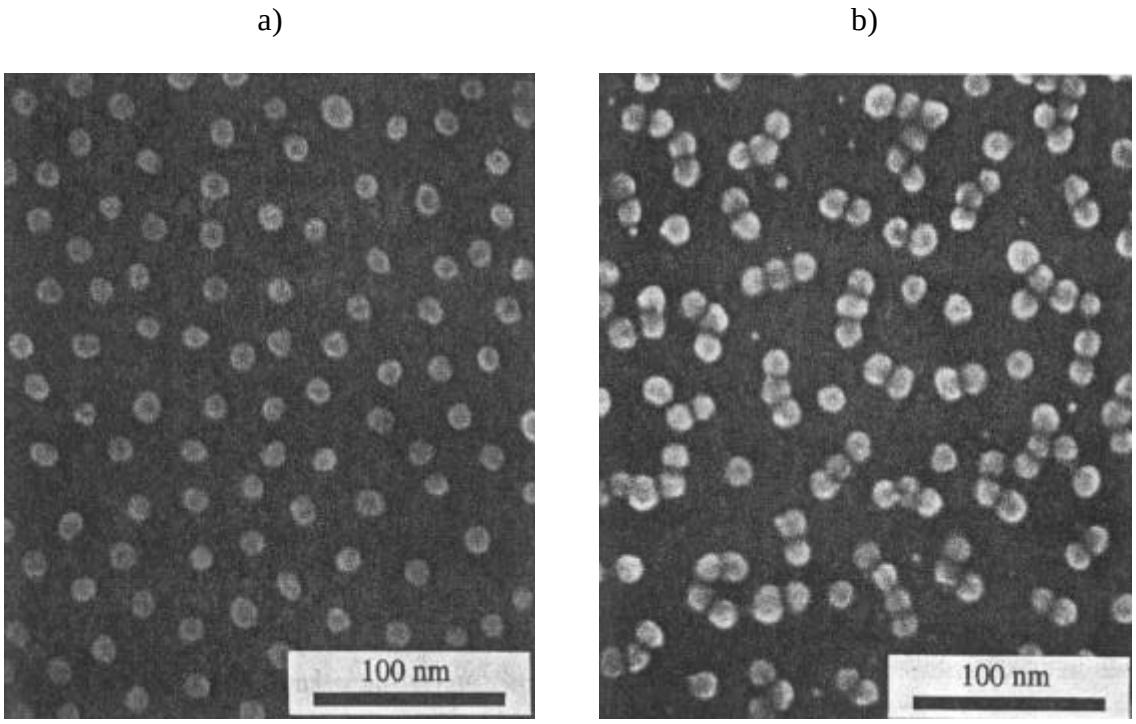

Fig. 2.4: Citrate stabilized particles were let to adsorb in an amine functionalised surface. After this step the substrate was dipped into an ethanol solution of very diluted hexane dithiol molecules for 24 hours, and back to the gold sol. SEM image of the layer before (a) and after dithiol (b). Figures are adopted from [57].

2.3.5 Electrical properties of arrays made of metal clusters

Modern microelectronics strongly tends to miniaturization of the circuit elements and to a larger degree of integration. The shorter distances between the elements on a chip lead to an increase in the performance speed and, therefore, to smaller delay times in the information exchange. That is why the investigation of the electrical properties of every arrangement made from metal clusters earns more and more interest in the recent years. In particular electrical studies on zero-, one-, two-, quasi-two- and tree-dimensional arrays of nanoparticles appear to give new ideas for their possible future application.

2.3.4.1. Zero-dimensional arrangements

There are two different methods for the study of single quantum dots. The simpler, and more spread-out technique is the Scanning Tunneling Microscopy (STM). In this case the tip is positioned above a cluster, the height feedback is turned off and a Scanning Tunneling Spectroscopic curve (STS) is measured [15], [44], [67], [68], [69], [76], [103], [104], [105], [131]. This means that the tunneling current is measured as a function of the sample voltage, or the distance between the sample and the tip. The preparation of quasi-monolayers needed for this technique is described in Chapter 2.3.3.1. The other techniques is the preparation of small nanocontacts with Electron Beam Lithography (EBL), and catch a cluster between them [55], [70], [71], [72], [106] as it is described in Chapter 2.3.3.1.
The electrical measurements show nonlinear *I-V* curves in case of both techniques, because of the so-called Coulomb-blockade (in details see Chapter 4.1). The nonlinearity is enhanced with the smaller particle size[15], and the lowertemperature[44]. This phenomenon is caused by the clusters, as it is proved by Reifenberger [68]. In this work he measured the STS curve when the tip was positioned above and next to a cluster. As can be observed on Fig. 2.5, when the tip is above a cluster, clear nonlinearity in the *I-V* curve is measured, however in the other case, simple Ohmic behavior is obtained.

a) b)

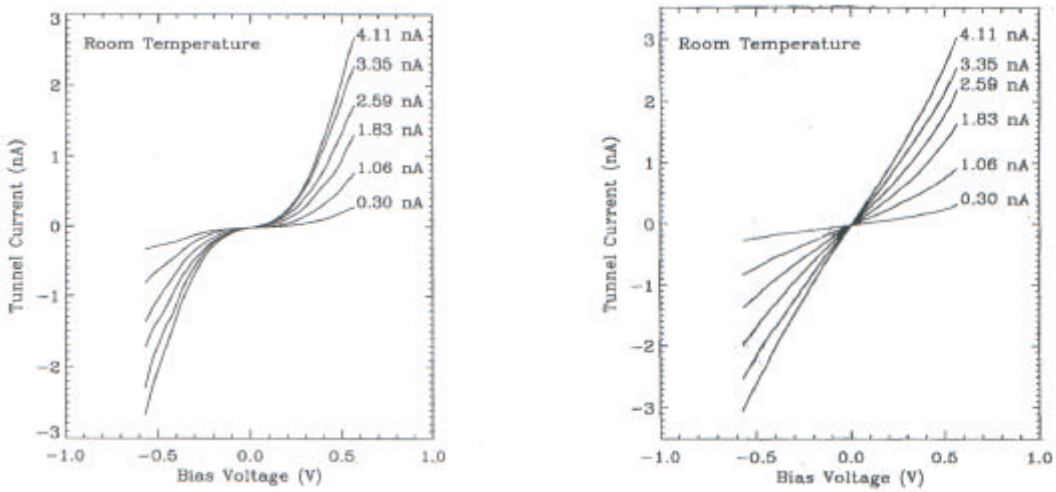

Fig. 2.5: STS curves measured above (a), and next to (b) a cluster. Figure is adapted from [68].

The differences between the two types of measurements are the length, and the height of the two tunneling barriers, on both sides of the metal core (Fig. 2.6). In the case of STS, the tunneling gate can be modeled by two different resistive-capacitive electric circles (RC circle), but in the other case the height of the two gaps is the same. Both situations are discussed by Korotkov [107] who reported that if the two tunnel barriers are really different, a Coulomb staircase behavior can be expected in the *I-V* measurements [67], [105], [131], but not in the other case [55], [70], [71], [72], [106].

a) b)

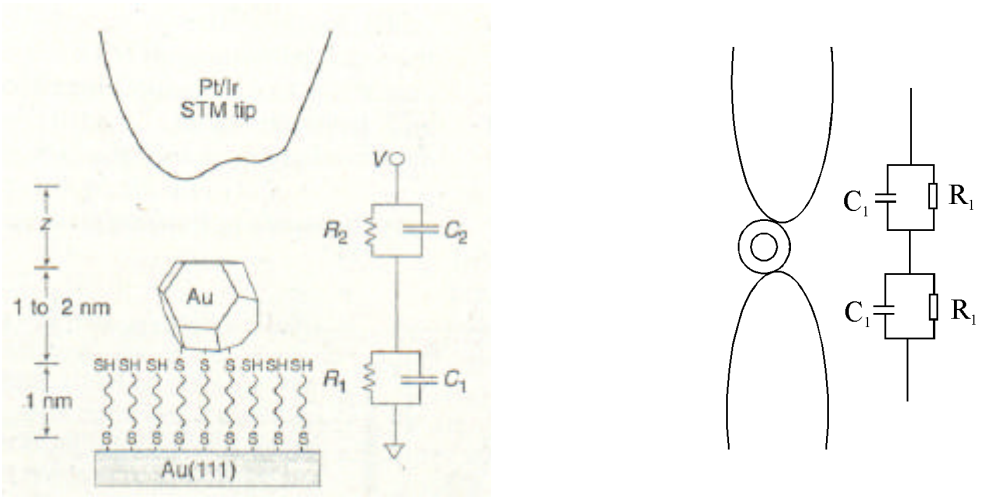

Fig. 2.6: STS arrangement (a), and cluster between two nanocontacts, fabricated with EBL (b). The height of the tunnel barrier is different in the case of a), so Coulomb staircase can be expected in the *I-V* curve, but the same in b). Fig a) is adapted from [69].

The fine structure of the *I-V* curve observed in the case of a cluster between two EBL fabricated nanocontacts shows the electron energy levels of the investigated cluster [55], [106].

2.3.4.2. One-dimensional arrangements

There are very few experimental data concerning the electrical properties of one-dimensional arrangements. As a main difficulty a very small disorder in the array of the cluster row can cause big differences in the measured data [108]. Although some previous one-dimensional structures of metal clusters are reported on the literature (see Chapter 2.3.3.2), the measurement of the electrical properties is still a big challenge.

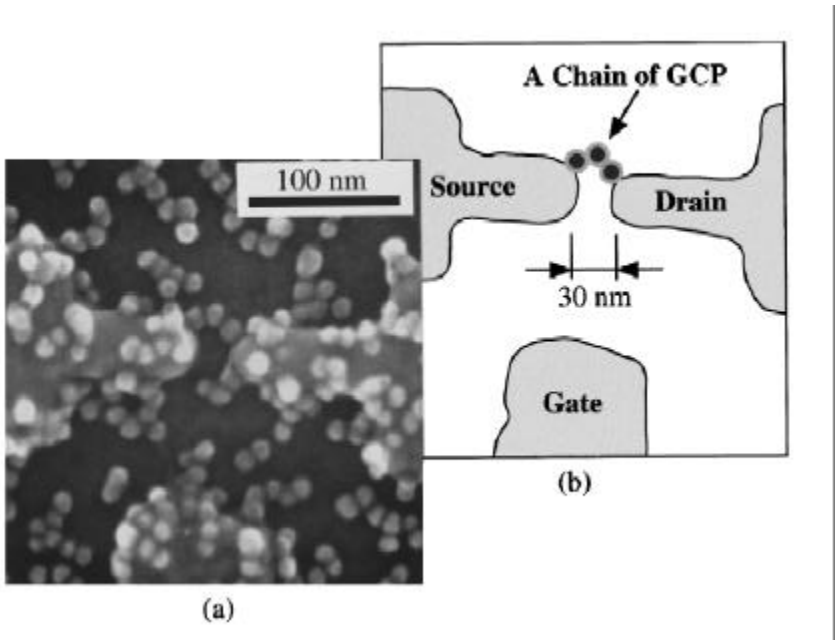

Fig. 2.7: SEM image (a), and a sketch (b) of a one-dimensional array of nanoparticles between two nanocontacts fabricated by EBL. The picture is adapted from [57].

The only example found as a real one-dimensional experimental result was the one made by Sato and coworkers [57]. The detailed information of the synthesis of the layer can be read in Chapter 2.3.2.3. As it is observable in Fig. 2.7, the nanocontacts are bridged by three clusters in a row. This is the first promising result for the preparation of a SET. The authors measured the *I-V* curve of this system and found both the Coulomb-blockade, and

the oscillation of the source-drain current in the function of the gate voltage. This is a convincing proof for a working as a SET.

2.3.4.3. Two-dimensional arrangements

The electrical behavior of the two-dimensional arrangements of bigger (d > 5 nm) particles is metallic. That is why not many measurements were published in this diameter range yet. Smaller particles can be investigated [44], [87], [109], [110] also with electrical methods. The first results in this area was obtained by Andres et al. [44]. They measured the *I-V* curve of a monolayer consisting of 2 nm clusters. The curve seemed to follow Ohm's law at room temperature and showed Coulomb-blockade at lower temperature (Fig. 2.8).

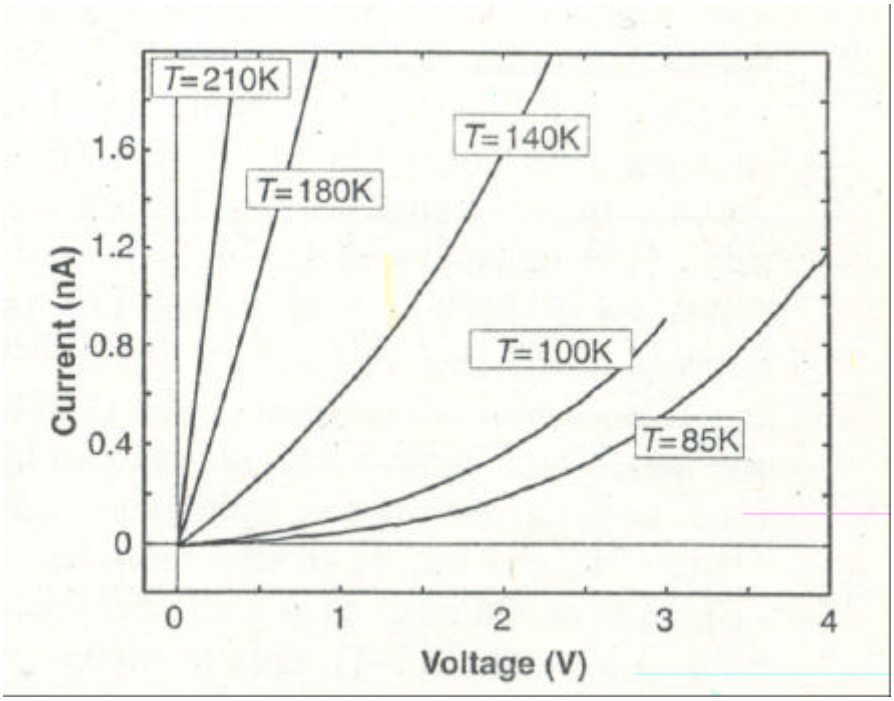

Fig. 2.8: The temperature dependence of the *I-V* curve of a cluster monolayer. Figure is adapted form [44].

2.3.4.4. Quasi-two- and three-dimensional arrangements

The resistance of a multilayer consisting of metal clusters with a core size bigger than 2 nm in diameter is normally too small to be measured [111]. This is also the case in three-

dimensional measurements. The results received for the two cases are comparable, that is why they are discussed in the same chapter.

If any electric information is needed from a film, smaller colloids or longer ligands have to be used, otherwise the resistance is too small to be measured. Murray and coworkers used 2.4 nm gold clusters with different thiols as ligands, [112], [113]. The alkyl chains varied from 4 to 16 carbon atoms. The simple Arrhenius model as well as the so-called granular model (see chapter 4.5.3) was fitted to the measured curves, and the activation energy was calculated with both theories. Brust et. al. [56] showed that this systems can be better explained with the granular model. It was elaborated for the electrical properties of cermets, and other metal-insulator composite materials (see chapter 4.5.3). According to this theory, electrons move through the material with hopping from one metal island to another in an insulator medium. In this case, the electrons jump from one cluster to another in an alkyl chain medium (see chapter 4.5.3). This model fits very well with other nanoparticle systems. Simon and coworkers applied the same theory for palladium clusters [114].

2.4 The Au_{55} cluster*

The Au_{55} cluster is different from the above-mentioned nanoparticles, because it presents a really monodisperse size. The important difference compared to the other particles resides in the fact that the number of metal atoms as well as the ligand shell are well-defined. This strict stoichiometrical composition means that it is a giant macromolecule, with the properties of a nanocluster. This is very important because it is known that in this size range small changes in the composition of the particles means by differences in its properties. Some characterizations require monodisperse particles. In the case of electrical measurements, for instance, a few bigger clusters in the material induced an increase of the conductivity of the sample.

---

* In the following chapters the sign Au_{55} denotes to the metallic core consisting of 55 gold atoms, surrounded by any ligand shell. If a particular cluster is mentioned, the name, or the sign will be always written exactly, like $Au_{55}(PPh_3)_{12}Cl_6$, or Normal Au_{55} (see chapter 8.1)

All of these characteristics make the Au_{55} cluster the smallest available clusters useful for nanoelectronic investigations. Its size and electron structure gives the possibility to it as a nanotransistor or a room temperature single electron device in the future.

2.4.1 The strategy for the synthesis of Au_{55} cluster

As it is explained in Chapter 2.3.1.1, many good strategies for the synthesis of metal clusters exist. To prepare Au_{55} the transition metal salt reduction method is used [1], [116], [117] (for details see chapter 8.2):

$$AuCl(PPh_3) + B_2H_6 \quad Au_{55}(PPh_3)_{12}Cl_6 \qquad 2.14$$

In this case $AuCl(PPh_3)$ is the transition metal salt, B_2H_6 is the reductive agent, benzene and toluene act as a solvent. B_2H_6 has a double function in this reaction: firstly, as a reductive agent it reduces the Au(I) salt, secondly, as a Lewis acid it reduces the concentration of the PPh_3 [1], and with this it assures the optimal parameters for the formation of the clusters. The PPh_3 is the stabilizing agent. As a Lewis base it coordinates to the gold atoms in the cluster, similar to the coordination in the $AuCl(PPh_3)$ salt, except that the oxidation number of the gold is different in the two cases.

The structure of the $Au_{55}(PPh_3)_{12}Cl_6$ cluster can be observed in (Fig. 2.9) [1], [116], [117]. It consist of two parts, a metallic core and an organic ligand shell. The gold core contains 55 gold atoms, which are crystallized in a cubic closed packed structure. That means, that the shape of the central metal core is cuboctahedral, with a diameter of 1.4 nm. The organic surrounding consists of 12 triphenylphosphine molecules; they are bound to the corners of the central polyhedron. The cluster contains also 6 chlorine atoms, which are aligned in the middle of the square sides of the cuboctahedron (Fig. 2.10) [120]. The whole cluster is 2.1 nm in diameter.

EXAFS measurements indicated that the Au-Au distance of the clusters is 0,280 nm corresponding to a slightly disordered cuboctahedral structure [127].

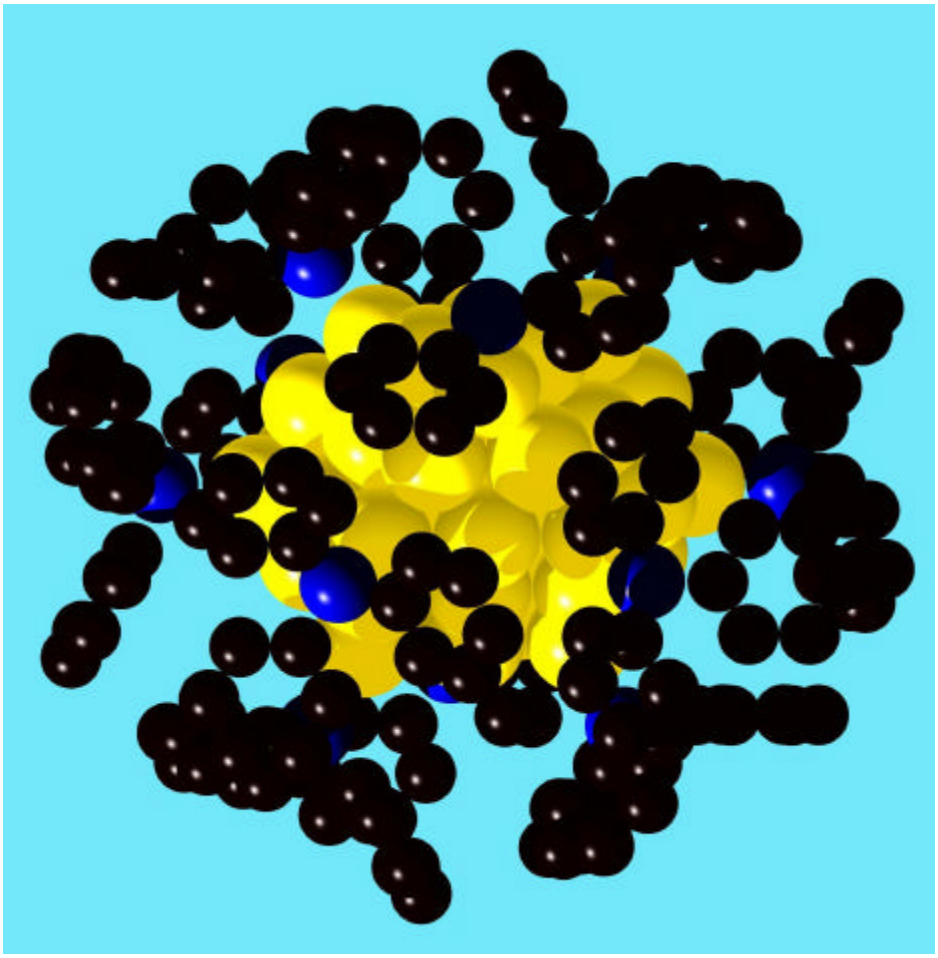

Fig. 2.9: The structure of the $Au_{55}(PPh_3)_{12}Cl_6$ cluster. Au atoms, P atoms, C atoms. The Cl and H atoms are missing from the figure.

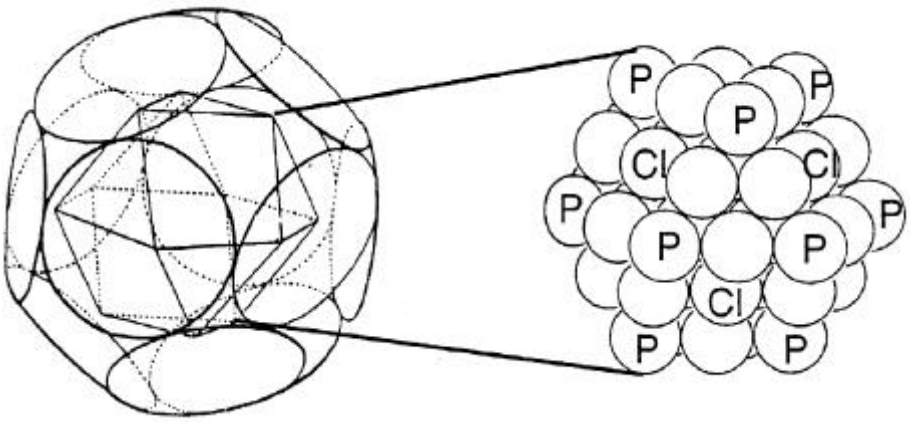

Fig. 2.10: The structure of the $Au_{55}(PPh_3)_{12}Cl_6$ cluster. On the first picture the big circles represent the PPh_3 ligands. On the second picture the signs show which ligand binds to which gold atom. Figure is adapted form [118]

2.4.2 "Magic" numbers in the cluster chemistry: specific stoichiometry of the metal cores

Using the same strategy for the synthesis of other metal clusters it turned out that there are some specific numbers of metal atoms, called "magic numbers", which are more stable than the others. These clusters, which consist of 13, 55, 147 etc. atoms, are full-shell clusters (Fig. 2.11). That means that they are like nanocrystals of metal atoms, crystallized in the closest packed structure, and the shape of the clusters are geometrically closed, which means that they have the minimum number of surface atoms for their size. So it can be spoken of one-shell, two-shell, and so on, clusters. In the case of metal clusters, this polyhedron is usually cuboctahedral. For the formation of this shapes particular number of atoms are needed, for the n^{th} shell ($10n^2 + 2$). The magic numbers N of a k shell cluster can be calculated with the formula:

$$N = \sum_{n=0}^{k} 10 \cdot n^2 + 2 \qquad 2.15$$

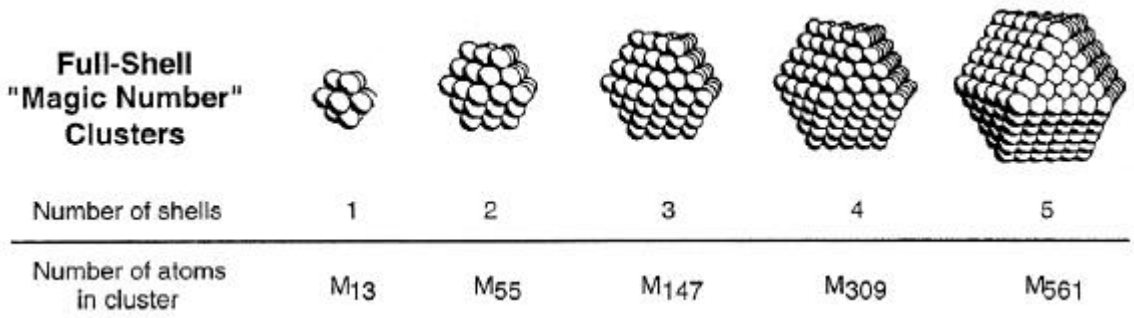

Fig. 2.11: The stoichiometry, and geometry of the full shell clusters. Figure is adapted from [118].

With the kinetic investigation of these reactions the "birth of a metal" can be followed (Fig. 2.12). It seems that the magic number clusters occupy a kind of energy minimum on the energy diagram of this reaction. That magic number which belongs to the first step local minimum of the curve that is deeper than the characteristic thermal energy in a certain reaction, depends on the synthesis parameters like temperature, the concentration of the solution, the reductive agent and the chemical nature of the ligand together with the metal. In the case of gold and PPh_3 the formed metal core consists of 55 gold atoms, by palladium and phenantroline it consists of 561.

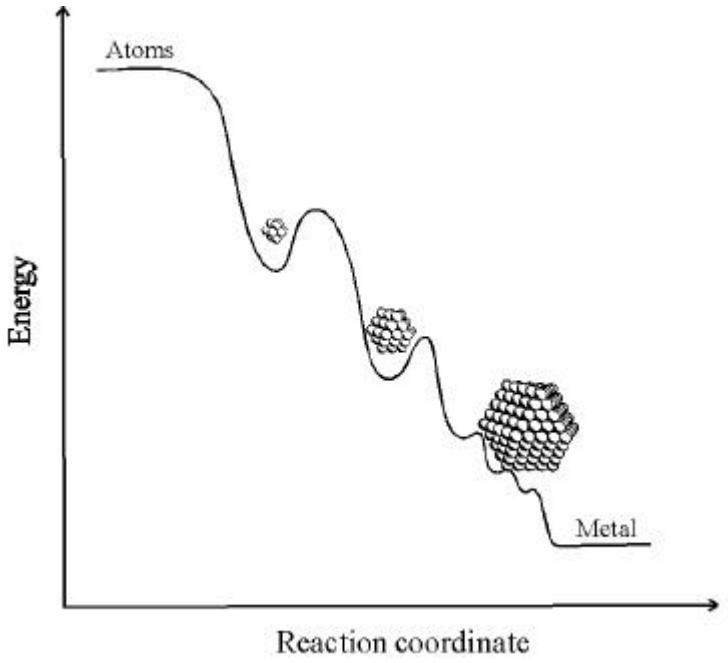

Fig. 2.12: The energetic curve of the birth of the metal. The images of the clusters are the same as on (Fig. 2.11).

2.4.3 The physical-chemical properties of the Au_{55} cluster

Because of its ligand shell, the so synthesized cluster is soluble in many organic solvents, especially in dichloromethane. The solutions are usually brown, depending on its concentration it can change from light brown (diluted solutions) to dark brown (concentrated solutions).

The UV-Vis spectra of cluster solutions do not show a plasmon resonance in the range of 300-800 nm, which is a unique feature of the clusters owning such small metal cores.

After the evaporation of the solvent, or the dropping of pentane to the dichloromethane solution, the clusters crystallize to give a dark brown powder consisting of air stable microcrystals (see chapter 2.4.5.5).

Mössbauer spectroscopic investigations show that there are four different types of Au atoms in the Au_{55} cluster: one bound to triphenylphosphine, a second to the chlorine, the third is an unbounded surface atom, and the last type situated the atoms inside the cluster [119]. The chemical shift, caused by the 13 inner atoms, is quite close to that of bulk gold, which means, that the 13 atoms build a metallic core. This point is very important for the

future use and explains why the electrical properties of the Au_{55} cluster must be investigated.

2.4.4 Importance and strategy of the ligand-exchange

As already mentioned, the organic ligands PPh_3 makes the Au_{55} cluster soluble in organic solvents and insoluble in water. In order to solubilize it in water, ligand exchange reaction is necessary using a phase transfer reaction (the method was already described in chapter 2.3.2) [120]. A dichloromethane solution of $Au_{55}(PPh_3)_{12}Cl_6$ clusters is mixed vigorously with a water solution of $PPh_2(C_6H_4SO_3H)$. During the phase transfer reaction, the other molecules, soluble in water, exchange the PPh_3. This can be visualized by a brown coloration of the colorless aqueous phase. The experiments showed that the $Au_{55}[PPh_2(C_6H_4SO_3^-)]_{12}Cl_6$ cluster is more stable in solution what is caused by the relative big charge hold by the particle.

The same strategy was followed also in the case of T_8-OSS [121] and disodium-mercaptoundecahydro-*closo*-dodecaborate (BSH) (Fig. 2.13). The affinity of these two ligands to Au_{55} is higher than that of PPh_3 molecule because of the thiol groups, so the Au_{55} is easily transferred to the aqueous phase. This transfer reaction helped also to purify the sample and to quantify the reaction, as it is written in chapter 2.3.2.2.

a) b)

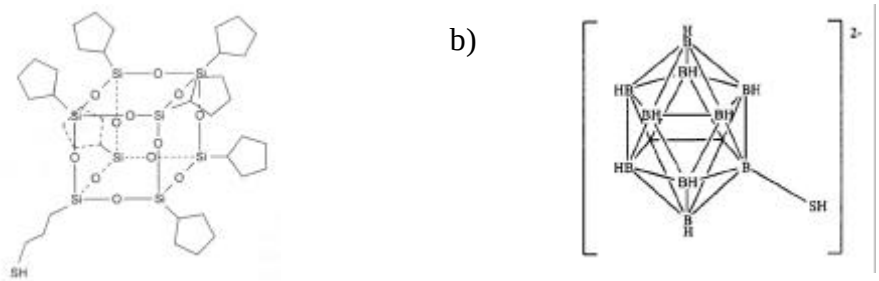

Fig. 2.13: The T_8-OSS (a) and BSH (b) ligands. Figure is adapted from [121] and [122].

The experience was that the exchange of the ligand shell changes the properties of the clusters dramatically. The $Au_{55}(PPh_3)_{12}Cl_6$ is relatively stable in solid phase under atmospheric conditions, but its lifetime in solution is not more than a few hours [120]. This is because of the equilibrium reaction, which takes place in the solution:

$$ML_y + k\,S \quad ML_{y-k}S_k + k\,L \qquad 2.16$$

where M in the metal core, L is the ligand and S stands for solvent molecules. If too many ligands become free, the weakly stabilized metal cores stick together, forming a bigger particle. `The aggregation can be observed by the change of the color of the solution. Letting the $Au_{55}(PPh_3)_{12}Cl_6$ cluster in solution for two or three hours the originally dark brown solution becomes purple, and in additional one hour, blue. After a night, a black precipitate can be observed, showing, that during the aggregation metallic gold is formed. The $Au_{55}(T_8\text{-}OSS)_{12}Cl_6$ cluster is stable in solution for almost infinite time. That is because the big ligand shell, which doesn't let the clusters too close to each other, but also, because of the reaction constant of the above explained reaction is very small, so there are simply no attackable metal core.

Of course ligands can also be exchanged by simply mixing the $Au_{55}(PPh_3)_{12}Cl_6$ clusters with a thiol ligand[114][123]. In this case the stronger Au-S bond can exchange the weaker Au-P bond. The problem of this synthesis usually is to get rid of the free PPh_3. As it is explained in chapter 2.3.2.3, the ligands can also be exchanged on the surface. For this, a thiol functionalised surface is used, and a solution of the $Au_{55}(PPh_3)_{12}Cl_6$ clusters. In this case the gold core is anchored to the surface with formation of an Au-S bond and some of the PPh_3 from the ligand shell become free.

2.4.5 Preparation and properties of zero-, one -, two–, *quasi*-two-, and three-dimensional arrays of Au_{55} cluster.

2.4.5.1 Zero-dimensional arrangements

Zero-dimensional arrangements of Au_{55} clusters can be prepared by dropping a very dilute solution onto a substrate. Using the same deposit method on a carbon coated copper grid, TEM measurements have shown, that the size of the metal core is 1.4 nm [1].

STM investigations of $Au_{55}[PPh_2(C_6H_4SO_3^-)]_{12}Cl_6$ layers were also realized. Such layers were obtained by a chemical method: a glass surface covered with cysteamine-hydrochloride was dipped into an aqueous solution of the water-soluble $Au_{55}[PPh_2(C_6H_4SO_3^-)]_{12}Cl_6$ cluster. The as-prepared monolayer was investigated by STM,

perpendicular to the surface [128][133]. These measurements gave an important result: with the STM method, the clusters are 2.1 nm high. That means, that the ligand shell also influences the mechanism of the electron transfer through a particle.

2.4.5.2 One-dimensional arrangements

There are four strategies for the preparation of one-dimensional arrangements of the Au_{55}-cluster:

- The first and oldest method is to immobilize the clusters in alumina nanotubes [134]. The clusters stabilized by T_8-OSS (diameter size: 4.2 nm), were introduced into the pores (diameter: 7 nm) by means of electrophoresis (Fig. 2.14). Inside the nanotubes, the clusters form a spiral-like structure, as it is illustrated in Fig. 2.14. The clusters, finding each other as well as to the pore wall by van der Waals interactions, since the T_8-OSS ligand has no functional group in the direction of the pore walls.

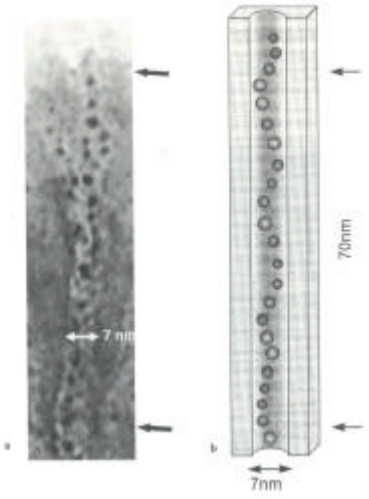

Fig. 2.14: Alumina nanotubes filled with Au_{55} $(T_8\text{-OSS})_{12}Cl_6$. The left picture is a TEM image of a nanotube inside, the right picture is a schematic drawing of the filled pore. Figure is adapted from [134].

- The second strategy couriers the use of DNA. *t* can also be used as a template to induce clusters arrangement via chemical interaction: a quartz platelet is dipped into a solution containing the DNA and clusters. The clusters arrange themselves along the DNA on the surface via specific bonds to form wires.

- Third strategy: Nanowires were generated by trapping the clusters between two nanocontacts with application of a voltage between the electrodes. A platelet with the contact structures was dipped into a $Au_{55}(PPh_3)_{12}Cl_6$ dichloromethane solution and 1V was applied between the electrodes. As long as the distance between the electrodes is 20 to 30 nm, a short row of clusters is trapped, arranging themselves along the lines of the electric force. As can be observed in Fig. 2.15, more cluster liner are formed during the preparation, drawing the lines of the electric force. The shortest line of these is, of course, the linear between the two contacts [155] (Fig. 2.15). This line in the middle of the picture seems to form a closed line which allows the flow of the electric charge through it. The electrical measurements through this line can be observed in chapter 2.4.6 and on Fig. 2.21.

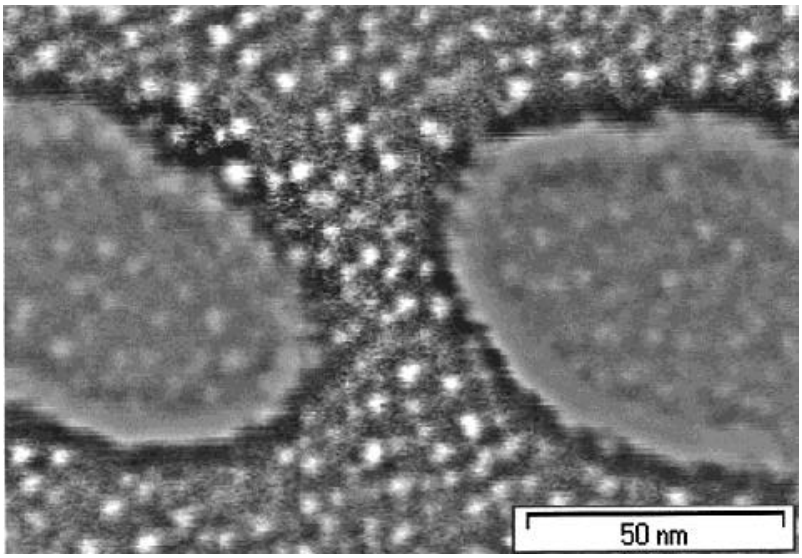

Fig. 2.15: Clusters arranged along the line of the electric force between two W tips. Figure is adapted from [155]

- The fourth trial is the preparation of *quasi*-one-dimensional structures using LB technique and the oscillation of the water meniscus. During the transfer process of the monolayer to a substrate, a periodic oscillation of the water meniscus induced a breake of the monolayer with the same periodicity [135] (Fig. 2.16). This movement allows the formation of stripes (thickness: 6 nm) parallel to the direction of the meniscus and perpendicular to the movement of the sample.

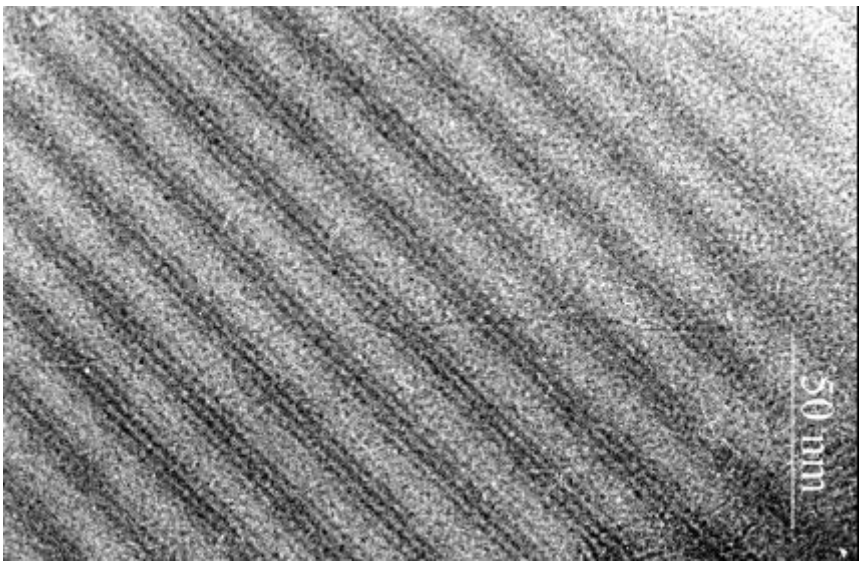

Fig. 2.16: Stripes prepared by LB technique. The sample is pulled out from the solution with a relative high speed, so that the meniscus breaks periodically. The stripes are parallel to the direction of the meniscus, and perpendicular to the movement of the sample. Figure is adapted from [135].

2.4.5.3 Two-dimensional arrangements

The preparation of two-dimensional arrangements of Au_{55} clusters was also a big challenge, and was solved during the last three years. Building large closed areas clusters is necessary to characterize them electrically.

As mentioned in Chapter 2.3.3.3, two main methods are available for the preparation of cluster monolayers. Chemical methods are starting with the modification of a surface, followed by specific adsorption of clusters. Physical methods are more or less based on modified LB techniques.

In recent years, the most important work concerning the chemical methods were realized by S. Peschel and M. Bäumle [125][126]. They worked mostly with layers based on ionic interactions, using polyethylenimine (PEI) as cationic polymer, and the water-soluble gold cluster as anionic cluster. Two kinds of acid-base ionic interactions are present: between the negative glass surface, and the positive polymer (the imino groups in the polyethylenimine receive a proton from the hydroxyl group of the glass surface) and between the positive polymer, and the negative clusters ($-SO_3H + -NH_2 \quad -SO_3^- + -NH_3^+$) [136][137]. This method was convenient for mica, silicon and glass substrates. For gold substrates another method was used: the surface was covered by small linker molecules like aminothiols, e.g.

cysteamine [125] (see chapter 2.3.2.3). With this technique smaller or bigger islands of closed monolayers were obtained, however, only small range ordering was observed..

Covalent bonds between surface and cluster were never used to obtain monolayers on different substrates. Specific interactions based on covalent bonds were used to immobilize clusters inside pores [138], but this technique was not convenient for preparing closed monolayers onto flat surfaces.

Some trials to order clusters onto different substrates using modified LB technique(s) were also realized [139] (Fig. 2.17). Some drops of a $Au_{55}(PPh_3)_{12}Cl_6$ dichloromethane solution were deposited onto a very diluted aqueous solution of different amphiphile compounds, like per-6-deoxy-6-thio-α-cyclodextrin or poly-vinyl-pyrrolidone. After evaporation of the solvent, a carbon coated copper grid was dipped carefully under the surface of the liquid and pulled out slowly to transfer the layer. The samples were investigated by TEM.

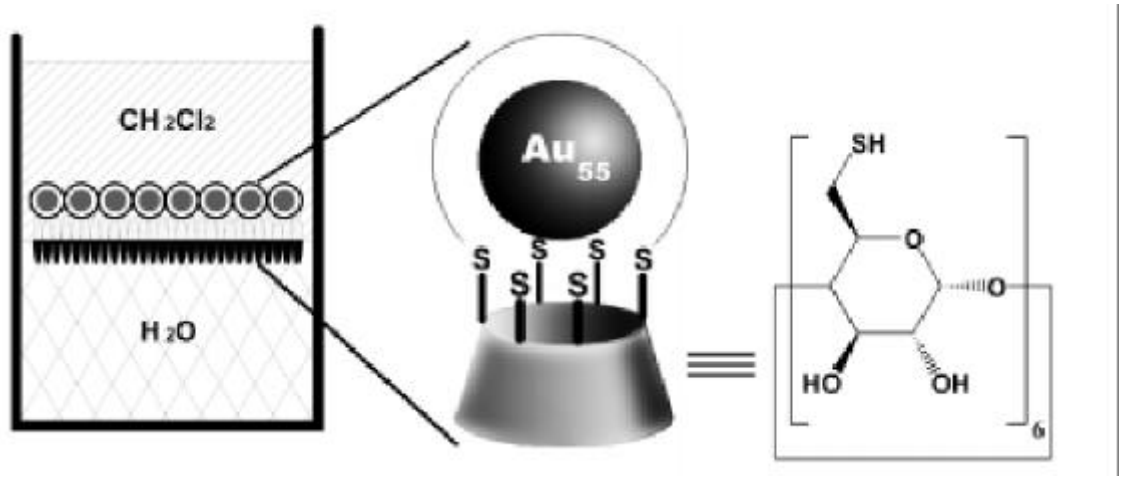

Fig. 2.17: Sketch of the cluster-amphiphile interaction on the interface between the dichloromethane and the aqueous solution. Figure is adapted from[139].

With this technique, relative big islands of ordered monolayers (up to 1 μm in diameter) were obtained. The clusters crystallized in two different forms: hexagonal arrays and square lattices.

2.4.5.4 Quasi-*two-dimensional arrangements*

Thin films of the Au_{55} clusters are prepared mainly by two methods: spin-coating, and layer-by-layer self-assembly.

During the spin-coating technique, the formation of thin film owning relative homogeneous thickness is possible [140][141]. A quartz plate is spinning with a certain speed and some droplets of a cluster solution is dropped onto its surface. The thickness of the film is controlled by the speed of the platelet and the concentration of the drops (Fig. 5.24).

The layer-by-layer self-assembly methods are working on the same basis as those using bigger particles, discussed in chapter 2.3.3.4. In this case mainly ionic self-assembled layers were used [125][126]. A monolayer of the Au_{55} clusters was prepared, as it is introduced in chapter 2.4.5.3 and the clusters dipped back to the PEI solution, which built up a second polymer layer on the surface. The sample then was dipped into the water-soluble cluster solution, arranging the second cluster layer, and so on.

2.4.5.5 Three-dimensional arrangements

Microcrystals of hexagonally ordered $Au_{55}(PPh_3)_{12}Cl_6$ cluster are easy to prepare, from CH_2Cl_2 solution by simple evaporation of the solvent.

Ordered cluster arrangements with different cluster spacings can be built using clusters with different ligand shells (see chapter 2.3.2). With PPh_3, for instance, the distance between the centers of two neighbored clusters is 2.1 nm, while in the case of T_8-OSS ligand is 4.1 nm. Spacers also can be used to get different lengths between the gold particles [123], [114], [41]. In this case, acid-base interaction between the SO_3H group of the $Au_{55}[PPh_2(C6H4SO4H)]_{12}Cl_6$ clusters and the NH_2 group of the ligands were used.

The tuning of the distance between the particles without changing their ligand shell is an important experiment [123], [114], [41] (Fig. 2.18).

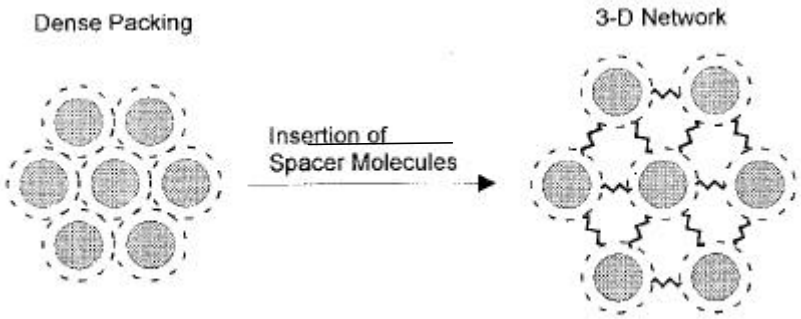

Fig. 2.18: Tuning the distance of the clusters with spacers. Figure is adapted from [41].

The easiest method to get such structures is to mix the aqueous solution of the water-soluble cluster and an α-ω-diamine and let it crystallize. In this case ionic bonds are formed between the $-SO_3^-$ and the $-NH_3^+$ groups, and the spacers are wedged in the cluster space. These reactions are not ligand exchange reactions, rather an inter-shell reaction with another spacer. Three different molecules were used for testing this reaction [125]: 4,4'-diamino-1,2-diphenylethan (DDE), bis{5-[(4-aminophenyl)ethinyl]-3-methyl-thien-2-yl}acetylen (BATA) and 1,4-bis{3-propionic acid[1-(8-N-pyridiniumbromide] octylester]}benzene (POB) (Fig. 2.19). With TEM and electrical measurements it was proved, that the inter-cluster distances were different according to the ligand used. (In details see chapter 5.2.3.1).

a) DDE

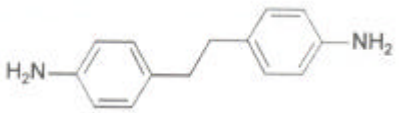

b) BATA

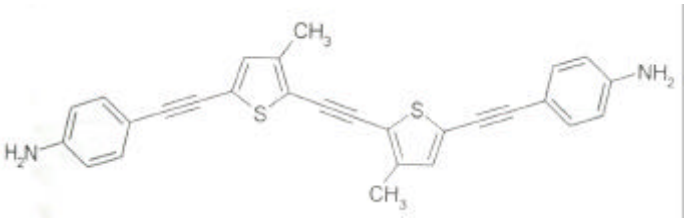

c) POB

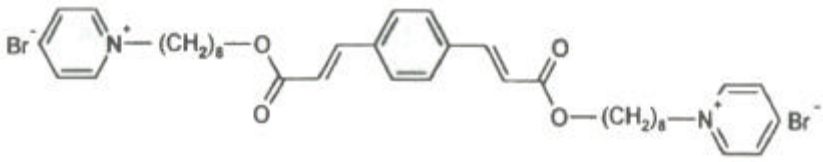

Fig. 2.19: The three molecules, used for tuning the distance between the clusters. Figure is adapted from [123].

For *quasi*-two-dimensional arrangements spin coating technique was used (see chapter 2.4.5.4 and Fig. 5.24). For the preparation of a monolayer a modified LB technique was applied (with a slight modification of the method described in Ref. [139].)

2.4.6 Electrical properties of arrays made of Au_{55} clusters

The size, the composition, and the shape uniformity of the Au_{55} cluster together with its very small capacitance makes it the optimal object for the investigations of easily producible room-temperature SET. This fact was proved by electrical measurements realized on both zero- [124][128] and one-dimensional [155] arrangements (Fig. 2.21).

If an STM tip is positioned above a Au_{55} cluster, the STS curve shows strong Coulomb-blockade. A Coulomb-staircase at low temperatures is also observable (Fig. 2.20).

It turned out that, using EBL fabricated nanocontact systems with a source-drain distance of 20-30 nm from each other, and a gate electrode a little farther (Fig. 2.15); nanowires of clusters can be trapped between the source and the drain (see chapter 2.3.4.1 and Fig. 2.15). Measuring the *I-V* characteristics of these systems, Coulomb behavior was obtained. The change of the gate potential causes a change in the *I-V* curve between the source and the drain, which indicates that a SET was fabricated [155] (Fig. 2.21).

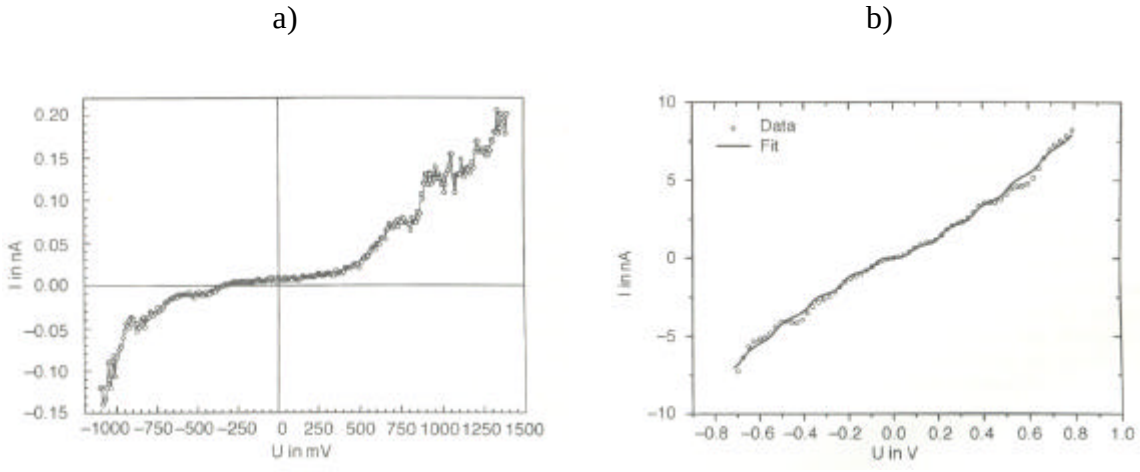

Fig. 2.20: The STM tip is positioned above a single Au_{55} cluster and *I-V* characteristics is measured. (a) The STS curve shows Coulomb-blockade behavior at room temperature. (b) Coulomb-staircase behavior at 90 K. Figure is adapted from [124].

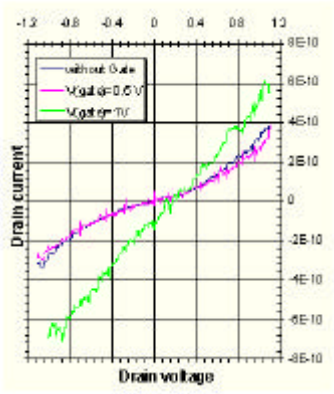

Fig. 2.21: The *I-V* characteristics of the first single electron transistor fabricated from the Au_{55} cluster. The changing of the gate potential leads to the change of the *I-V* curve between the source and the drain, which indicates that a SET was prepared. Figure is adapted from [155].

Many difficulties concerning the electrical characterization of the monolayers are exist. First of all, the resistance of the $Au_{55}(PPh_3)_{12}Cl_6$ cluster systems are too high to be measured with simple methods. These cluster systems behave as insulators also in 3D. The resistance of a system consisting of two electrodes and the sample depends also on the size of the electrodes (see chapter 4.3.3). In the case of two-dimensional measurements the "area" of the electrodes are very small.

On the other hand, these monolayers consist of closed-packed cluster islands in most cases. To be sure to really contact them, conducting paths with very small distance have to be used. This also useful, because decreasing the electrodes distance involves a decreasing of the system resistance.

Furthermore, the monolayers prepared until now were mostly layers based on ionic bonds (see chapter 2.4.5.3). In this type of arrangements conductance of the layer caused by the ionic movements in the residue water and the polymeric medium can be one or two magnitude higher, than the conductance of the clusters.

Thin films of the clusters are easier to measure than the monolayers. The areas of the electrodes used are bigger, since the thickness of the layer is bigger, and with spin-coating technique, for instance, homogeneous and quite thin films can be prepared (see chapter 2.4.5.4). Using $Au_{55}(PPh_3)_{12}Cl_6$ clusters no ionic interactions are used, so no movable ions in the layer can interact and this point represents the biggest advantage of this synthesis

technique. Because of the bigger electrode area and because the film is much more homogeneous than in the case of a monolayer, bigger electrode-distances can be used.

The most obvious idea to study the conductivity of a sample having relative big resistance is the three dimensional characterization. In this case depending on the used geometry, the electrode surfaces can be relative big compared to their distance, so the conductivity can be increased into the easily measurable range. The pioneering work in this field was made by L. J. de Jongh and coworkers [142]. They measured the temperature dependence of the conductivity of three-dimensional Au_{55} systems and observed, that the kinetics of the electron transport in this systems doesn't follow the Arrhenius law, because the logarithm of the conductivity is not linear as a function of the reciprocal temperature, just as a function of the square root of the temperature. (see chapter 4.5.3) This observation makes the Au_{55} cluster systems similar to the so-called cermets, which are metal-insulator composite materials.

The authors discuss numerous theories to describe this behavior, and find that the variable range hopping models namely the thermally activated stochastic multiple-site hopping process fit the measured data best. At high temperatures the nearest neighbor hops dominate (see chapter 4.5.3).

A simpler explanation of this behavior was worked out by Mott in 1969 [149][150][151]. This is the Mott's conduction theory for the Variable Range Hopping (see chapter 4.5.3).

3 Aim of this work

The investigations focused on the following points:

1. Experimental conditions for the electrical measurements
2. Dependence of the charge transfer mechanism and the activation energy on the ligands
3. Electronic properties of Au_{55} monolayers

The studies will be carried out separately for two-, *quasi*-two-, and three-dimensional arrays of Au_{55} clusters. From the viewpoint of the experimentalist, the following problems have to be solved for the two-dimensional-samples:

1. A monolayer consisting of large, dense-packed Au_{55} islands should be prepared. For successful electrical measurements, this layer should not contain movable ions like Na^+ or traces of conducting solutions (aqueous solutions, impurities).
2. The monolayer has to be transferred onto the substrate applied with the electrode system. This electrode system should contain electrodes in a suitable geometry and size range.
3. Suitable parameters should be elaborated for the cross-linking reactions, without changing the structure of the monolayer.

For the *quasi*-two-dimensional samples:

1. Multilayers of Au_{55} clusters should be prepared, without movable ions or traces of ion-conducting solution.
2. A suitable method should be found for the chemical attachment of the multilayer onto the substrate surface.

For the three-dimensional samples:

1. Conjugated α,ω-dithiols should be synthesized to function as bridging ligands.
2. Cross-linking of the clusters with ligand-exchange reactions.

The conductance of samples with quasi-two- and three-dimensional cluster arrangements can be characterized with the methods elaborated by U. Simon. However, novel measurement techniques need to be developed for monolayers with a two-dimensional cluster architecture.

4 Discussion of the charge-transfer mechanisms in nanoparticle systems

To understand the problems and the results, which will be discussed in the following chapters (chapter 5 and 6), some principle studies on the electron transfer mechanisms of different cluster arrangements is necessary. It will be shown, how the charge transfer mechanism of a complicated three-dimensional sample can be built up from the flow of current trough single nanoparticles. In the following this background will be overviewed and discussed.

4.1 Conduction mechanism of zero-dimensional systems (tunneling through a quantum dot)

The literature overview of the tunneling through a quantum dot is discussed in chapters 2.3.4.1 and 2.4.6. The main and common points in these measurements are that the capacitance of the central island in a SET has to be decreased, to increase the temperature threshold of the single electron tunneling effects. The basics of the single electronics is discussed in chapter 2.2. There are mainly four signs that indicate a SET: the Coulomb-blockade, the Coulomb-staircase, and the oscillating dependence of the source-drain *I-V* characteristics on the gate potential. This is supplemented with the Size Induced Metal-Insulator Transition effects (SIMIT effects) in the case of small metal particles, which is not strictly a sign of the presence of a SET, but influences the shape of the *I-V* curve.

A single electron transistor consists of a small metal island (metal nanoparticle) and three electrodes: the source and the drain are close to the central island, the gate is a little farther, coupled capacitively to the central island (see Fig. 2.2). Using the single electronics language, the set consists of a double junction system, with an electrode (gate) capacitively coupled to the central island. If the electron pass through the first junction, it charges the central island, which causes the voltage drop to change with a value of e/C (where e is the charge of the electron, and C is the capacitance of the junction). This is the cause of the Coulomb-blockade effect: the tunneling is suppressed at voltages $|V|<e/2C$. If the Coulomb-blockade do not exist, than at voltages $V<e/2C$ the tunneling would increase the elec-

trostatic energy of the capacitor $C(V \pm e/C)^2/2 > CV^2/2$. The Coulomb-blockade is determined only by the first junction: if the two junctions are different, asymmetry in the *I-V* characteristics can be observed, which is caused by the two different Coulomb-blockades from the two different directions (normally this is the case by STS measurements. See E.g. Fig. 6.2). Concrete examples for the Coulomb-blockade behavior can be observed in Fig. 2.5 and Fig. 2.20.

If the tunnel junction of the SET is considerably different, then the *I-V* curve shows substantial periodic oscillations with a period of $\Delta V = e/C_1$ (for $R_1 >> R_2$, where R_1 and R_2 are the tunneling resistances of the two junctions). This is the Coulomb staircase. Each period of the staircase corresponds to an additional electron on the central island [107]. This effect is typical for the STS measurements, because the tunnel junction between the conducting particle and the substrate is usually much smaller, then those between the tip and the particle.

The third effect is that the value of the Coulomb-blockade depends on the background charge of the central island. This can be controlled by a third electrode (gate), which is capacitively coupled to the central island, in order to control its charge. Using the theoretical equations of the SET, it can be concluded that the Coulomb-blockade completely disappears, if the background charge is equal to (k+1/2)e (k is an integer) because the states with effective charges of e/2 and -e/2 have equal energy.

The transition from single atoms or molecules to the metallic state contains many dramatic changes in the electron energy levels. These effects are the so-called quantum size effects (QSE) (Fig. 4.1) [124][129]. In this transition (Size Induced Metal to Insulator Transition, SIMIT), there is no well-defined threshold, the change is continuous, and the results depend strongly on the measurement method.

The *I-V* characteristics of a SET transistor with a level discreteness contains step-like features which appear, when the discrete level in the island crosses the Fermi-level (HOMO electron level in the metals) of the external electrode. The SIMIT can interfere with the Coulomb-staircase forming a quite complicated electronic behavior. Sometimes it is difficult to distinct between the two effects (Fig. 2.20), except when the Coulomb staircase has

equal periods, while the SIMIT effects are random, depending on the energy level of the nanoparticle.

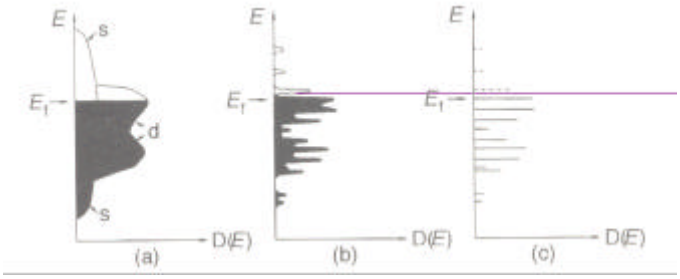

Fig. 4.1: Electronic situation in (a) bulk metal particle with quasi-delocalized d and s electrons forming a band structure. In (b) the electrons begin to form discrete energy levels which are completed in the molecular state (c) with fully localized bonding electrons. Figure is adapted from [124].

Reifenberger and coworkers [152] have investigated the influence of the chemical nature of the ligands on the STS curve. They measured the STS curve of conjugated molecules with different functional groups at the ends. They have found that STS spectra can be really different when a molecule is linked to a substrate or to a STM tip with different chemical interactions. This effect can be explained by the conductance of the molecules through the HOMO or the LUMO orbitals. The place of the Fermi level is changed according to the LUMO of the investigated molecule, depending on the chemical nature of the function group. In the case of an STS measurement the voltage drops on the molecule is 1 4 V, which can cause the distribution of the electrons between the HOMO and the LUMO: the electrons can be really excited from the Fermi level of the substrate or the STM tip to the energy of the LUMO of the spacer molecule. The same effect has also to be taken into consideration in the case of nanoparticles: the nature of the chemical interaction between the substrate and the particle can influence its conductivity. It will be discussed later that this is not the case at measurements with higher dimensionality (see chapter 5.2.3.4).

4.2 Conduction in one-dimensional arrangements

One-dimensional arrangements of metal nanoparticle systems cannot be considered as a double-junction system any more, but like a multi-junction system. In other words, there

are two electrodes and many tunnel junctions between them. That arises two kinds of problems in the case of ligand-stabilized clusters. The first is that the separation of conducting particles is larger, so the junction is thicker, because the distances between the metal cores are equal to the length of two ligand shells. The thickness of the junction increases the tunneling resistance, which depends exponentially on the distance between the particles. In the case of smaller clusters this effect generates experimental difficulties.

The second problem is the question of the possible disorder in this system. Small disorder in the arrangement causes big differences in the measured data [108]. The authors have discussed the impurities effect (smaller particles in the array) and the packing defects (the inter particle distances are very different at certain places). The main conclusion was that the impurity increases the potential at that point, which may lead to, at least, localization: the single electron in the array may be trapped. The packing defects influence the capacitance at that point of the array.

The conduction in disordered nanoparticle systems with a higher dimensionality occurs trough conducting paths. These are one-dimensional rows of clusters inside an array with higher dimensionality. These rows were chosen by the flowing current, because the resistance of these ways is smaller than any other in the region. (For better understanding see Fig. 4.3).

The two main experimental results, which give peaces of information about the electrical behavior of one-dimensional arrangements, are discussed in chapters 2.3.4.2 and 2.4.6.

4.3 Conduction in two-dimensional arrangements

4.3.1 The effect of the impurities and displacements

Adding one more dimension to the system the conduction becomes even more complicated.

The problem of the impurity does not pose problems any more, because the conduction paths (the way of the electrons through the arrangement) choose directions among the clusters, which are in the absence of this small disorder effects (Fig. 4.2a). The same can be

predicted for small numbers of displacements in an ordered lattice (Fig. 4.2b), system "heals" itself.

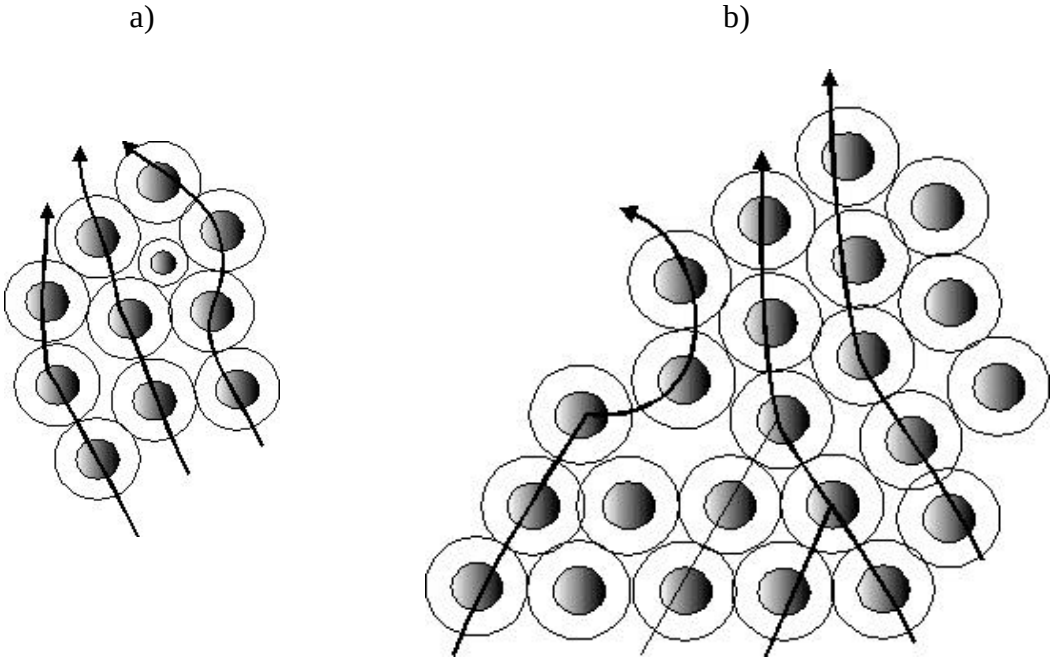

Fig. 4.2: Conducting paths in the case of the presence of an impurity (a) or displacements (b).

4.3.2 The conducting paths

In the case of island-like structures of a monolayers (which is quite common in nanoparticle systems) the conductance mechanism is more complicated.

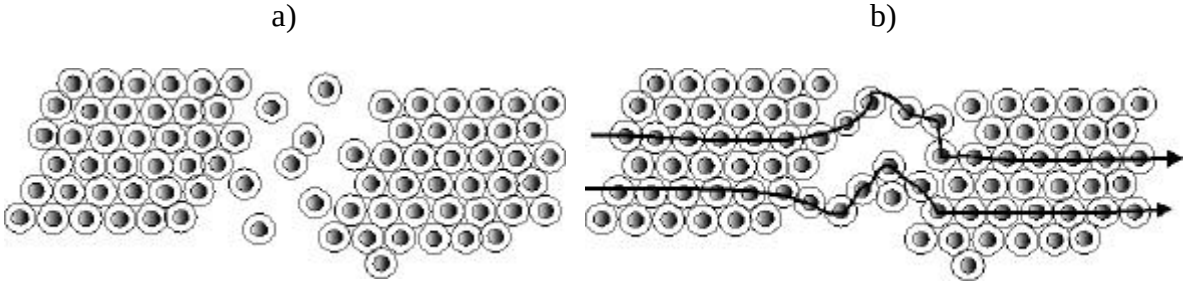

Fig. 4.3: Island-like structure of a nanoparticle system. In the inter-particle region the clusters arranged statistically (a) or build up conducting paths (b).

In this case, more or less ordered islands alternate with regions of smaller conducting particles density (Fig. 4.3). The charge transfer mechanism of these arrangements can be explained with a theory, which is similar to the Brick layer model developed for three-dimensional samples, and discussed in chapter 4.5.2 in details.

Two possibilities can be observed (see Fig. 5.10 and Fig. 5.11). The first corresponds to a statistical arrangement of the particles in the inter-island region (Fig. 4.3a, Fig. 5.10). In this case there is no conducting path between the islands: it is the insulator case. The activation energy of the sample is very high: the clusters have to move to build conducting paths. In Fig. 4.3b another arrangement can be observed (see also Fig. 5.11): the particles build conducting paths in the inter-particle regions. This model is also discussed in details in chapter 4.5.2. So, these regions have larger resistances than the intra-particle regions, but this can be explained by the smaller number of the conducting paths.

A nice example concerning to the building of conducting paths can be observed in the case of comb structures with relative high applied voltage (Fig. 4.4). In this picture every second white line (tungsten wire) are electrically connected with each other: the 1^{st}, 3^{rd}, 5^{th} and so on upwards, as well as the 2^{nd}, 4^{th}, 6^{th} and so on downwards (see Fig. 8.5). That means, that if voltage is applied to the electrodes, this voltage falls between the neighboring wolfram lines, represented by the white lines in the figure. If the applied voltage is high enough, the clusters can move to build conducting paths, as it can be observed in the circled areas in Fig. 4.4.

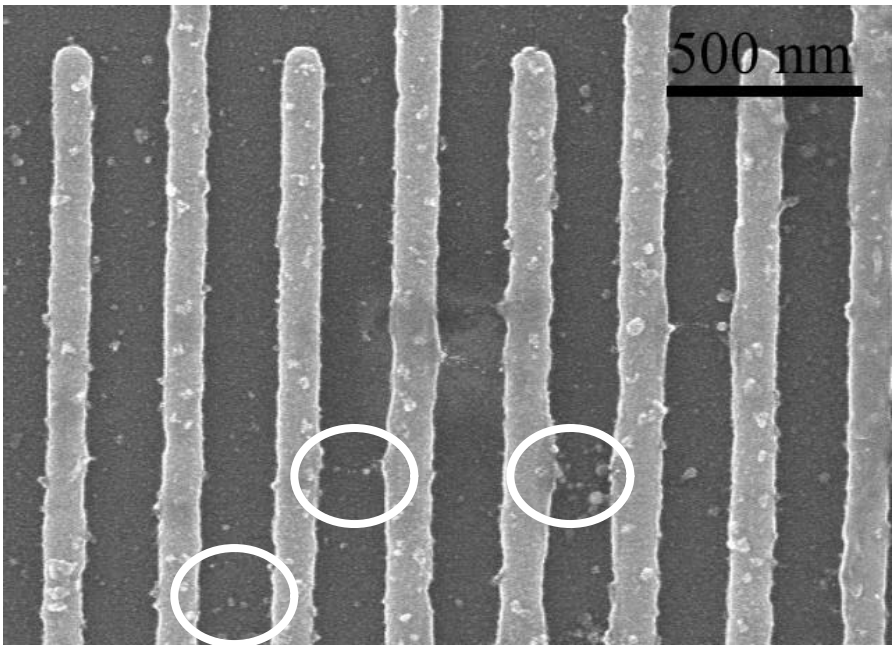

Fig. 4.4: Conducting paths built as an effect of the high applied voltage.

4.3.3 The effect of the electrode-geometry

In the case of a homogeneous sample with "infinite"* long electrodes on the surface, a clear Coulomb-behavior should be observed. That means that in the metallic case the *I-V* curve is simply linear, or in the presence of SET effects it is a Coulomb-blockade with two linear branches on the sides (Fig. 4.5). Measuring on real samples, even in the case of practically infinite long electrodes (comb structures) nonlinearity effect can be observed. That means that the I-V curve is not linear in any voltage regions. This can be explained with the different lengths of the conducting paths: at small voltages (small activation energies) only the shortest paths are available, at higher voltages can others also become active. The individual currents of the different paths are superimposed to give the macroscopically measurable current I.

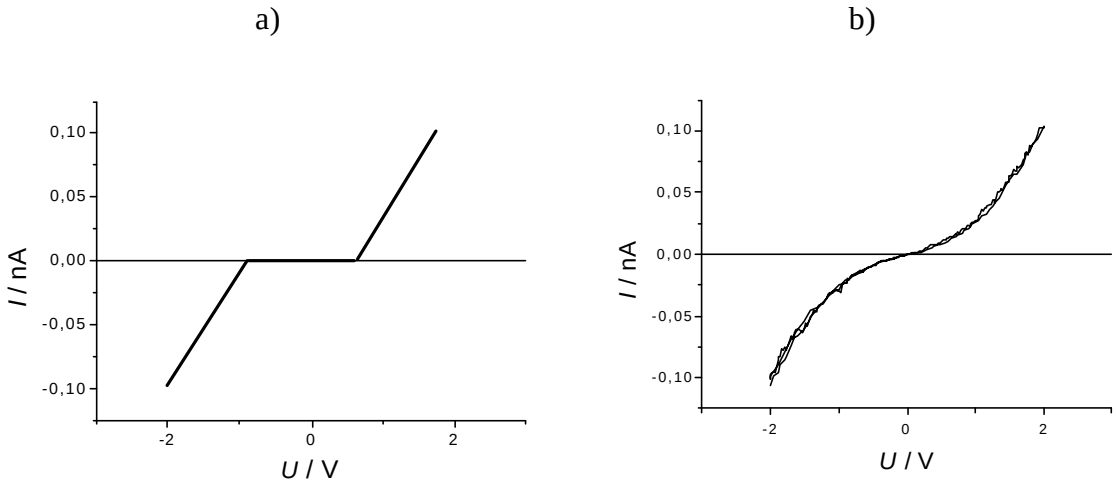

Fig. 4.5: Theoretical (a), and measured (b) I-V curves in the case of homogeneous layers between two not infinite electrodes.

In the case of non-infinite electrodes even the electric measurement of a homogeneous layer results in a nonlinear *I-V* curve (Fig. 4.5).

* "Infinite" long in this sense means that the length of the electrodes on the surface perpendicular to the direction of the flowing current is very long comparing to their distance.

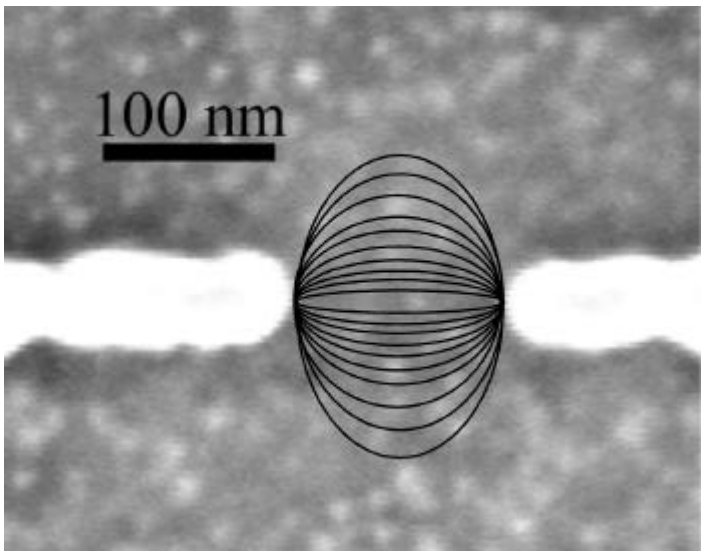

Fig. 4.6: Conducting paths of a homogeneous sample in the case of non infinite electrodes.

This effect is caused by the different conducting paths, which are more and more available with the increasing of the voltage (Fig. 4.6). In Fig. 2.15 this effect can be observed. This sample was prepared by applying a voltage between two electrodes in a $Au_{55}(PPh_3)_{12}Cl_6$ solution. The clusters arranged along the electric force lines as it is discussed in chapter 2.4.6. The conductance of this sample is nonlinear, because with increasing of the voltage more and more paths become active. The currents flowing trough the individual paths are summed up: the conductance of every individual path is linear, but they become conductive on different voltages, so their sum is not linear any more.

4.4 Conduction in *quasi*-two-dimensional arrangements

In thin films built by superposition of many nanoparticles monolayers, the number of the conducting paths increases and the possibility of having statistically arranged areas decreases, so the activation energy and the resistance of the layers are dramatically decreased.

The rules that determine the conductance in a thin film are exactly the same as in two and in three dimensions. It is a transition state, which results in a transition behavior. Numerous monolayers piled up may behave as well as a monolayer with many conducting paths,

and as a thick film like a three dimensional arrangement. One sign of this effect might be the dependence of the activation energy on the layer thickness.

4.5 Conduction in three-dimension (conduction in non-homogeneous solids)

4.5.1 The absence of the Coulomb-blockade

With the increasing of the thickness of a *quasi*-two-dimensional layer into three-dimensional the parameters of the layer become constant. These values are average values of the microscopic characteristics. Models are developed to understand this situation, which will be discussed in the following.

The first and most apparent behavior of the three-dimensional systems is the absence of the Coulomb-blockade. This effect is clear and undisturbed in zero- and one-dimensional samples. In the two-dimensional arrangement, the Coulomb-blockade can always be observed if Au_{55} is used. In *quasi*-two-dimension, it depends strongly on the temperature, the ligand shell and the thickness of the layer, and in three-dimension there is no Coulomb-blockade behavior. There are two effects at the origin of this phenomenon. First, on a three-dimensional sample, numerous conducting paths, with numerous microscopic capacitance are present. The longer is a conducting path, the smaller is the capacitance of it, which means, that a longer conducting path has a bigger Coulomb-blockade value. In the case of a macroscopic sample these values follow continuously each other, which result in a soft border of the zero conductance.

On the other hand, an increasing of the thickness of a layer results ultimately in an increased number of conducting paths. That means, that the capacitance of a three-dimensional arrangement decreases so, that the Coulomb-blockade effect disappears.

An evolution of the Coulomb-blockade can be observed on the following pictures: In the case of $Au_{55}(PPh_3)_{12}Cl_6$ cluster the conductance curve of the monolayer can be observed in Fig. 5.19, those of an asymmetrical thin film on Fig. 6.3 and the thicker film with bigger electrode on Fig. 5.26.

The same transition happens in a smaller thickness range in the case of the cross-linked systems: the conductance curve of the monolayer is on Fig. 5.21, and those of the thin film is on Fig. 5.31.

4.5.2 Brick layer model

There are many models that can be used to explain the conducting properties of non-homogeneous solids. The Brick layer model [153][130] (Fig. 4.7) proved to be the most useful for our Au_{55} systems.

Originally the brick layer model was developed to explain the conductance of cermets. These are metal-insulator composite materials, with metal islands inside, separated metal-oxide insulators. A typical example is the evaporation of Al in the presence of different amount of oxygen. If the percentage of O_2 is large, mainly Al_2O_3 forms. Without the presence of oxygen Al metal grows. Between these two limits there is a threshold ratio. If the sample contains more Al than this value, more and more metal islands will be formed inside the material, which gives the possibility of conductance. It will be pointed out in the following, that this material has numerous similarities in the conductance mechanism with the cluster systems. This is not very surprising, since the clusters are also metal-insulator composite materials, with the metal cores as metal islands and the ligand shell as insulator medium.

The “bricks” constitute the main part of the material. The grain boundaries are the small areas with exceptional behavior. If the conductance of the grains is smaller than that of the grain boundaries, the electrons move trough the grain boundaries without disturbing the grain interiors phases. If, however, the conductance of the grains is larger, the grain boundaries act as a gap in the way of electrons. In this case the electrons have to hop through the higher resistance regions. The conducting path can be built up, or can simply exist inside the grain boundaries. These are paths where the resistance is smaller than at other places in the grain boundaries.

In the terminology of cluster systems, bricks or grain interiors are the densest packed regions, where the electrons can tunnel through the hopping bands. This material is an isolator or a semiconductor, depending on the ligands. The impedance spectrum of this process

is a simple Debye semicircle [130], equivalent to a simple Resistance-Capacitance (RC) circle, indicating the regularity of the electron-conducting arrangement. The grain interior phases are cluster displacements in the lattice, or impurities, which disturbs the regular densest packed order in the material. The electrons have to hop through these regions following a temperature-activated process.

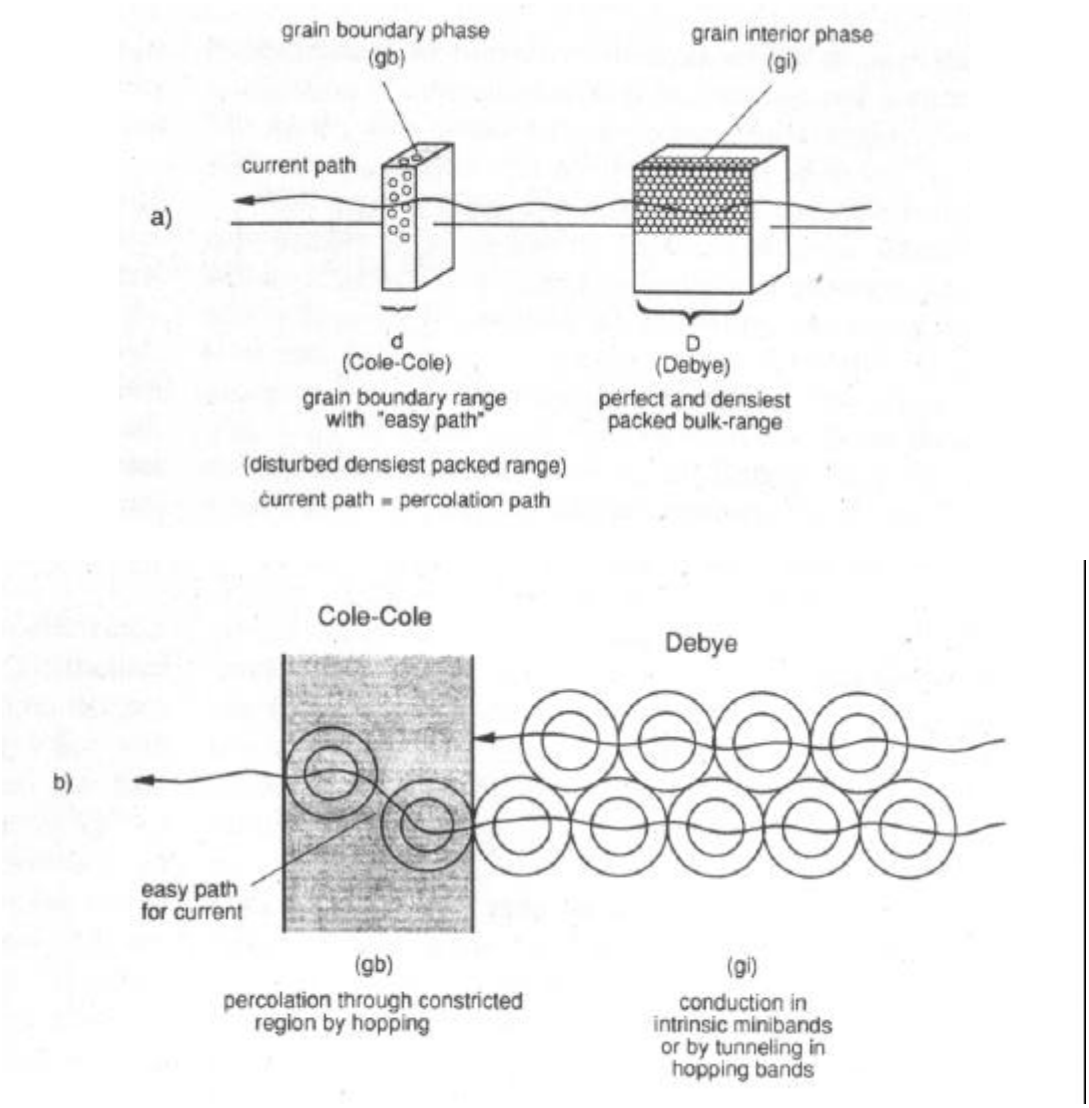

Fig. 4.7: Description of the brick layer model: (a) the bricks are the densest packed cluster groups inside the material, the grain boundaries are the disturbed regions. (b) Inside the bricks the conduction mechanism is the tunneling in the hopping bands, opposite to the hopping inside the grain boundaries. The figure is adapted from [130].

The impedance spectrum of this process is the not so regular Cole-Cole curve, which is equivalent to a resistance coupled parallel with a so called constant phase element, (CPE) [153]. This curve implicates the irregularity of the system (Fig. 4.8).

The in chapter 4.3 explained nonlinearity of the *I-V* curve will now be discussed in terms of the brick layer model. Depending on the activation energy and the thickness of the grain interiors, an increase in voltage increases the number of the available easy paths (one-dimensional conducting paths), resulting in a nonlinear *I-V* behavior.

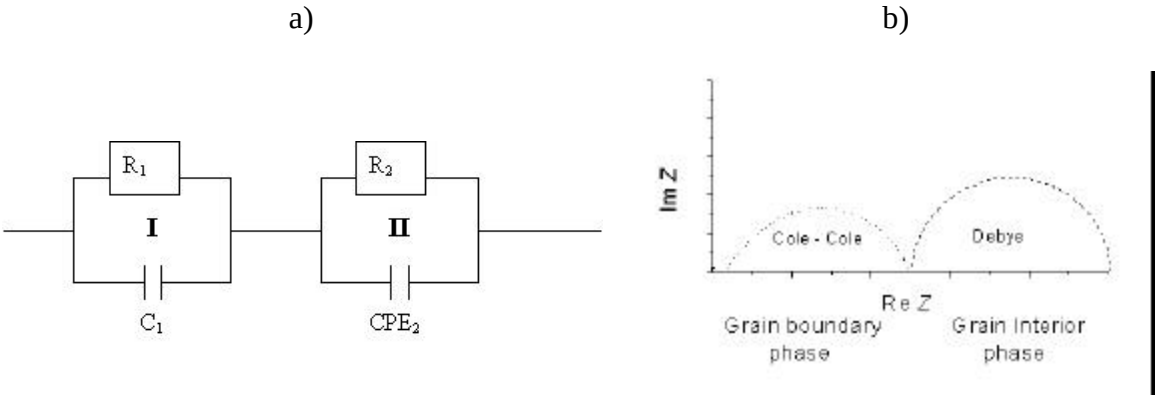

Fig. 4.8: Impedance of the system, which can be characterized by the Brick layer model. The sign I on the (a) figure is the Debye semicircle, and the Sign II shows the electric circle of the Cole-Cole process. On figure (b) impedances of the two process can be observed.

4.5.3 Variable range hopping models

For simple reactions, the temperature-dependence of the reaction rate for a follows the empirical Arrhenius law. This proclaims, that the logarithm of the reaction rate depend linear on the reciprocal of the temperature. The conductance of the semiconductors, being a temperature-activated reaction, also follows this rule. The conductance of metals is in contrast not a temperature-activated reaction, since there is no energy gap around the Fermi level. The temperature dependence of the resistance depends therefore on an other effect, namely on the electron phonon scattering.

The conductivity of cluster systems should at first approximation be similar to that of semiconductors. This is true at high temperatures. As mentioned in chapter 2.4.6, the pioneering work of de Jongh showed, that in analogy with the cermets the temperature-dependence of the conductivity of Au_{55} cluster systems also follow $\ln C \propto (1/T^{1/2})$ proportionality [142], (where C is the conductance and T is the temperature).

This behavior can be explained with Mott's conductance law for the Variable Range Hopping model. That means, that the single charge carriers are moving with hopping between the neighboring clusters. Mott's law proclaims [149][150][151], that:

$$C = C_0 \exp\left(\frac{-E_A R}{T}\right)^g \qquad 4.1$$

where E_A is the activation energy, and R is the gas constant.

Mott's theory assumes, that

$$g = \frac{1}{d+1} \qquad 4.2$$

where g is a constant, and d is the dimensionality.

At all dimensionalities of Au_{55} cluster arrangements g = ½ was measured experimentally in our work, in spite of the *quasi*-two- and three-dimensional arrangements. There are several approaches to explain this behavior. Efros and Shklovskii [154] have developed a model which assumes, that the density of states depends quadratic on the energy. Other and simpler explanation is, that the conductance – in spite of the dimensionality of the sample – occurs through one-dimensional paths, that is the easy paths. The effective dimensionality of the conductance, independent from the real dimensionality of the sample is therefore d = 1.

On the other hand, at high temperatures the charge transfer occurs through temperature activation of the electrons. They have to hop from an uncharged cluster to another uncharged cluster, forming so a charged cluster pair. At smaller temperatures, this hopping occurs between cluster grains: the electron is delocalized on the whole grain, and the charge transfer occurs between such cluster groups, as opposed to individual clusters. That is also one possible cause of the deviation from the Arrhenius behavior (see chapters 5.2.2.1, 5.2.2.3 and 5.2.3.2).

5 Results and discussion of the electrical properties of molecularly cross-linked Au_{55}-systems

The clusters can be linked with and separated from each other using different organic ligands. Three kinds of interactions are possible: van der Waals bonds, ionic bonds, and covalent bonds. If the connection between the ligand stabilized metal particles is of Van der Waals or ionic type the system is called physically linked system. If covalent bonds are present, the system is called chemically cross-linked system.

The physically linked systems are conventional "ligand stabilized particles". They are usually soluble in organic or inorganic solvents, which destroy the link between the particles, and after that the clusters are recrystalisable in quadratic and hexagonal microcrystals.

The chemically linked systems are usually more rigid than the physically linked ones, usually not soluble at all, since "space polymers" are inside. They cannot be chemically manipulated and build mainly microcrystals with a hexagonal network.

The synthesis of the physically linked systems is summarized in chapter 2.4.5.5.

5.1 Sample preparation

The possible synthesis techniques for covalently and physically cross-linked systems are discussed in chapter 2.3.4. The experimental descriptions of the synthesis of Au_{55} systems is introduced in chapter 8.5 and 8.6. In the following chapters, the problems, and the discussion of the synthesis methods will be presented.

5.1.1 Preparation of layers

Quasi-one-dimensional structures of physically cross-linked systems were prepared by using a very diluted aqueous cluster solution of 15 nm gold colloids. This solution was dropped onto a quartz platelet, and the solvent was let to evaporate (for details see chapter 8.6.1.1). With this technique so-called "dropping circles" are gained (Fig. 5.9). These structures were contacted with conducting silver spots at different distances (50 and 75 µm).

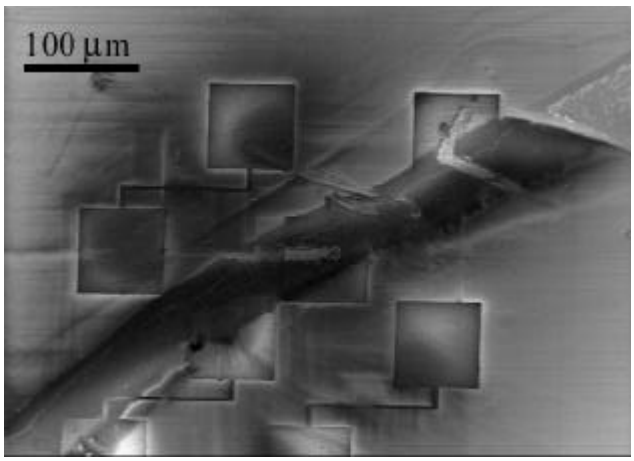

Fig. 5.9: SEM image of a thick dropping circle on an EBL fabricated sample.

The detailed preparation of mono- and multilayers of Au_{55} is reported in chapter 8.6.

Quasi-two-dimensional structures of physically cross-linked systems can be obtained with the same method, but with the use of much concentrated solution. Disadvantage of this method, that the thickness of the sample is not homogeneous. To get flat surface spin coating technique has to be used (see Fig. 5.24).

Physically and chemically cross-linked monolayers can be obtained with the use of the LB technique (see chapter 2.4.5.3). In this work for the preparation of $Au_{55}(PPh_3)_{12}Cl_6$ monolayers a dichloromethane solution of normal Au_{55} was dropped onto aqueous PVP solution containing already a substrate dipped inside. After evaporation of dichloromethane, the layer was transferred to the substrate, (cover-glass (8x8 mm), or any other sample), with pulling it out from the liquid. With this technique islands of closed Au_{55} monolayers could be obtained (Fig. 5.10).

The use of the same method in the case of a carbon coated TEM grid resulted in large areas of ordered cluster structures (up to 1 µm) (see chapter 2.4.5.3) [139]. It might be also the case if another substrate is used, if it is assumed, that the substrate doesn't influence too much the structure of the layer. This assumption is not very strict, since the arrangement of the cluster layer is directly influenced by the PVP layer and just indirectly by the substrate. The truth of this assumption cannot be proved with the available methods, since it cannot be decided nor with the use of nor AFM or SEM (too small resolution), or with TEM (the glass substrate is not "transparent" for the electron beam).

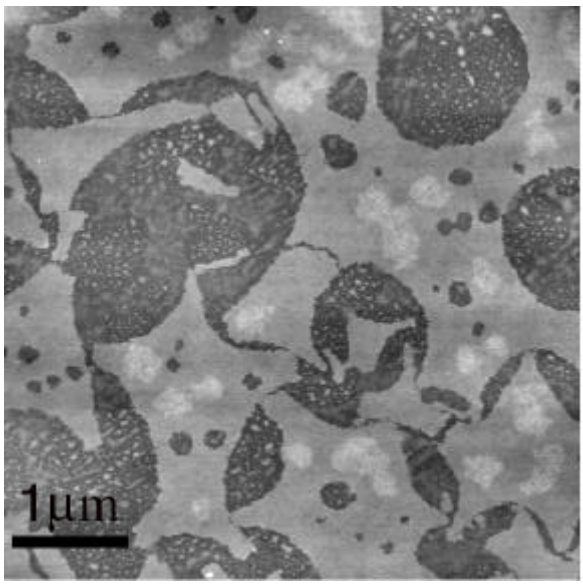

Fig. 5.10: Monolayer of $Au_{55}(PPh_3)_{12}Cl_6$ prepared by a modified LB technique. The height difference between the lighter, and darker regions is about 3 nm, which is equal with a 2 nm high cluster layer, and a 1 nm thick polymer film underneath.

The physically cross-linked layer can be transformed to a two-dimensional covalent cluster-polymer, with spreading the dithiol solution onto the water surface covered by the physically cross-linked Au_{55} layer. The gained arrangement can be transferred onto a substrate with the same method, as before. The AFM and TEM picture of the obtained layer is showed on Fig. 5.11.

a) b)

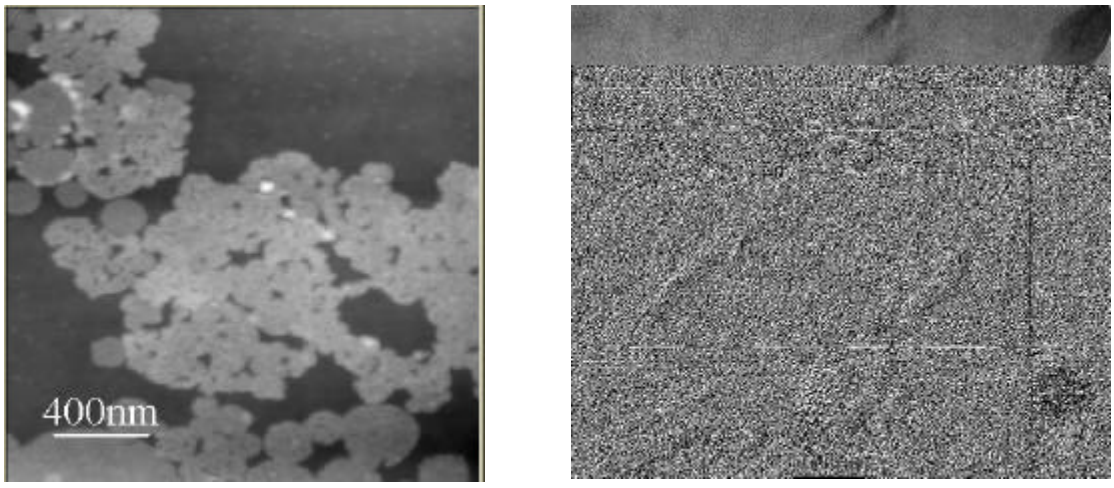

Fig. 5.11: Monolayer of a cross-linked Au_{55} system prepared by a modified LB technique. (a) is an AFM image. The height difference between the lighter and the darker regions is 4 nm, which is more-or less equal with an Au_{55} cluster core (1,4 nm) with a 1 nm thick ligand shell. (b) is a TEM image. The clusters inside the layer can be observed. There is no evident sign of high range ordering.

The monolayers obtained using the LB technique were carried out on a water surface (acid base catalyst) in presence of oxygen. Using this method, monolayers with oxidized thiol groups were fabricated (Fig. 5.12).

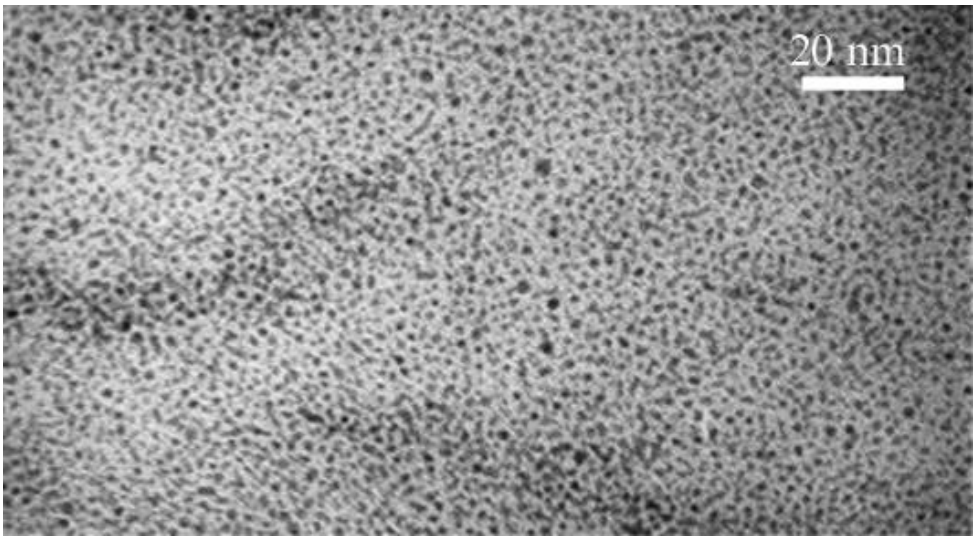

Fig. 5.12: TEM image of a cross-linked monolayer of Au_{55} clusters, prepared by LB technique.

As can be observed from Fig. 5.12, the distances between the particles are relative big, compared to the cluster size. In one TBBT molecule the distance between the two sulfur atoms is approximately 1 nm, an oxidized TBBT molecule has a length of maximum 2 nm. In this picture it can be observed, that the distance of the metal cores is larger than their diameters. This implicates that the TBBT molecules are oxidized during the formation of this rigid film.

Using this method for the preparation, the purification of the sample is wholly impossible, so there is no information about the residual PPh_3 and dithiol in the system.

Monolayer with large closed areas can be also prepared with the silanisation of a substrate. The so prepared layers contain only covalent bonds. The experiment was divided into 4 steps: a glass substrate was first dipped into a HCl solution and then into 3-chloropropyl-dimethylsilan-carbamate under N_2 atmosphere. After washing the sample carefully with pentane to remove the excess of the silane, it was heated for making the silane-oxygen silane bonds irreversible on the surface. The thickness of the silane layer measured by AFM was smaller than 0.5 nm. Thereafter, the sample was successively dipped in an ethanol solution of KSH, washed with ethanol, to remove the excess of the KSH, dipped into a

$Au_{55}(PPh_3)_{12}Cl_6$ dichloromethane solution, and finally washed with CH_2Cl_2. With this method a monolayer was obtained with relative big closed islands of clusters (up to 10 µm). To cross-link the deposited particles, the sample was dipped into a dithiol solution and washed with the solvent selected to solubilize the linker used (the solvents list is presented in Tab. 8.2). The obtained layer is shown on Fig. 5.13.

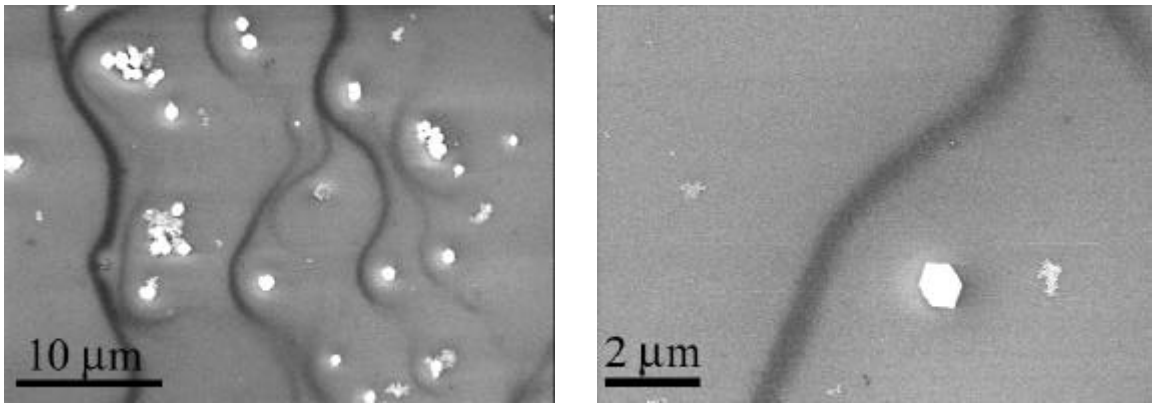

Fig. 5.13: SEM images of a monolayer of a cross-linked Au_{55} system prepared by silanization. The right picture is a zoom on a part of the left one. The darker regions show cluster free areas, the lighter ones the areas covered by monolayer, and the white points show smaller cluster-microcrystals.

In the case of these silanized samples this problem of the purification can take also place, however, the clusters are stronger attached to the surface by a chemical sulfur-gold bonds, so they cannot move so easily. They are also bound to the surface, so the solvation of the excess of the dithiols, and the free PPh_3 is an easier problem. On the other hand, an exchange between the bound clusters-surface and clusters-thiol groups can take place. This could bring a reorganization of the clusters arrangement at the surface or the dissolution of the clusters into the solvent. To minimize these phenomena, the sample was dipped into the ligand solution 15 min.

Another difficulty with the silanized samples is, that with the use of a multifunctional silane (like $(MeO)_3Si$-R, with any organic R) a polymerization can occur during the silanization of the surface. That may cause that the surface becomes more rough, which makes it difficult to cover it homogeneously with the small Au_{55} clusters. That is why the multilayer was synthesized by the use of TMSPCl and for the monolayer-preparation KDMSPCl was used.

5.1.2 Three-dimensional systems

Three-dimensional Au_{55} systems were prepared by the one-step cross-linking and precipitation method (chapter 2.3.4.1) [53]. The detailed parameters are presented in chapter 8.5.

In this case, the cross-linker groups used were thiol molecules because of their strong affinity to the gold core. Cross- linking can take place following two different ways: a direct connection cluster-ligand-cluster, or a cross-link via a S-S bridge in an oxidative medium, as a cluster-ligand-ligand-cluster connection.

The preparation of an cluster-ligand-cluster connected cluster system was realized under N_2 atmosphere, or without the presence of any acid-base catalyst (hexane as solvent [50][51]) to avoid any oxidation. The ligand solution was dropped into the cluster solution. The reaction was very slow (3-5 weeks). The first step, the exchange of the triphenylphosphine to thiols, is a fast reaction. This reaction is followed by the the building of the bridges between the clusters. For this the two ligand shells have to penetrate through each other. This is a rather time consuming step.

The preparation of the cluster-ligand-ligand-cluster connected systems was realized in the presence of oxygen and an acid-base catalyst (like water, or DMF). The reaction was relative fast; it presented the precipitated space polymer in 1-2 hours after the dropping of the ligand solution into the cluster solution, because of the fast thiol oxidation (Fig. 5.15). It turned out that traces of water in the dichloromethane is enough for acid-base catalyzing the deprotonation of the thiols, so the oxidation reaction.

It is also possible to oxidize the dithiol molecules by adding I_2 during the reaction. However, I_2 becomes part of the ligands of the cluster-polymer formed and the sample is not stable enough to be pressed: it becomes metallic. This shows, that if many thiols are exchanged by I_2, the ligand shell doesn't protect enough the clusters against the aggregation and their manipulation is more difficult.

Working with this technique involves two problems: the purification of the sample is difficult, and the cluster polymer presents chemical non-uniformity. To synthesize and precipitate, the cross-linked systems need just some thiol-Au bonds so some of the thiol groups still free, even after precipitation of the product. On the other hand, mainly in the case of the oxygen atmosphere, since the ligands are accessible, an "overoxidation" can take place.

which means that between two clusters there are not just two, but more ligands. These two effects make the determination of the real coordination number of the gold core rather difficult.

TEM investigations show (Fig. 5.14), that the diameter of the clusters did not change during the reaction. The detailed preparation of the three-dimensional arrangements is discussed in chapter 8.5.

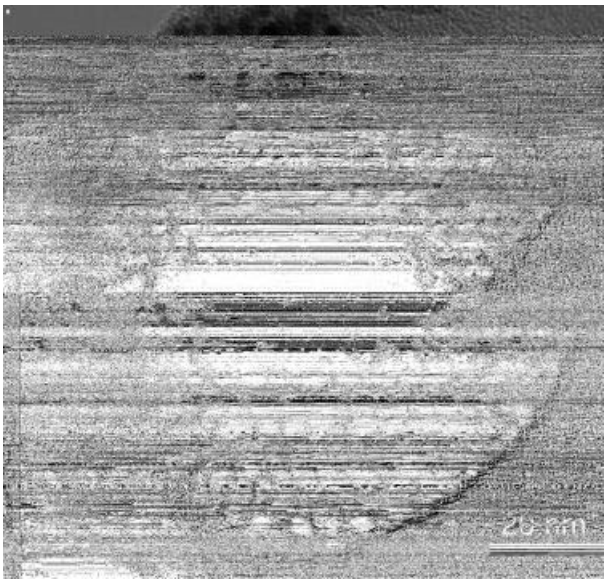

Fig. 5.14: TEM image of $(Au_{55}(purine)_{20})_n$.

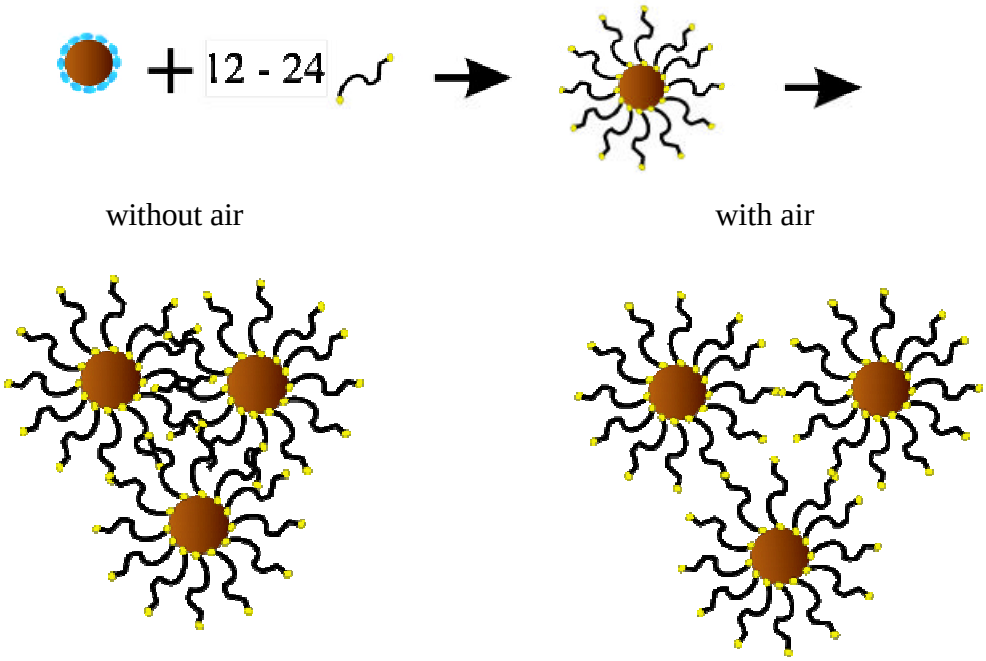

Fig. 5.15: Cross-linkage of the clusters, with terminal dithiols. •: PPh_3, •: -SH, •: cluster core.

5.2 Electrical properties of chemically cross-linked Au_{55} systems

In the following, the electrical properties of physically and chemically cross-linked samples will be compared. For the presentation of the results in a wide grasp, results are also presented, which were not measured in this work. It is tried to give all the citations in its place, but here at the beginning an overview is presented about this:

- The electrical characterization of the Au_{55} monolayers was done during this work. The only experiment mentioned in chapter 5.2.1 which is not a part of this work is presented on Fig. 5.22 in chapter 5.2.1.3, which was published in Ref. [109], and the report of the modification of the LB film in the same chapter, which was discussed in Ref. [87].
- The electrical characterization of the Au_{55} multilayers which was contacted with contacting silver spots was made during this work. The measurements with the use of the EBL fabricated electrode system in chapter 5.2.2 was published in Ref. [140] and [141].
- The conduction properties of the physically cross linked three-dimensional systems was studied by U. Simon, and was published in [114], [129] and [130]. The Au_{55} cluster system, which was cross-linked with oxidized hexanedithiol was also measured by him. Every other measurements was done during this work, with his support.

5.2.1 Two-dimensional systems

5.2.1.1 Conduction properties of $Au_{55}(PPh_3)_{12}Cl_6$ monolayers

Two methods were used to prepare $Au_{55}(PPh_3)_{12}Cl_6$ monolayers (for more details see chapter 8.6).

First, the EBL fabricated samples with contact tips (Fig. 8.3) were used to obtain information about the electrical properties of the $Au_{55}(PPh_3)_{12}Cl_6$ monolayers. However the resistance of the chemically and physically prepared layer was too high to be measured, even using electrodes less than 20 nm in distance (for details see chapter 6).

As a second trial comb structures were used (Fig. 8.5). With this method both chemically and physically prepared samples could be measured. Three different electrode systems were used: it was found that the resistance decreased with the increasing of the electrode area (Fig. 5.16).

Physically prepared layers:

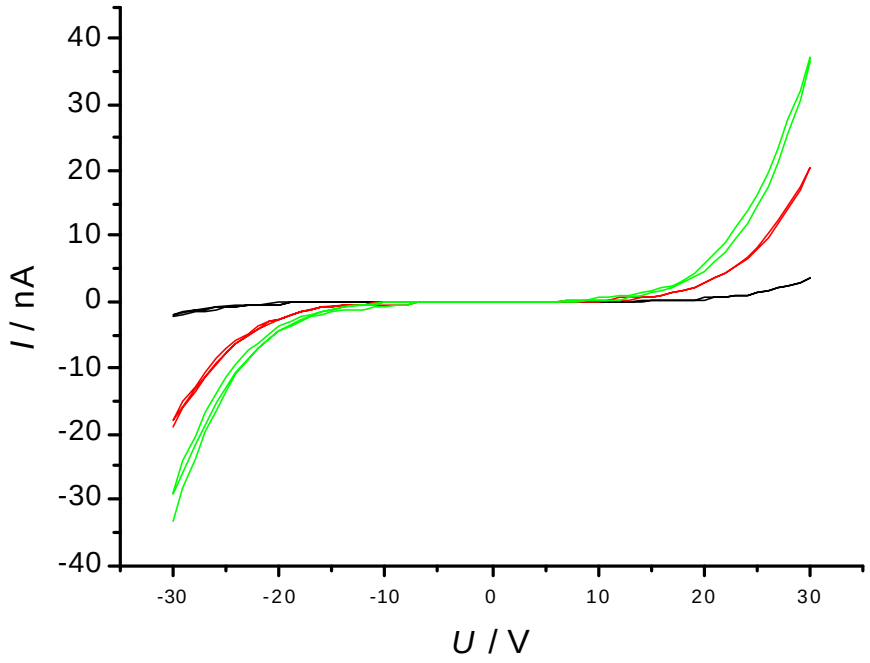

Fig. 5.16: *I-V* curves measured on a sample prepared with LB technique on three different comb structures: : A, : B, : C (The letters refer to those in chapter 8.7.1.2).

In Fig. 5.16 a very high nonconducting gap can be observed. Coulomb-blockade behavior is expected in the *I-V* characteristics of monolayers (see chapter 4.3.3 and 4.5.1), but this gap is too large to be explained by Coulomb-behavior (see chapter 2.2). In the sample, small islands of closed packed clusters are present. At the island-boundaries, the conducting paths have quite high activation energies: these might be an explanation to the lack of the Coulomb-blockade. That means that, in the case of physical layers, the *I-V* characteristics of the sample depends on small architectural differences. These differences can be caused by different island structures (which are not so easily visualizable by SEM, but easily observable in the quantitative analysis of the measured *I-V* characteristics), or some

contamination on the surface (Fig. 5.17). The asymmetrical localization of this contaminates can lead to asymmetrical *I-V* curve.

a) b)

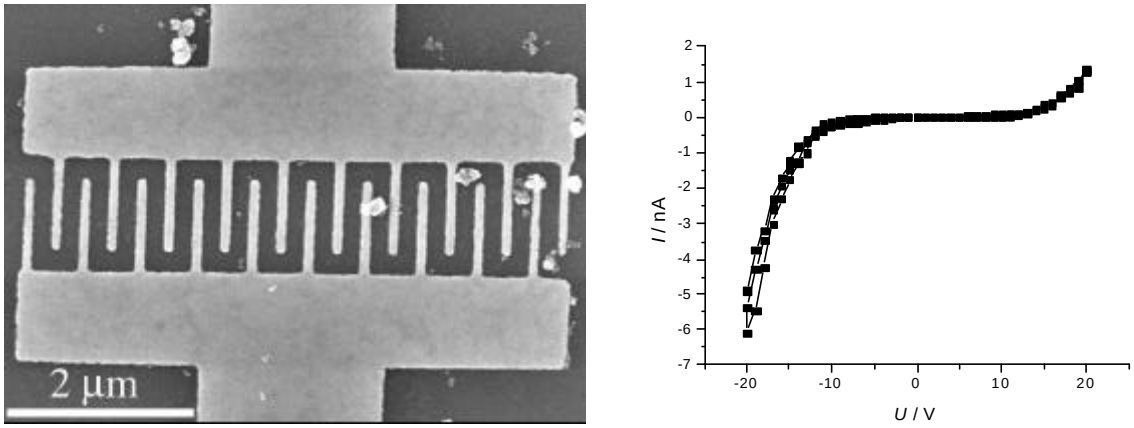

Fig. 5.17: A SEM image of a comb structure with architectural mistakes (a) and the *I-V* curves measured on a sample prepared with LB technique (b).

Chemically prepared layers:

The layers prepared by silanization of the EBL fabricated sample are robust. It is also possible to use this kind of substrate to build up closed-dense packed islands on the micrometer scale (Fig. 5.13) The presence of these big islands were demonstrated also by the *I-V* characteristics, with an evident presence of smaller a gap than the physically prepared layers (Fig. 5.18). The non-linearity of the curve may be caused by the different current paths (see chapter 4.3.2)

a) b)

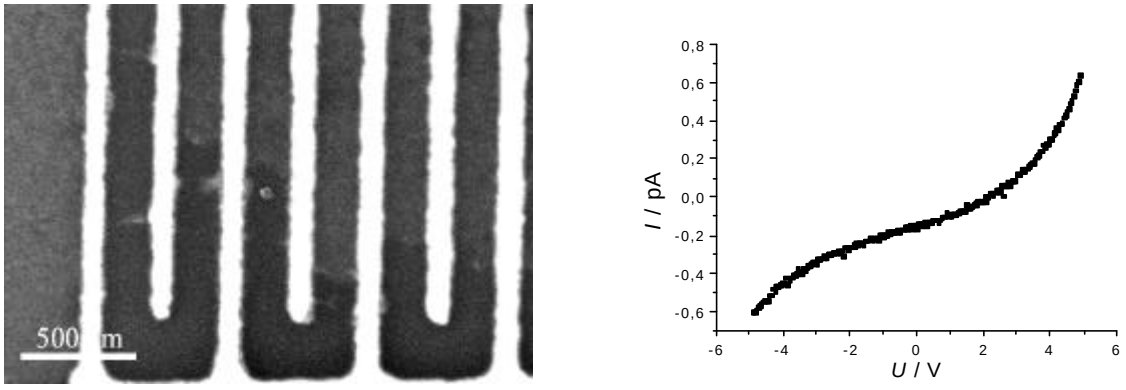

Fig. 5.18: A SEM image of a comb structure with chemically prepared layer (a) and the *I-V* curves measured on this sample (b).

5.2.1.2 Conduction properties of chemically linked Au_{55} monolayers

After the deposition of both types of layers onto a substrate, the samples were dipped into a solution of TBBT. Different behaviors in the *I-V* characteristics were observed

Physically prepared sample:

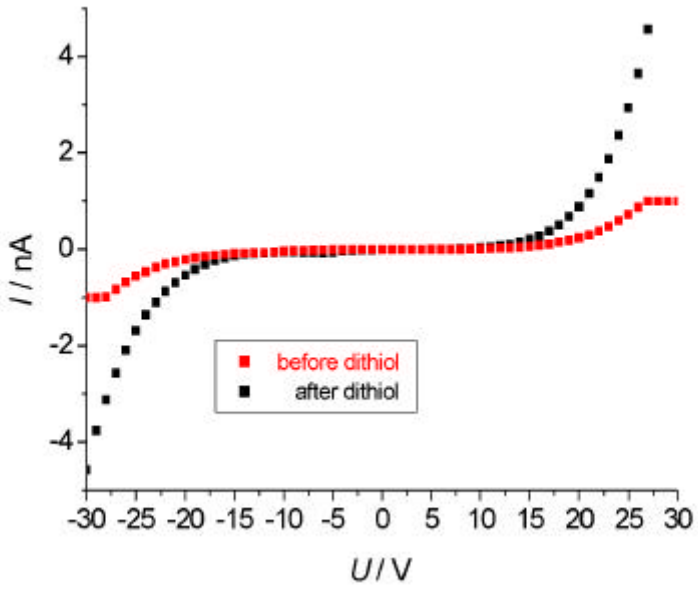

Fig. 5.19: *I-V* curves measured on a sample prepared with LB technique : before and : after dipping it into the dithiol solution.

During this dipping procedure, some Au_{55}-clusters, weakly bonded to the surface, can be dissolved back by the dithiol ligands. On the other hand, if the polymerization of the dithiols is fast enough, it will stay on the surface because of its big molecular weight and form a thin film. Surely both reactions happen statistically, but the resulting *I-V* characteristics show smaller resistance than the non-polymerized cluster system, in spite of the probably smaller number of the clusters on surface (Fig. 5.19).

An alternative to this method was to try to cross link the layer *before* its transfer onto a substrate, using the LB method (see chapter 2.3.4.2 and 8.6.1.2). A dichloromethane cluster solution was spread onto a water surface and after evaporation of the solvent, an ethyl acetate solution of dithiol was added. The choice of this second solvent was governed by 3 parameters: insolubility of Au_{55}, not miscible with water and has a smaller density than the

water. The solvent used was ethyl-acetate (EtAc). After evaporation of the EtAc, the surface was compressed and transferred onto the EBL fabricated sample (see chapter 8.6.1, Fig. 5.11,).

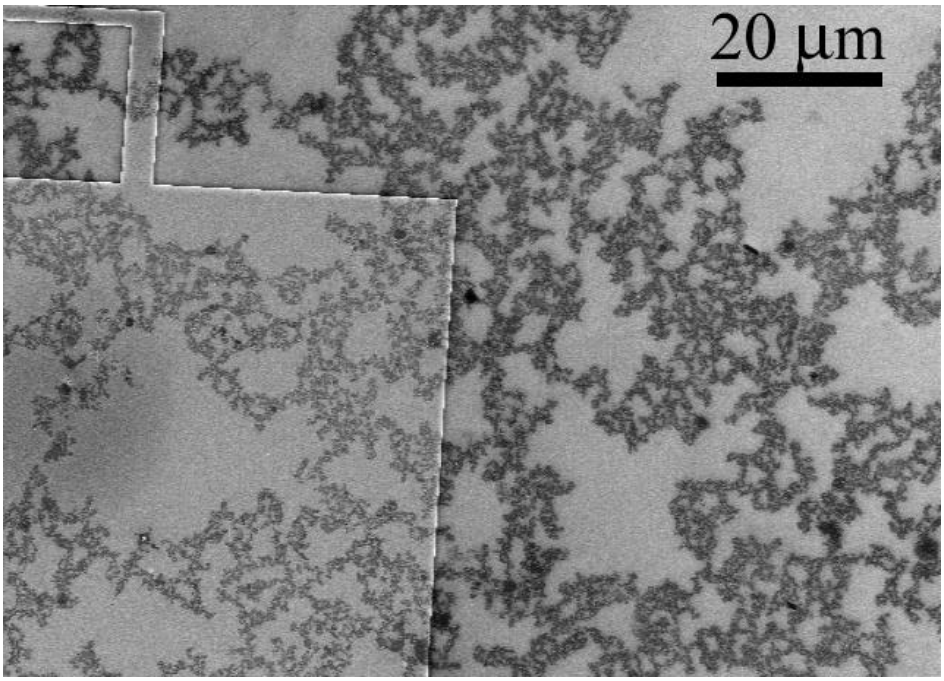

Fig. 5.20: SEM image of a sample prepared with the cross-linker LB technique. The black regions of the sample are the cluster islands. On the left side of the picture a contact pad can be observed.

Because of the shape of the cluster islands (they look like more like a network and not like islands) (Fig. 5.20) the probability to find a good area between the contact tips was quite small, and the resistance of such layer was not measured.

Chemically prepared samples:

The particles in the silanized monolayer are not mobile; they are sticked to the surface by strong chemical bonds (Fig. 5.21). The changing of the resistance in this case is much bigger than by the physical layers. The resistance is one order of magnitude smaller by the cross-linked layer.

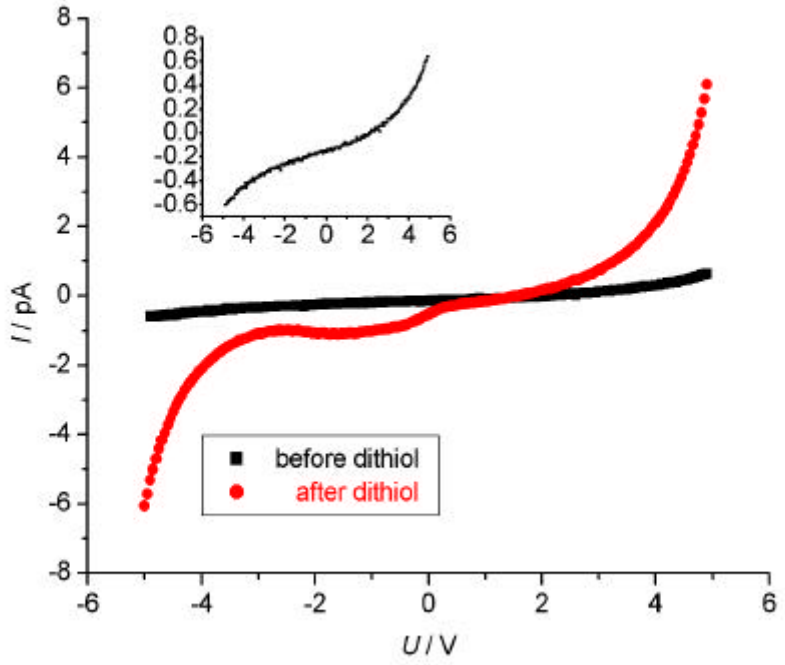

Fig. 5.21: *I-V* curves measured on a sample prepared with silanization : after and : before dipping it into the dithiol solution. On the inserted figure the magnification of the curve measured before dipping into the dithiol solution can be observed.

5.2.1.3 Comparison and discussion

A Coulomb blockade effect was measured by Reifenberger and coworkers in the case of bigger gold clusters [109]. They have shown that there is a direct dependence between the chemical properties of the ligands and the current-voltage characteristics. (Fig. 5.22)

Effectively, a layer with clusters separated from each other by two ligand shells, presents a higher resistance than a layer containing particles covalently cross-linked. Two explanations concerning this phenomenon are possible (Fig. 5.22): the linker molecule with a conjugated Π system supports the electron transfer, or it is induce a smaller distance between the particles in the cross-linked case.

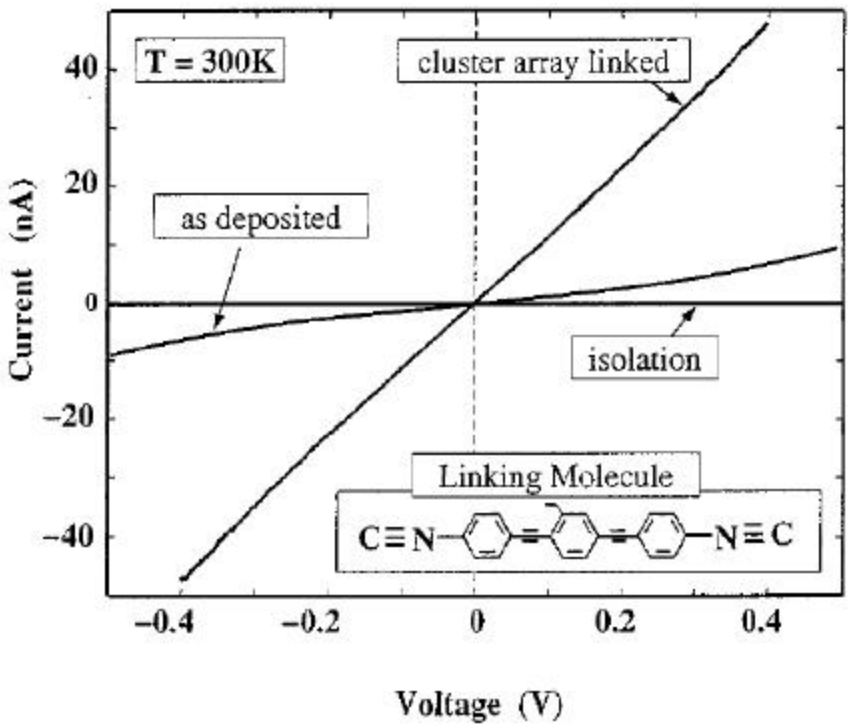

Fig. 5.22: The dependence of the *I-V* curve on the chemical properties of the ligands. Figure is adapted from [152].

The difference between the covalently cross-linked and the van der Waals bonded clusters were also investigated in the case of a LB film, where the particles were cross-linked by dipping a LB monolayer into a dithiol solution [87]. It was found that the resistance becomes smaller, if the gold particles are interconnected with dithiols. Nonetheless, the length of the dithiols used in this work was smaller than the length of the two ligand-shells, so the smaller resistance obtained cannot be attributed only to the presence of the bridge ligand. Because of the experimental procedure, the lower resistance can also be a result of a possible rearrangement, which occurred during the dipping process. In the worst case even multilayer can be formed.

The same phenomenon was observed also in the case of Au_{55} clusters (see chapter 5.2.1.1 and 5.2.1.2), but in this case, the length of the ligands (ox. TBBT is approximately 2 nm) was longer than the ligands of the not cross-linked molecules (two PPh_3 ligands 0.7 nm).

5.2.2 *Quasi*-one and *Quasi*-two-dimensional systems

5.2.2.1 Conduction properties of quasi-*one-dimensional gold colloid systems*

The detailed preparation of such systems made of citrate stabilized gold colloids with a diameter of 15 nm is discussed in chapter 5.1.1 and 8.6.1. The measured *I*-*V* curves exhibit a simple Debye semicircle (Fig. 5.23), which shows that the system contains easy paths for the electron transfer. The non-metallic behavior of the system indicates that the arrangement of the colloids is not ordered, so the conductance has to occur through easy paths.

a) b)

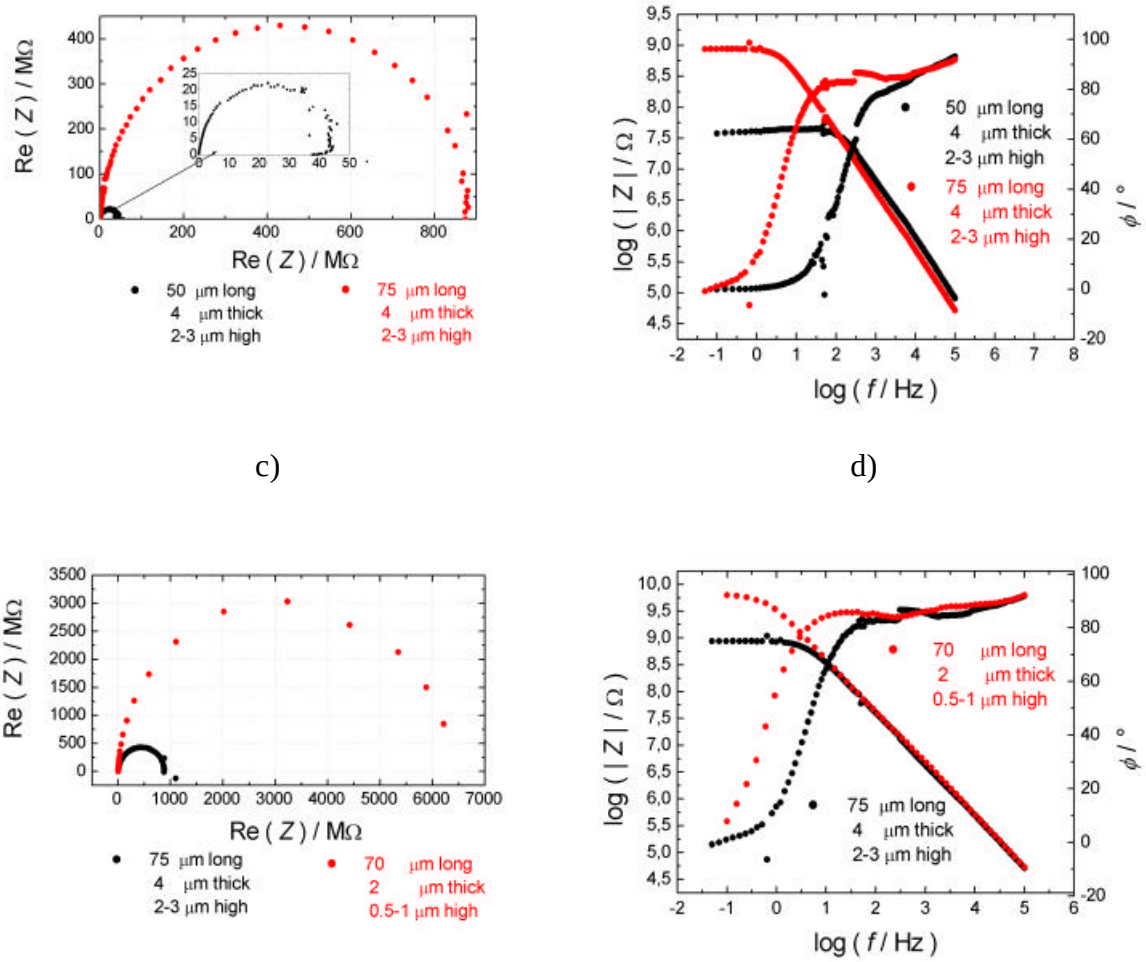

c) d)

Fig. 5.23: The impedance of the *quasi*-one-dimensional systems built up from 15 nm gold colloids.

It is clear to be seen, that the conductance of the wire depends linear on the cross section: a sample with a 8 to 6 times bigger cross section (8-12 and 1-2 ηm^2) has a 7 times bigger resistance (see Fig. 5.23 c and d). The conductance varies exponentionally with the distance between the contacts: the 1.5 times longer wire (50 and 75 ηm) has a more than a magnitude bigger resistance (see Fig. 5.23 a and b).

5.2.2.2 Conduction properties of $Au_{55}(PPh_3)_{12}Cl_6$ multilayers

The samples for these measurements were prepared by spin coating technique (see chapters 2.4.5.4 and 8.6.1, Fig. 5.24). The as-fabricated films are not crystallized and usually not ordered (Fig. 5.24).

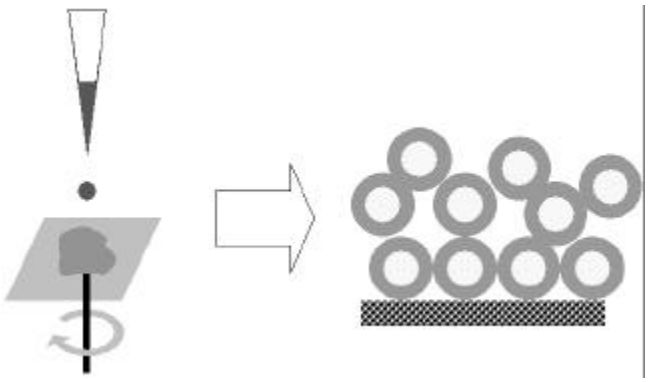

Fig. 5.24: Spin-coating technique. A quartz platelet is spinning with a certain speed and a cluster solution is dropped onto its surface. On the right side of the schematic features of the obtained film can be observed.

Wybourne and coworkers [140][141] measured the *I-V* characteristics of three types of 50 nm thick films prepared by spin-coating technique from $Au_{55}(PPh_3)_{12}Cl_6$ (Fig. 5.25). After measuring the *I-V* curve of the sample, they exposed it to an electron beam having 40 keV energy.

As a third experiment a layer of gold clusters stabilized by octadecanethiol (prepared by ligand exchange reaction from $Au_{55}(PPh_3)_{12}Cl_6$) was spin coated onto a substrate. The *I-V* characteristics of all three samples can be observed in Fig. 5.25 b.

a) b)

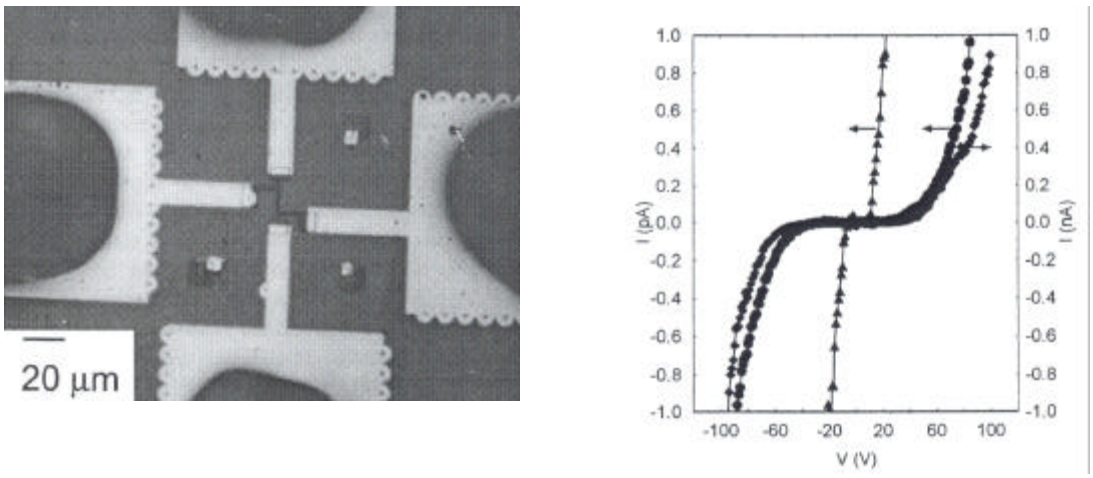

Fig. 5.25: (a) Optical image of nanocontacts 15 µm from each other, fabricated with EBL. Between the electrodes there is a 50 nm thick film prepared with spin coating technique from different types of Au_{55} clusters. (b) I-V curve of this system, using: : $Au_{55}(PPh_3)_{12}Cl_6$ clusters, : octadecanethiol stabilized Au_{55} clusters, : $Au_{55}(PPh_3)_{12}Cl_6$ clusters exposed with 40 keV electron beam. Figure is adapted from [140] (a) and [141] (b).

It is clearly recognizable that the electron beam "activates" the cluster system. The resistance of the irradiated samples is smaller than the non-irradiated ones. On the other hand, the authors experienced a higher stability of the irradiated samples. According to the authors, the increased conductance is the result of a cross-linking mechanism between ligand shells, which lock the cluster cores better to their places.

The authors reported, that on Fig. 5.25 b Coulomb-blockade can be observed in all three cases. In the non-exposed cases, a value of the gap of 60-100V is observable: this one is too high to be a Coulomb blockade (see chapter 4.1 and 5.2.1.1).

Thicker layers of $Au_{55}(PPh_3)_{12}Cl_6$ clusters were investigated during this work. The detailed preparation of them is discussed in chapter 8.6.1 (Fig. 5.24). The *I-V* curve measured at different temperatures show linear behavior from 300K down to 150K (see chapter 4.5.3 and Fig. 5.26).

As it can be observed the Arrhenius curve is almost linear in this temperature region, so the granular model doesn't fit better in this case. The activation energy of the 300 nm thick layer is 0.20 eV, and in the case of the 500 nm thick layer 0.18 eV (see chapter 4.4).

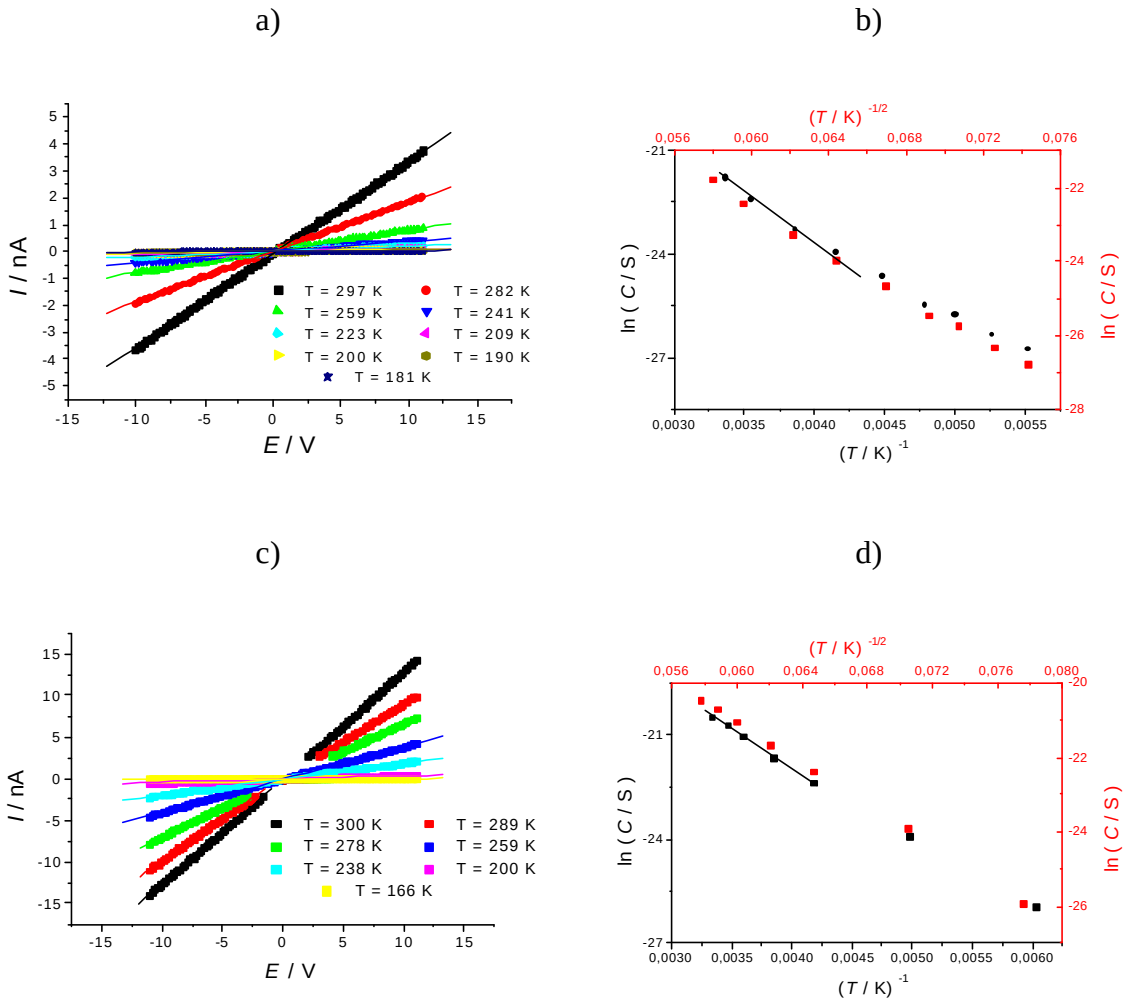

Fig. 5.26: I-V curves measured on 300 (a) and 500 (c) nm thick layers, and the temperature dependence of the conductivity of the 300 (b) and 500 (d) nm thick layer.

The Impedance of the same samples show clear Debye behavior, and the resistance was independent from the applied voltage (Fig. 5.27). This sample seems to follow the classical Ohmic law of the conductance. This fact indicates that the layer contains many easy paths, or, in other words, the clusters are arranged in a highly crystallized order (4.5.2). This assumption is confirmed by SEM images (Fig. 5.28).

Comparing the work of Wybourne [140][141] with the 50 nm thick layer, and the other with the 500 nm thick layer it can be concluded that the 50 nm thick sample gives an *I-V* curve more similar to those of the monolayer (see chapter 5.2.1.1, and compare Fig. 5.16 and Fig. 5.25), whereas the *I-V* characteristic of the thicker layer is similar to the three-

dimensional samples (see chapter 5.2.3.1). For the explanation of this phenomenon see chapter 4.4.

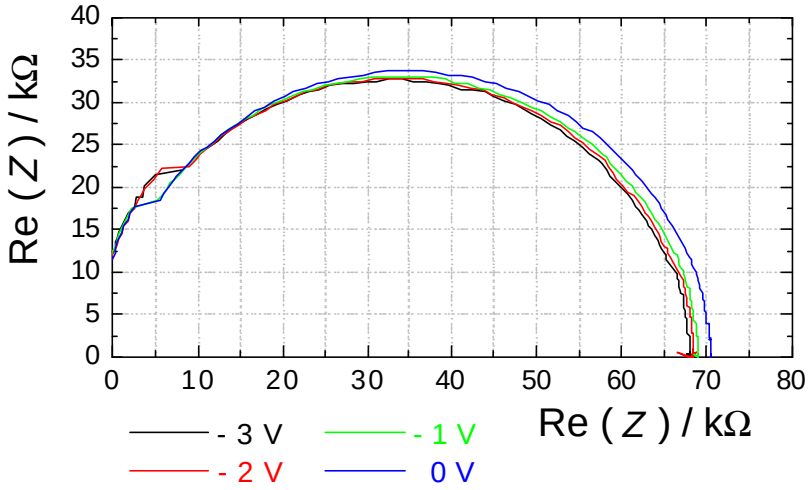

Fig. 5.27: Impedance measured on a 500 nm thick layer of $Au_{55}(PPh_3)_{12}Cl_6$ clusters perpendicular to the surface. The different colors show different voltages.

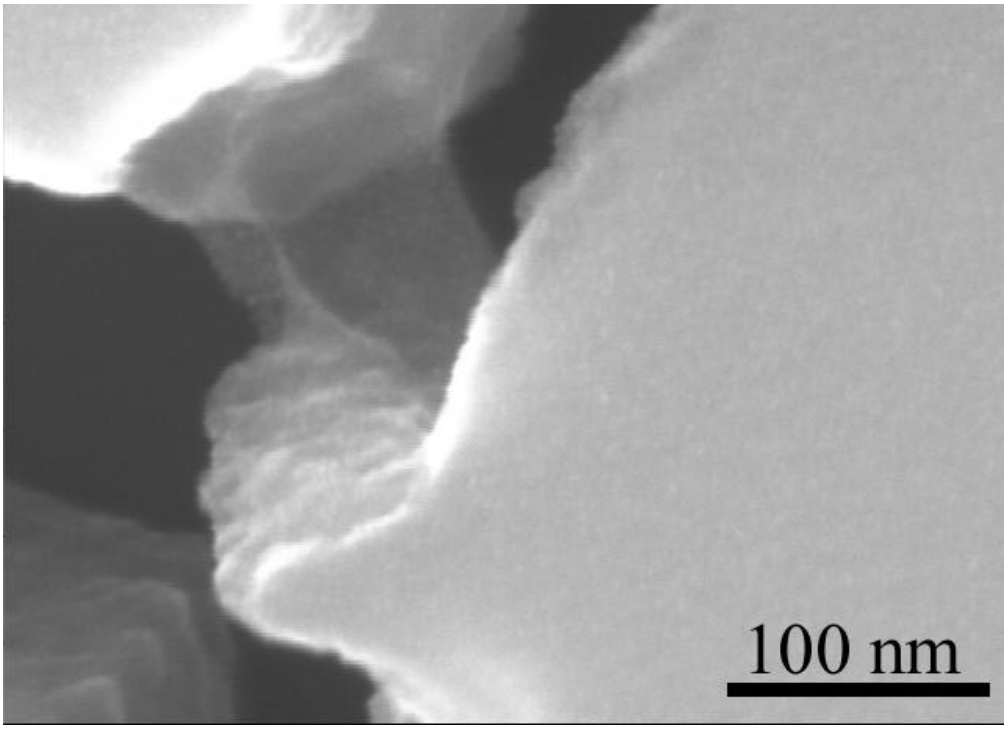

Fig. 5.28: SEM image of a sample prepared by the spin coating technique (see chapter 8.6.1).\

5.2.2.3 *Conduction properties of $Au_{55}(PPh_2C_6H_4SO_3H)_{12}Cl_6$ multilayers*

The detailed preparation of this system is described in chapter 8.6.1 (Fig. 5.24). The water soluble $Au_{55}(PPh_2C_6H_4SO_3H)_{12}Cl_6$ cluster shows different *I-V* curves compared the normal Au_{55}, That indicates different conducting mechanisms (Fig. 5.29).

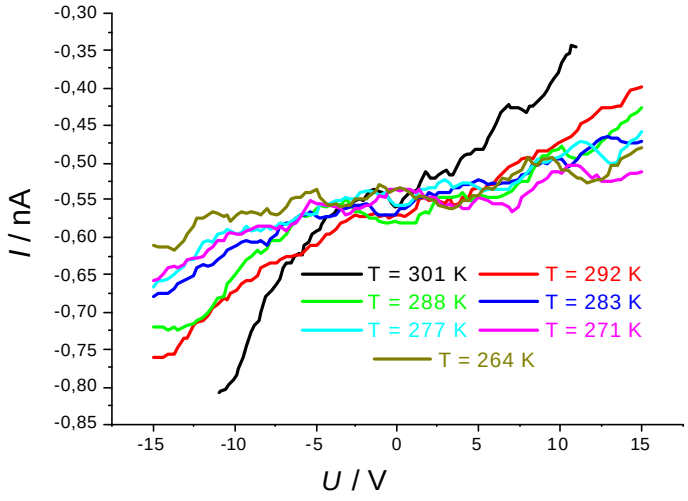

Fig. 5.29: I-V curve of the water soluble $Au_{55}(PPh_2C_6H_4SO_3H)_{12}Cl_6$ cluster on different temperatures. The layer thickness is about 500 nm.

In the case of the ligand $(C_6H_5)_2C_6H_4SO_3Na$, non-linearity effects have been observed. Two explanations can be imagined for this phenomenon. The first is that in the cluster layer mobile Na^+ ions are present. Together with the residual water in the layer this ions can act as charge carriers. The second explanation assumes that the cluster layer is not ordered. This fact can also be a cause of nonlinear *I-V* characteristics (see chapter 4.5.2).

Coherent to the *I-V* measurement, the water soluble cluster systems show a voltage-dependent impedance spectrum.

A decreasing of the impedance with an increasing of the potential U can also be a consequence of the movable Na^+ ions, or a disorder in the cluster arrangement (see chapter 4.5.2). The model function, based on to the“ easy path“ theory has been fitted to the measured curves (see chapter 4.5.2 and Fig. 4.8). The capacitances and the exponent of the CPE have been found to be voltage- independent, hence the resistances depend on the applied voltage. This information is not enough to decide between the two possible effects.

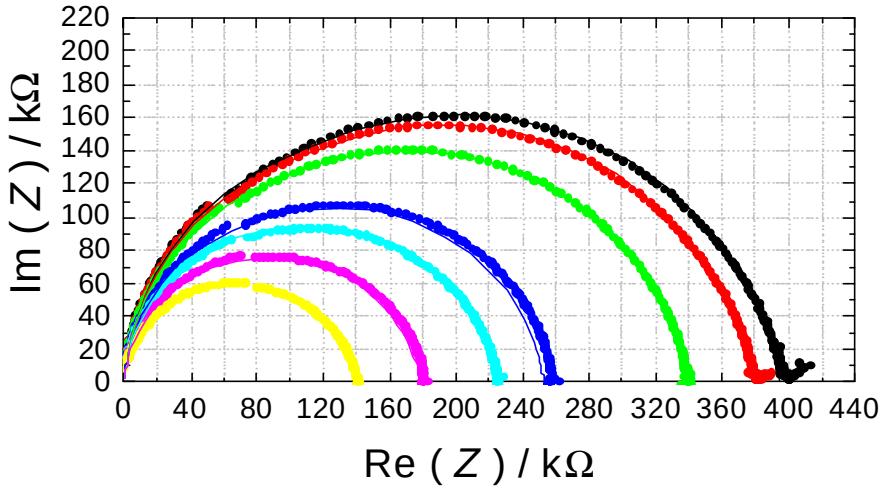

Fig. 5.30: Impedance measured on a 1µm thick layer of $Au_{55}(PPh_2C_6H_4SO_3H)_{12}Cl_6$ clusters perpendicular to the surface. The different colors show different voltages: • 0.0 V,• 0.1 V, • 0.2 V, • 0.4 V, • 0.5 V, • 0.7 V, •1,0 V. The fitted curves (solid lines, almost invisible) cover perfectly the measured datasets.

5.2.2.4 Conduction properties of chemically cross-linked Au_{55} multilayers

The detailed preparation of these films is described in chapter 5.1.1, 5.2.2.2 and 8.6.2. The *I-V* characteristics of these layers show linear behavior between 300 and 90 K (Fig. 5.31).

a) b)

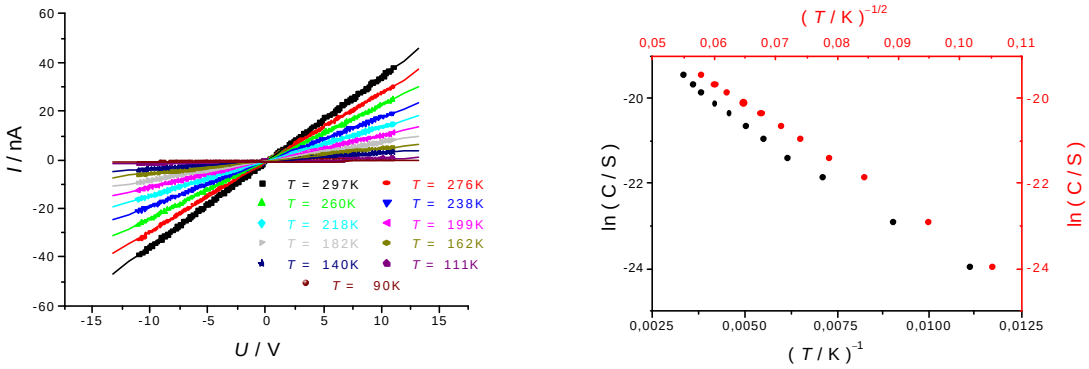

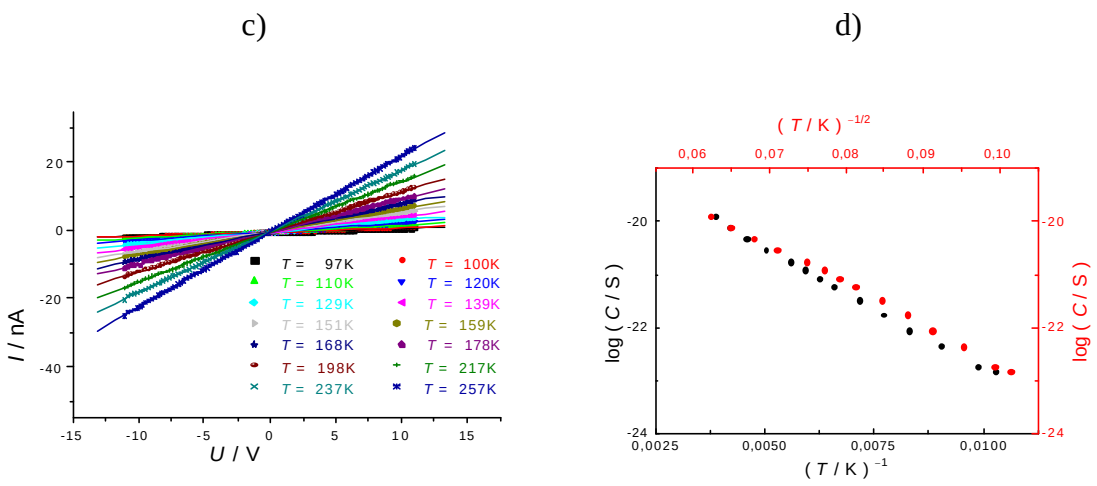

Fig. 5.31: *I-V* curves measured on 5 times (a) and 6 times (c) repeated circle (see chapter 8.6.2), and the temperature dependence of the conductivity of the 5 thiol-cluster layer (b) and 6 thiol-cluster layer (d) nm thick layer.

The resistivity of the chemically prepared layers was smaller than in the case of physical multilayers. The chemical layers , measured in this work, were maximum 50-60 nm thick. It can also be observed that the Arrhenius curve is almost linear, at least in the case of the thicker film. With the thinner film a higher nonlinearity is observed. That means that by means of activation energy calculations, only the higher temperature points have to be taken into account (see chapter 4.5.3). Here and in the further chapters just the conductivity data, belonging to temperatures >200K will be used for the determination of the activation energy. The activation energies of the two samples are: E_{A5}(layers) = 0.043 eV, E_A(6 layers) = 0.039 eV.

The measured impedance spectra show a simple Debye behavior (Fig. 5.32).

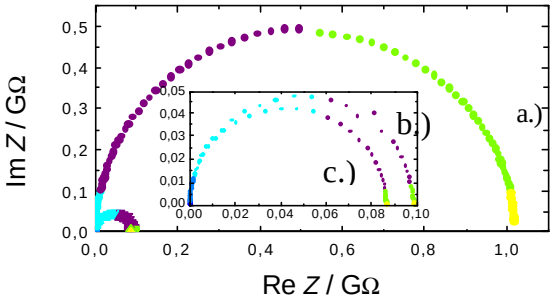

Fig. 5.32: Impedance measured on 4 times,(a) 5 times (b) and 6 times (c) repeated circle (see chapter 8.6.2). The different colours symbolise different frequencies. Yellow: 0.1–1 Hz, green: 1-10 Hz, purple: 10-100 Hz, cyan: 100-1000 Hz, blue: 1000-10000 Hz.

The simple Debye behavior implicates that inside the samples easy paths to follow the classical Ohmic behavior are accessible. That means that inside the layer the clusters are organized in a highly crystalline order (see chapter 4.5.2).

5.2.2.5 Comparison and discussion

Three different electrical behaviors were found. In the first (chapter 5.2.2.2) (physical layer) and the third case (chapter 5.2.2.4) (chemical layer), the layers showed clear Ohmic behavior, which was explained by a highly crystalline arrangement of the clusters. In the second case the electric behavior turned out to be different, which may be caused by the ionic conductance, or the disorder in the film (see chapter 5.2.2.3). The dependence of the shape of the curve on the range of crystallization is the main similarity between the chemically and physically prepared layers. Another similar effect is the dependence of the activation energy on the layer thickness.

The main difference between them is their resistance, and the value of the activation energy. The covalently cross-linked systems have five times smaller activation energy, than the physically prepared layers.

5.2.3 Three-dimensional systems

The Au_{55} was the only nanoparticle, in which case the three-dimensional conductance was measured and investigated. This is because the resistance of these systems is relative high. The advantage of the three-dimensional measurements is, that they don't hold other possible structural defects as the measuring on two-dimensional arrangements, but they are more robust. That means that they are not so sensitive for small changes in the synthesis parameters and the stochastic effects, than the two-dimensional arrangements. Also, the number of the conducting paths is larger, so architecture problems don't play as a big role as in the case of the monolayers.

5.2.3.1 Conduction properties of physically cross-linked systems

One of the most important questions in this field was to investigate, how the activation energy of the electron transfer depends on the chemistry and the size of the ligand shell. This work was done mainly by U. Simon et. al. [114][129][130][144]. They measured the temperature-dependence of the conductivity in compressed pellets of clusters, stabilized by 9 different ligands: PPh_3, $PPh_2C_6H_4SO_3H$, $P(C_6H_4CH_3)_3$, $P(C_6H_4OCH_3)_3$ [129], T_8-OSS [121], BOS [122] (Fig. 2.13), and the $Au_{55}(PPh_2C_6H_4SO_3H)_{12}Cl_6$ cluster, linked with different spacers, like DDE, BATA and POB [114], [143] (Fig. 2.19). The temperature-dependence of the conductivity of these 9 ligands indicates mainly three different rules: the very first results [129] showed a charge-transfer kinetics depending mainly on the small disorders in the material. The second measurements with different spacers denoted to a correlation between the distance of the cluster cores and the activation energies [114], [143]. The investigations with the sulfide ligands show, how the strength of the organic backbone effects the conduction mechanism [143].

In Ref. [129] results are summarized on the mentioned ligands. The authors pressed the powder of the cluster sample into small pellets, and compared their density to the theoretically calculated one. They measured also impedance to obtain information about the kinetics of the reaction. The results show that two elementary reactions exist. They calculated the activation energy for both reactions in the case of all three particles. The results show that the disorder rate of the pellet influences the activation energy. In Ref. [130] the authors explain the measured phenomenon. According to this theory in the sample, closest packed islands are separated with slightly disordered regions (see chapter 4.5.2).

Measuring the temperature-dependence of the charge transfer of the $Au_{55}(PPh_2C_6H_4SO_3H)_{12}Cl_6$ cluster, linked with different spacers, it was observed that the activation energy doesn't depend on the chemical properties of the spacer, just on the distance between the metal cores [114].

As a next step the $PPh_2C_6H_4SO_3H$ ligands were exchanged to T_8-OSS and BOS (see Fig. 2.13). With this change the coordinative bonds on the surface of the cluster core were exchanged from a Au-P bonds to Au-S interaction. This means a difference in the electron

configuration of the formed complex. In spite of this, the charge transfer behavior of the cluster system didn't show deviation from the rule explained before [143] (Fig. 5.33).

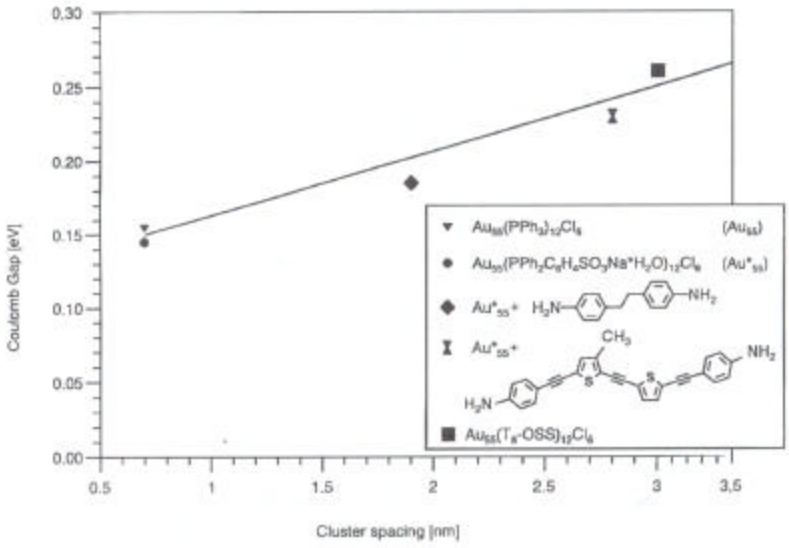

Fig. 5.33: The dependence of the activation energy of the conduction from the distance of the particles. The figure is adapted from [143].

The extrapolation of the activation energy for a 0 nm distance (Fig. 5.33)) gives a value of 0.137 eV for the charge transfer. This energy is needed for the classical charging of a sphere shaped capacitor, with the geometrical parameters of our cluster system. The charging energy of a capacitor depends linear on the distance between the two metallic parts. Speaking chemically, the activation energy for the disproportion reaction of a cluster pair depends directly on their distance. The reaction is thermally activated. The mechanism of the charge transfer is based on this reaction and can be explained by the variable range hopping models (see chapter 4.5.3).

5.2.3.2 Electron energy levels of the used ligands

As it is explained in chapter 5.1 and 8.5, dithiols were used to cross-link the particles. 4 different ligands were used here both in the non-oxidized and in the oxidized form: TBBT, Purine, 1,5NDSH, 1.6NDSH (Tab. 8.2). Oxidized forms mean dimerization of the thiol to a disulfide. The detailed synthesis is described in chapter 8.5.

Except for the TBBT, all the ligands used (Tab. 8.2) were rigid and aromatic systems. This implies a total electron delocalization, even in the S atoms of the thiol groups, which participate with their nonbonding electron pairs in the delocalization. To prove this, chemical calculations were made for all ligands used, in order to get an impression from the value of the HOMO-LUMO gap and to see the degree of the delocalization.

	1.5 NDSH	OX 1,5 NDSH
Structure	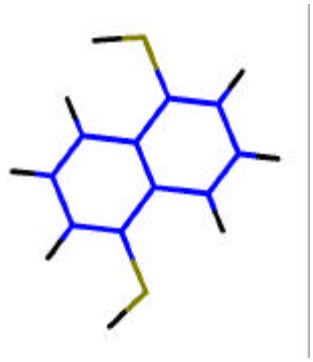	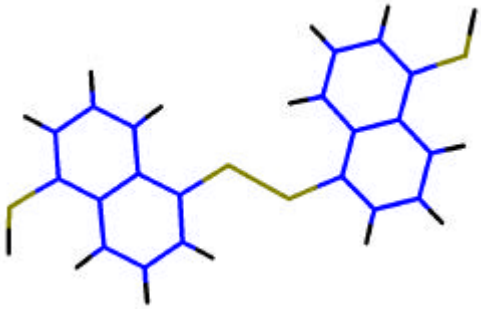
HOMO	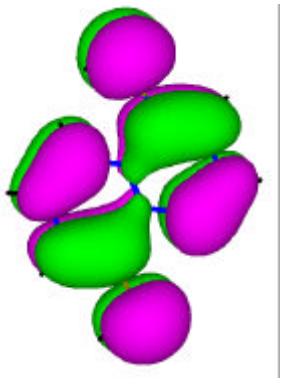	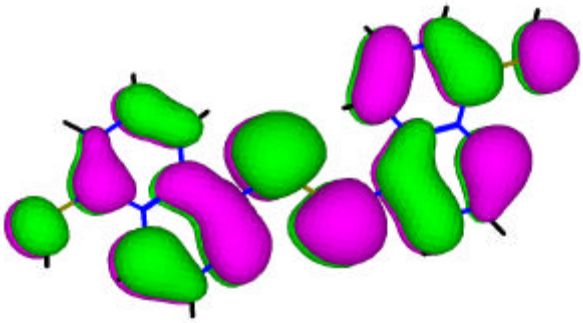
LUMO	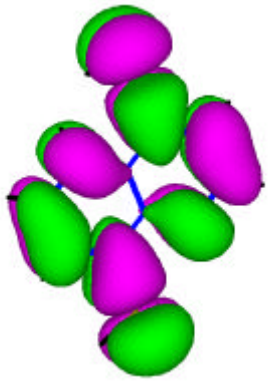	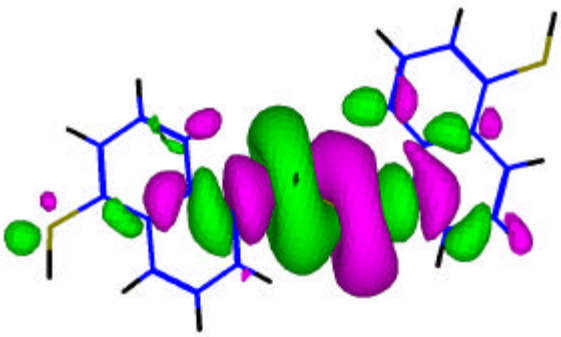

Tab. 5.1: Structure, HOMO and LUMO orbitals of the !,5 NDSH and the ox. 1,5 NDSH. The different colors show the different phases of the electron wave-function

The geometry was optimized by molecular-dynamical calculations; the shape of the wave functions and their energy was calculated with the semi-empirical Extended Hückel method. For the calculations the program Hyperchem 6 was used.

As it can be observed in Tab. 5.1 all electrons of the sulfur atoms participate in the delocalization of the electrons. The same effect can be observed in the case of the 2,6 NDSH, Purine, and all the oxidized forms.

In the case of TBBT, two benzene rings are separated by a S atom, but the electron configuration calculations proved that even in this case the energy levels of the molecule show the delocalization of the nonbonding pairs of the sulfur atom: by this molecule the geometry was optimized by Hartree-Fock calculation. The geometry of the wave-function was also calculated with the Extended Hückel method (Fig. 5.34):

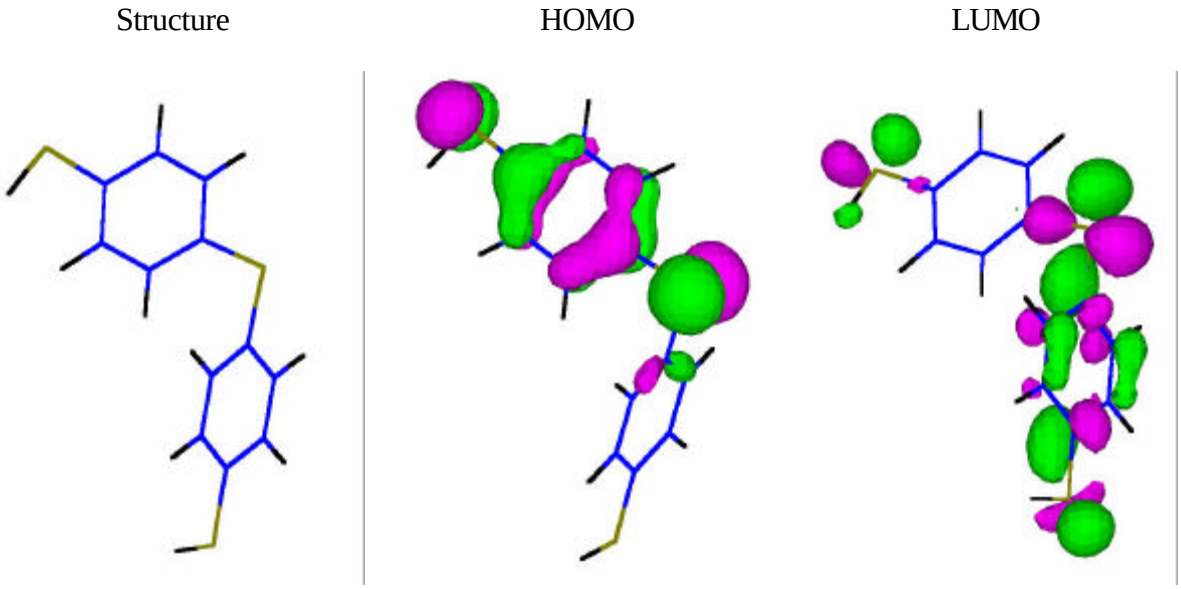

Fig. 5.34: Structure, HOMO and LUMO orbitals of the TBBT. The different colors show the different phases of the electron wave-function

The optimal values of the geometrical parameters of the TBBT are: middle C-S-C angle: 99º, torsion angle between the two phenyl rings (C-S-C-C torsion angle): 87º. The screening around this values shows that at room temperature almost no change in the C-S-C bond is available, but the torsion angle can change by 1-2º. If the distance of two terminal sulfur atoms is investigated then, according to the calculations, the molecule can be claimed as rigid.

That means that the cluster polymer may preferably form ordered arrangements (Fig. 5.35), because the molecules keep a constant distance between the clusters. On the other hand, in an aromatic molecule the electron energy levels are quite close to each other. That means, that the HOMO-LUMO gap is small. This effect may support the charge transfer between the clusters.

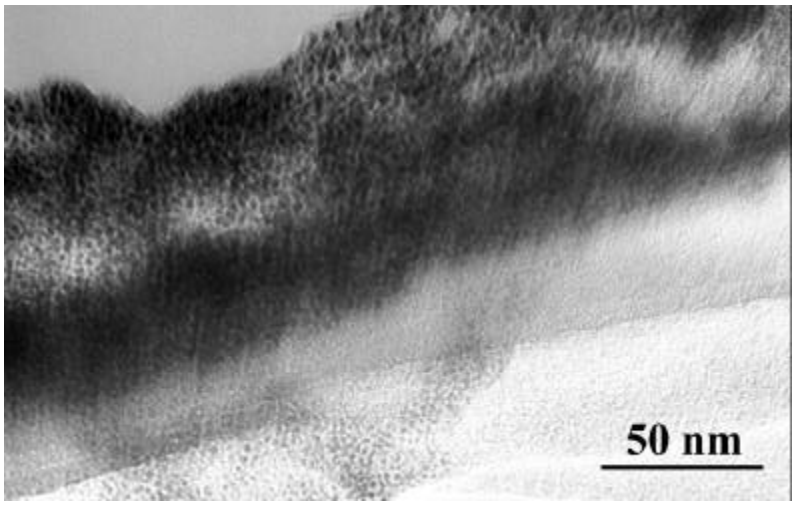

Fig. 5.35: The structure of TBBT polymerized Au_{55} cluster system.

The HOMO-LUMO gap of all the molecules, calculated with the Extended Hückel method, remains <2,5 eV (Tab. 5.2) which also induces the delocalization of the electrons.

	TBBT	PURINE	1,5 NDSH	2,6 NDSH
normal	2.2 eV	2.3 eV	2.5 eV	2.45 eV
oxidized	1.7 eV	1.9 eV	1.6 eV	1.6 eV

Tab. 5.2: the values of the HOMO and LUMO gap calculated with Extended Hückel model.

5.2.3.3 Conduction properties of chemically cross-linked systems

The temperature dependence of the conductance was measured between 300 and 4 K in the case of TBBT, and 310 to 77 K for the other molecules. The measured *I-V* curves are slightly nonlinear at higher temperatures, but become linear for temperatures less than 230 K. The Coulomb behavior remains up to the smallest measured temperature, 4 K, or 77 K indicating the existence of a large number of closest packed conducting paths (see chapter 4.5.2).

The temperature dependence of the conductivity is not linear, but follows the $C \propto 1/T^{1/2}$ rule (see chapter 4.5.3) (Tab. 5.3).

Because the Arrhenius equation is not applicable to the whole temperature range, the activation energy was calculated from the high temperature part of the curves.

In the case of the non-oxidized Purine the curve has a transient behavior. At higher temperatures the activation energy is higher than that of every other cluster systems, under the transient temperature the slope of the curve is in the same region, as those of the curves usually measured for other Au_{55} systems. This behavior can be caused by the higher asymmetric structure of this material, the existence of bigger clusters, or the presence of enclosed free ligand islands (see Tab. 8.2).

	WITHOUT OXIDATION	WITH OXIDATION
TBBT	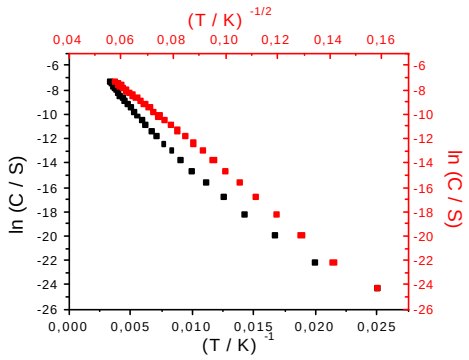	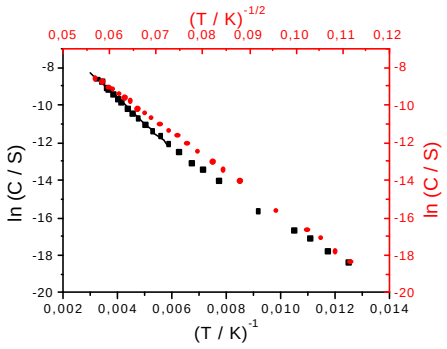
Purine	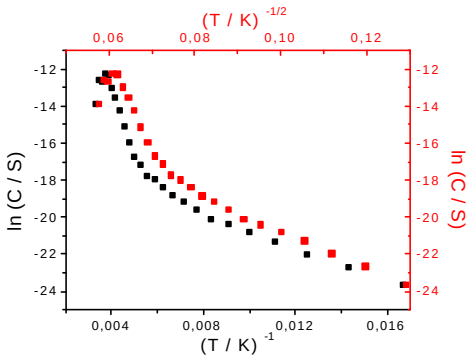	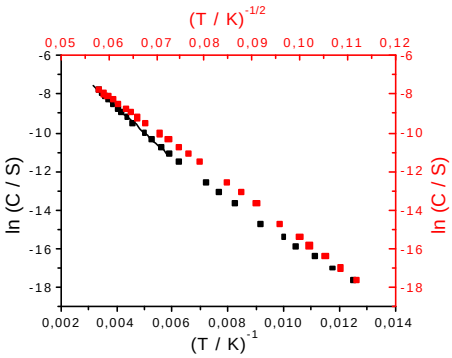

1,5 NDSH	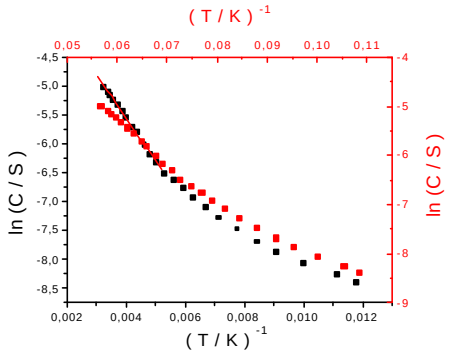	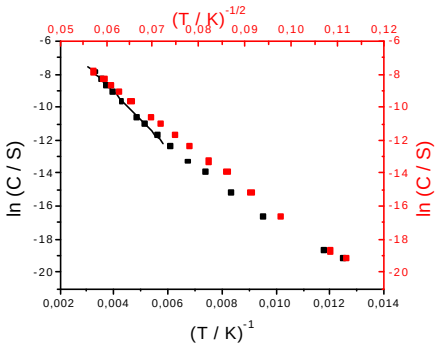
2,6 NDSH	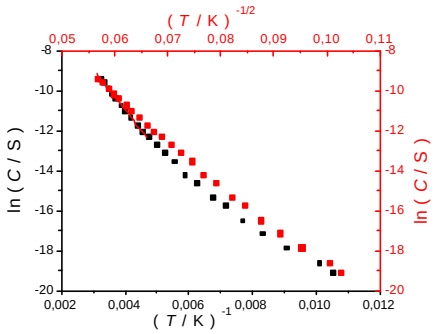	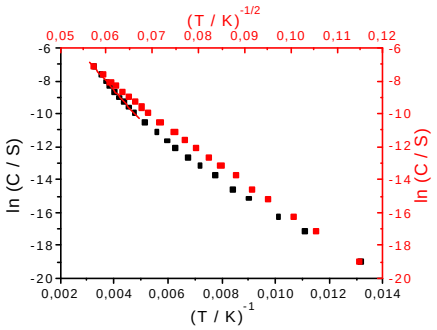

Tab. 5.3: Temperature dependences of the conductance by different ligands.

Impedance spectra were also measured of these systems. Two typical impedance spectra are shown in Fig. 5.36.

a)

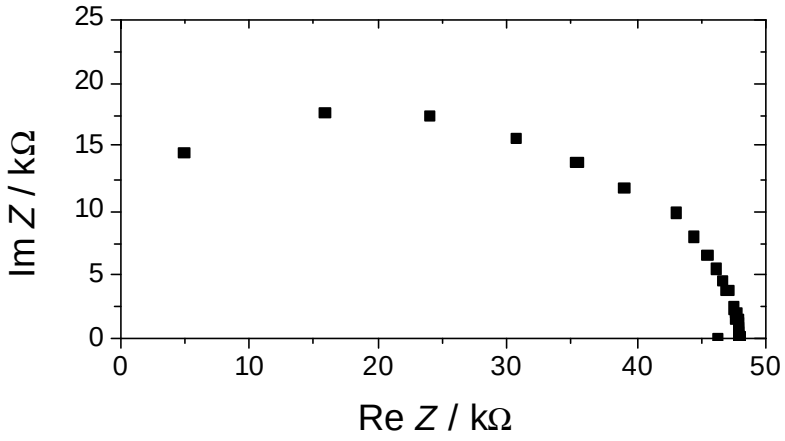

b)

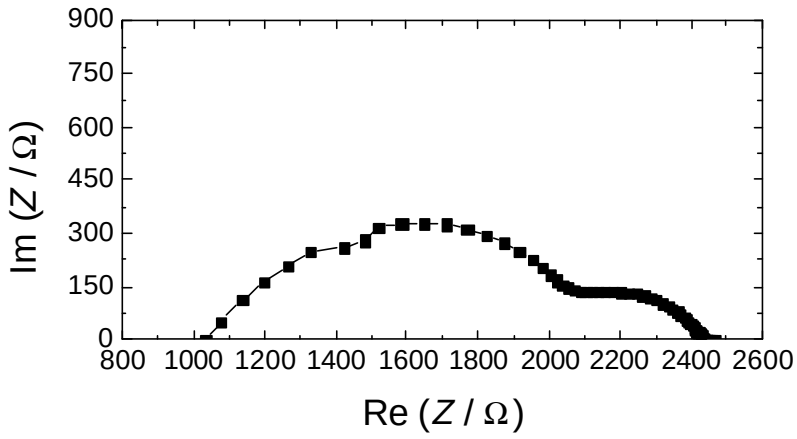

Fig. 5.36: Typical impedances at room temperature of the three-dimensional chemically cross-linked systems. The ligands are (a) Purine, (b) TBBT.

The Au_{55} system polymerized with Purine has the same shape of the impedance, as in the case of the *quasi*-two-dimensional samples (see chapter 4.5.2 and 5.2.2): it is probably the result of a sum of a Debye semicircle and a Cole-Cole process. In the case of the TBBT polymerized samples the shape of the impedance spectrum is quite surprising, because it indicating a quite complicated charge transfer mechanism, despite of the apparently ordered structure observed in the TEM images (Fig. 5.35). One possible explanation of this behavior is, that one of the processes showed by the impedance spectrum belongs to the redox process of the central S atom in the TBBT.

5.2.3.4 *Comparison and discussion*

Spacer	Name	Distance	E_a
Au_{55} 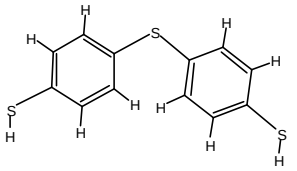 Au_{55}	TBBT	1.0 nm	0.095 eV

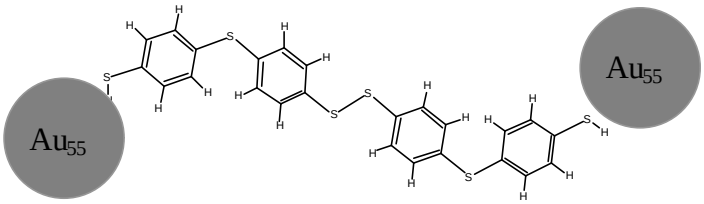	Ox. TBBT	2.0 nm	0.12 eV
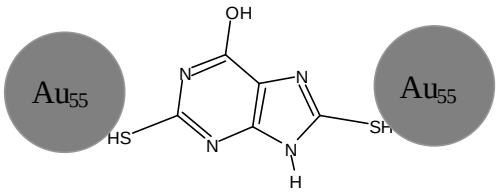	Purine	0.7 nm	0.07 eV (small temperatures)
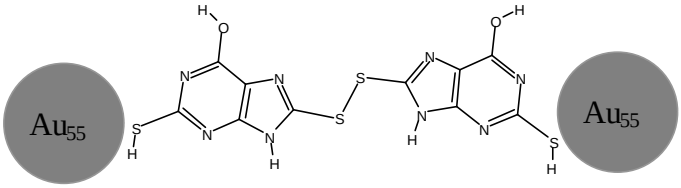	Ox. Purine	1.4 nm	0.11 eV
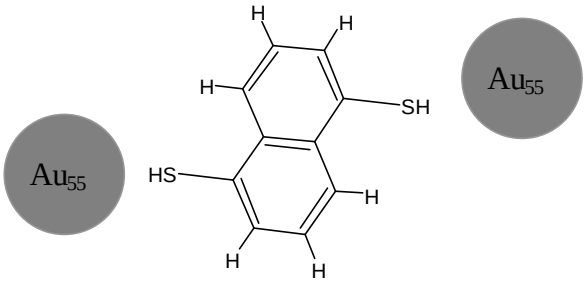	1,5 NDSH	0.75 nm	0.064 eV
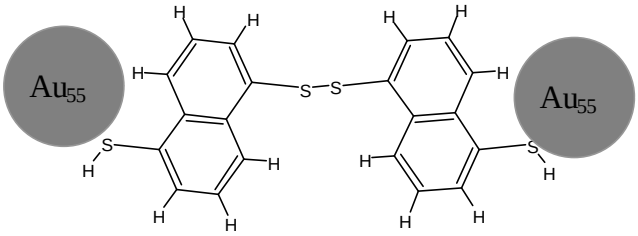	Ox. 1,5 NDSH	1.5 nm	0.15 eV
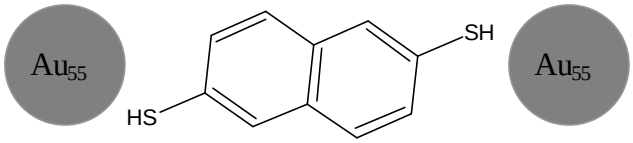	2,6 NDSH	0.8 nm	0.17 eV (possibly wrong synthesis)
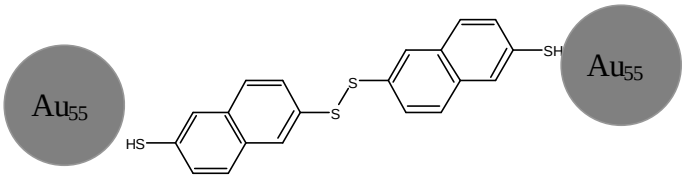	Ox. 2,6 NDSH	1,6 nm	0.14 eV

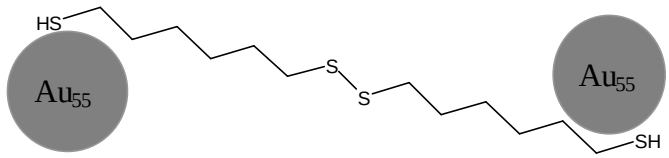	Ox HexDSH*	1.8 nm	0.15 eV
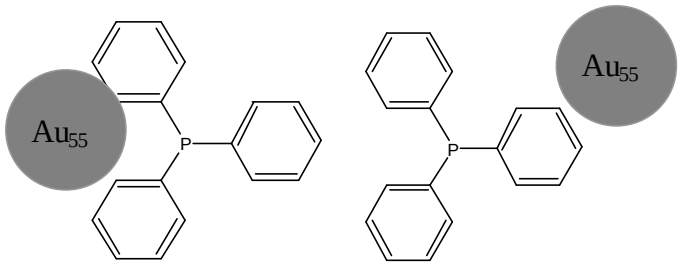	PPh_3*	0.7 nm	0.16 eV
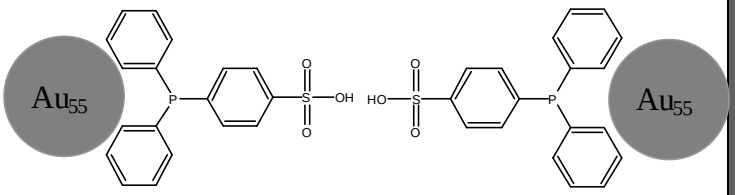	PPh_3-SO_3H*	0.7 nm	0.16 eV
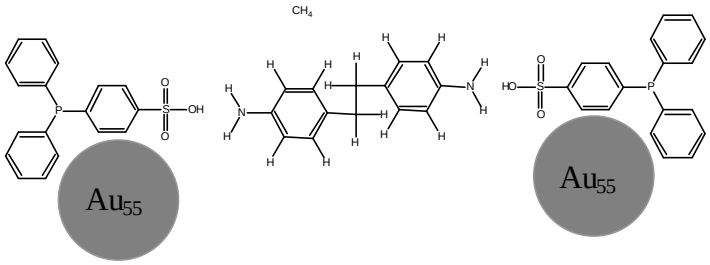	DDE*	1.9 nm	0.17 eV
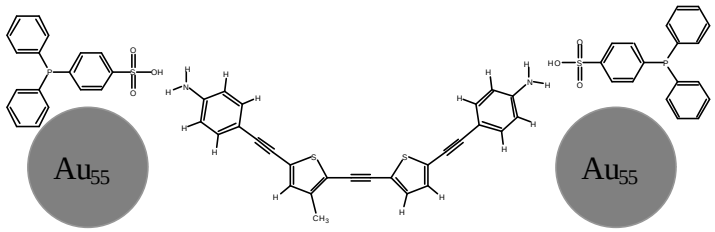	BATA*	2.8 nm	0.23 eV
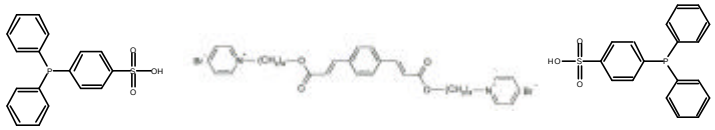	POB*	3.5 nm Eff: 1.4 nm	0.20

* The activation energy of this system, together with the not chemically cross-linked systems was measured by U. Simon [114].

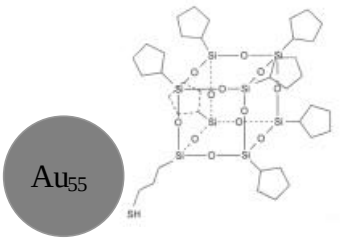	TOS*	3.1 nm	0.26 eV

Tab. 5.4: Conformation and activation energy of different cluster systems and the distance between the clusters. : covalently cross-linked : there is at least one ionic bond between the clusters : there is at least one van der Waals bond between the clusters

In Tab. 5.4 are collected the spacers used for all measured ligands, the distance between the clusters and the activation energy obtained for the systems. The numerical values are graphically depicted in Fig. 5.37. As it can be observed, the activation energies of the charge transfer are definitely smaller in the case of the molecularly bridged systems, than by the not-cross-linked ones.

The effect itself that the activation energy is smaller then it can be expected after the length of the molecule is not surprising since most of the molecule can be folded, so decreasing the distance between the clusters. This is well known, and measured in the case of the POB spacer (Fig. 2.19 c). In this case the inserted $-CH_2-$ chains can be folded. The effective length of the molecule can be calculated from the activation energy of the cluster system prepared with the use of the $Au_{55}(PPh_2C_6H_4SO_3H)_{12}Cl_6$ cluster and the POB spacer [114].

One thing still surprising on Fig. 5.37 is that the activation energy of the cross-linked systems are smaller, than the activation energy extrapolated for 0 nm distance from the model explained in chapter 5.2.3.1. This is important because it is a proof that this effect cannot be explained just by the simple folding of the molecules.

The effect also cannot be explained with the distribution of the electrons between the HOMO and the LUMO, simply because the voltage drop on one cluster is in the range of 10^{-6} V, opposite to the STS investigation, in which case it can be up to 4V (see chapter 4.1).

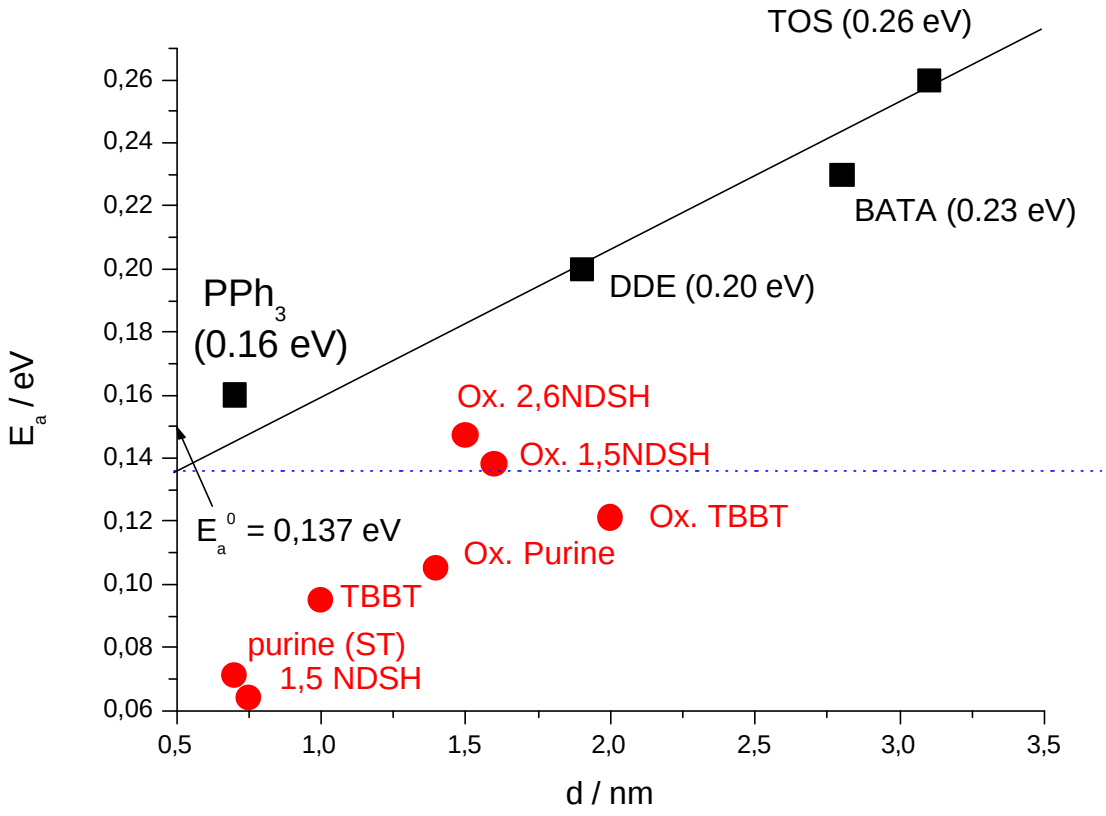

Fig. 5.37: Activation energies vs. the distance between the clusters by different ligands. : physically cross-linked systems : chemically cross-linked systems. ST means small temperatures.

Inner-sphere and outer-sphere electron transfer mechanisms, reported first by Taube [158], [159], are well known in the field of aqueous complex chemistry. The theory proposes that the charge transfer between two, with a ligand bridge connected metal ions, can be up to 10^8 times faster than without this cross-link. The reason for the smaller activation energy is that the electrons can use the electron states of the bridging ligand, and don't need to quit the inter-molecular space. At cross-linked clusters this mechanism implies that the electrons don't have to leave the molecule to tunnel between them, but they can move through a highly conjugated electron system. This effect reduces the activation energy of the charge transfer between two clusters.

a) b)

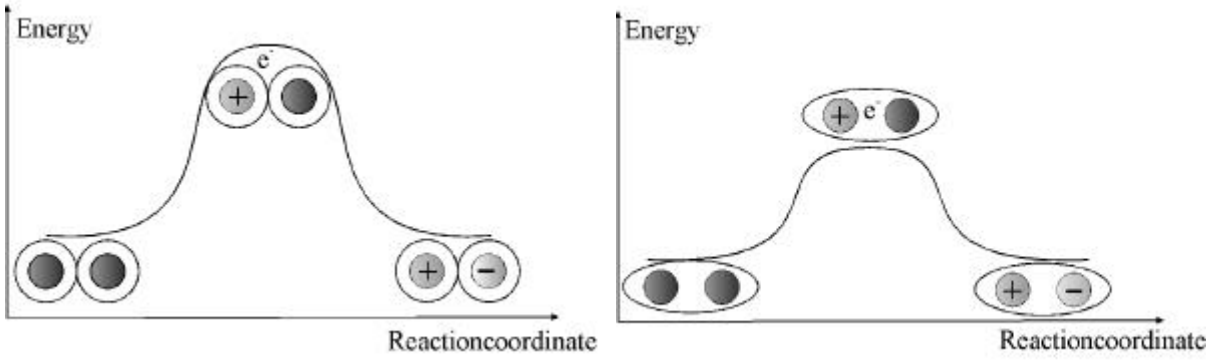

Fig. 5.38: The mechanism of the formation of the charged cluster pair in the case of the physically (a) and chemically (b) linked system. On Fig. (a) the activation complex is two cluster with an electron outside both clusters, on Fig. (b) it is two cluster and the electron is somewhere in the ligand sphere.

5.3 Summary and conclusion

It has been shown in the previous chapters that the resistance and the activation energy of the covalently cross-linked systems are evidently smaller than those of physically cross-linked ones. This phenomenon may be explained with the generalization of the inner and outer sphere mechanism from the solution chemistry to all charge transfers between two particles in any size range. For the two limiting cases the theory was validated thus far: for atomic/ionic entities the effect was proved first by Taube ([158], [159]) and later by many others. For macroscopic samples it is also clear that between two metallic bulbs there is a better electrical contact, if they are connected with a conducting wire. In this work the availability of the theory for one of the middle size particles was also shown.

6 Results and discussion of the diode behavior in asymmetrically ordered Au_{55}-monolayers

A diode is originally a heated anode and a cathode in a glass bulb under vacuum (Fig 6-1.*a*). If the cathode is positive, the electrons fly through the vacuum, and a certain current, flowing in the diode, can be measured. But, if the cathode is negative, it repulses the electrons, so they can't reach this electrode. That is why the original diode rectifies the alternating current and voltage (Fig. 6.1).

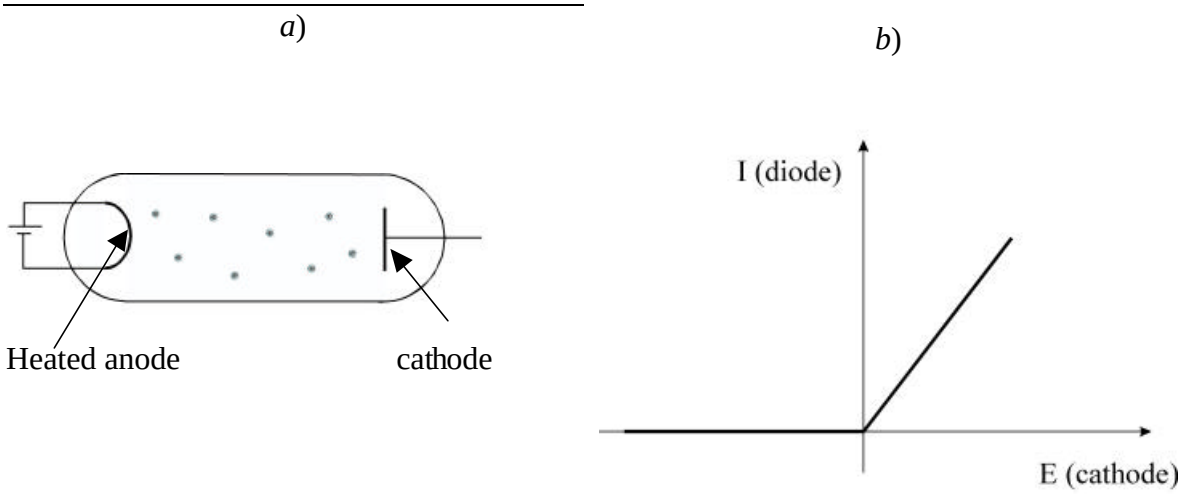

Fig. 6.1**:** Ideal original diode (*a*), and its characteristic *I-V* curve (*b*)

The diode today consists of two opposite doped semiconductor parts. It conducts, when the *n* doped part is negative, and the *p*-doped part is positive. If we apply the voltage in the opposite direction, then charge doesn't go through this circuit element. The *n-p* junctions in the today computer technique are really important: every building unit in a chip consists of different number of this transitions.

Later it was recognized that in every case, when at least two materials with two different electronic properties are in contact with each other, a small asymmetry in the *I-V* curve is observable [157] [132]. The same occurs by almost every STS measurement of cluster or colloid systems, because the resistance and the capacitance between the tip and the particle, and between the particle and the substrate, are in general not equal [128][131] (Fig. 6.2 *a*). It means, that it is easier for the electron to tunnel through one of the junctions, than through the others. In this case, the electron movement needs less voltage to flow through first the smaller resistance, than in the opposite direction. This asymmetry explains the higher gap at the left side of Fig. 6.2 *b*. Voltages between the absolute value of the right

sided and left sided Coulomb-blockade can be rectified, because the system by these potentials let the current flow just in one direction, but not in the other. Of course by STS measurements the position of the tip can be chosen for almost symmetrical *I-V* curve.

a) *b*)

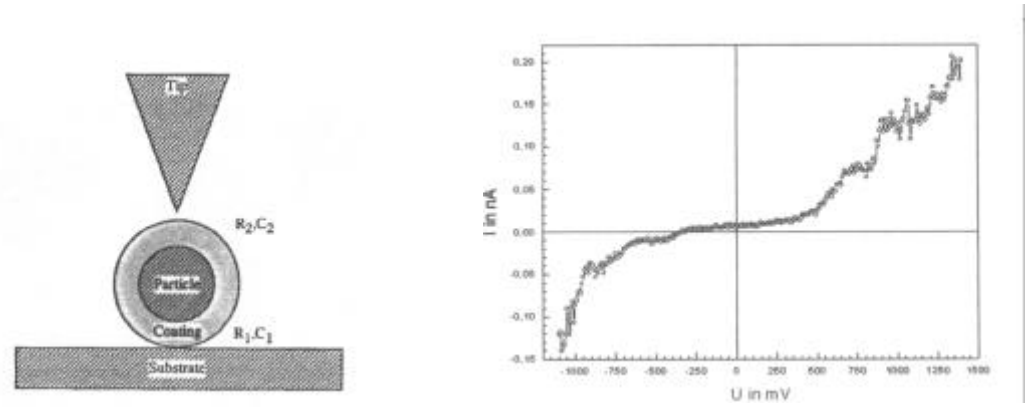

Fig. 6.2**:** *a*): A schematic description of the double junction system, showing the resistance and capacitance of each individual junction.[131] *b*): a typical *I-V* curve, measured above a single cluster[128].

6.1 Asymmetrical multilayers

Fig. 6.3 *a* shows a SEM image of a Au_{55} cluster film with a thickness of about 100 nm. It is clearly noticeable that a drop of water or dichloromethane has flowed between the two contact tips during the preparation. The leftover material builds an asymmetric arrangement in the layer which has a diode-like *I-V* curve (Fig. 6.3 *b*). The asymmetry is about 3 V. That means that for voltages between 3 and 6 V current can flow only in one direction, but not in the other.

6.2 Sample preparation

For the determination of the electrical properties, a two dimensional arrangement of a $Au_{55}(PPh_3)_{12}Cl_6$ monolayer, prepared by a modified LB technique (see chapter 8.6.1) was transferred onto a substrate, fabricated by EBL (see chapter 8.7.1.2). The dichloromethane solutiopn of the normal Au_{55} cluster solution was dropped onto a very diluted aqueous PVP solution, which contains the EBL fabricated substrate dipped inside. After the pulling out the substrate from the solution a monolayer is formed on its surface. Its structure is: the

substrate is covered with a thin (1 nm) PVP film. On this film there is a monolayer of Au_{55} cluster. At least 50% of the surface was always covered by the cluster layer, and with a good chance that there were also particles between the contact tips (Fig. 6.4).

a) b)

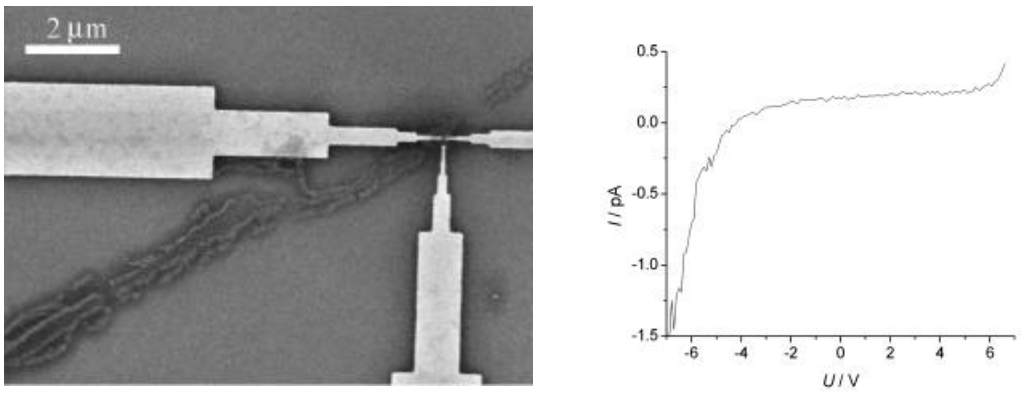

Fig. 6.3**:** Asymmetrical film arrangement (*a*), has a diode-like *I-V* curve (*b*). The thickness of the film is about 100 nm.

a) b)

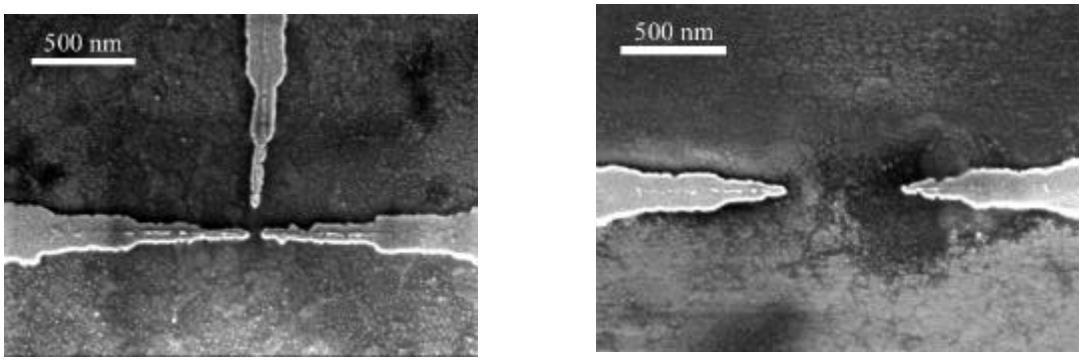

c) d)

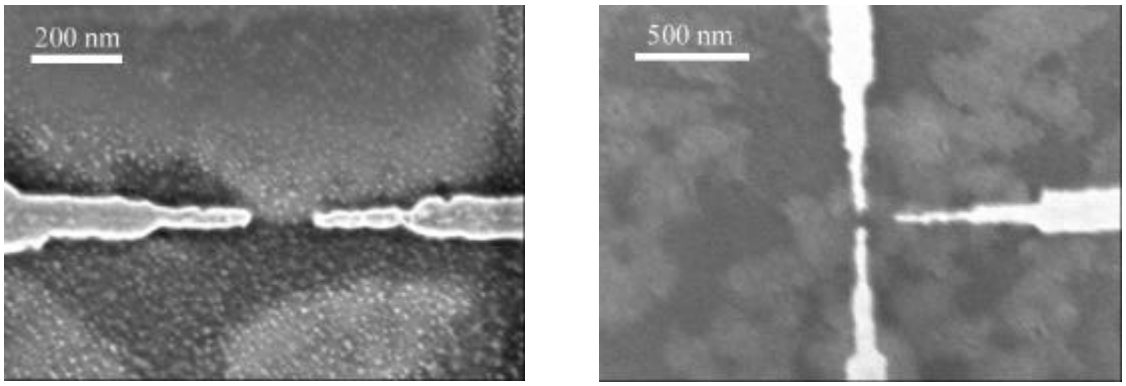

Fig. 6.4: SEM images of the different cluster arrangements between the contact tips. It is incidentally occurs, if there is nothing (a), between the tips, or just the half of the interstice is covered (b), or there is a cluster island asymmetrically (c) or symmetrically (d) connecting the tungsten contacts.

It turned out that the roughness of the sample supports the transfer: effectively the used surface is very smooth, but some 25 nm high tungsten contact structures are present on it. With EBL a “smooth-rough surface” can be prepared: there are great smooth areas, namely on the tungsten and SiO_2 surfaces, but the absolute corrugation is 25 nm. This fact seems to help the monolayer to remain on the surface, in contrast to the too smooth surfaces.

6.3 Activation of Au_{55} cluster monolayers with electron beam

It is well known, that the electron configuration of the Au_{55}-clusters are in between bulk and molecule. That means, that their energy levels are quasi continuous, with a small band gap between the HOMO and the LUMO orbitals [129]. This involves that the Au_{55} clusters are similar to semiconductor materials. A silicon platelet can be doped and its conductivity enlarged, generating holes in the valence band or additional electrons in its conducting band. To reach this goal in the case of Au_{55} a monolayer, deposited on a sample made by EBL, was irradiated with a small energy electron-beam, for 10 s. As it is clearly noticeable in Fig. 6.5 *b*, the resistance of the sample after irradiation is at least two orders of magnitude smaller than it was before. Other reasons may explain this resistance reduction. One of them is that during the irradiation, the ligands and the polymer film under the gold clusters can be destroyed, to form a thin carbon film, which is a conductive medium. Another reason can be in relation with the electron beam: a too long exposition to the electron beam may diminate aggregation of the clusters. This phenomenon is well known in the case of TEM measurement. At high energy, a long time irradiation can destroy the sensitive particles. Finally, in the SEM a thin carbon film is formed: it can disturb the measurement because it can behave as an insulator, semiconductor, or metallic conductor. Clarke [140][141] assumed that the activation phenomenon could be explained with the cross-linking of the ligand shells. To find the right reason of this effect, some further measurements were required.

The stability of this activated state was determined (Fig. 6.6). It is clearly observable, that the probe relaxes. On the other hand, even 39 hours after the irradiation the current is higher, than before irradiation. A certain nonlinearity of the curves is also noticeable, what

is not surprising in the case of these small particles (see chapter 4.3.3). It can be proposed that after exposure, some rearrangement occurs, working against the activated state of the layer.

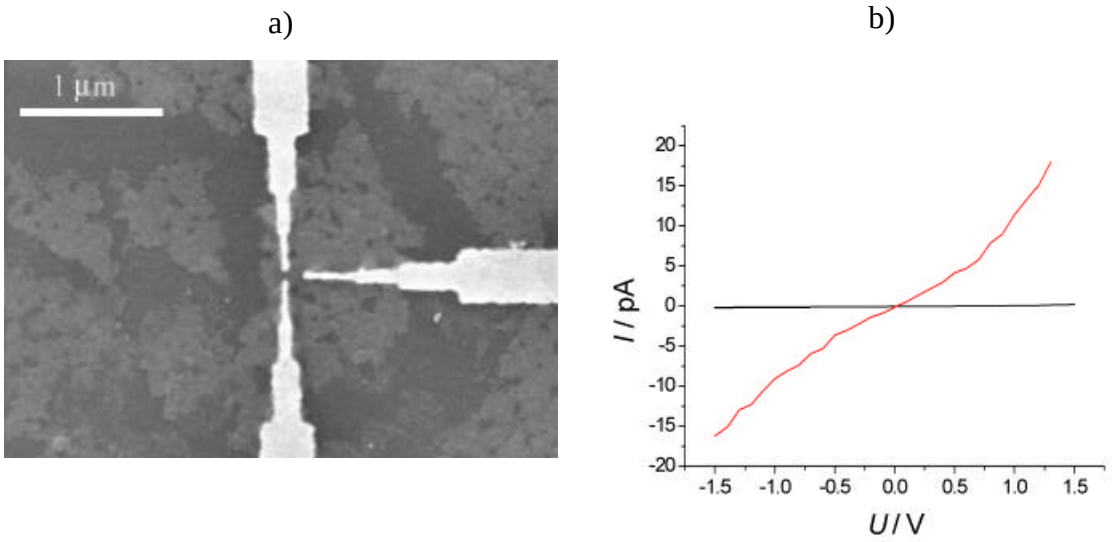

Fig. 6.5: SEM image of the Au_{55}-monolayer between the contact tips (a), and its I-V curve (b) before (black line) and after (red line) the irradiation with an electron beam energy of E = 10 keV for t = 10s. The thickness of the SiO_2 layer D = 80 nm.

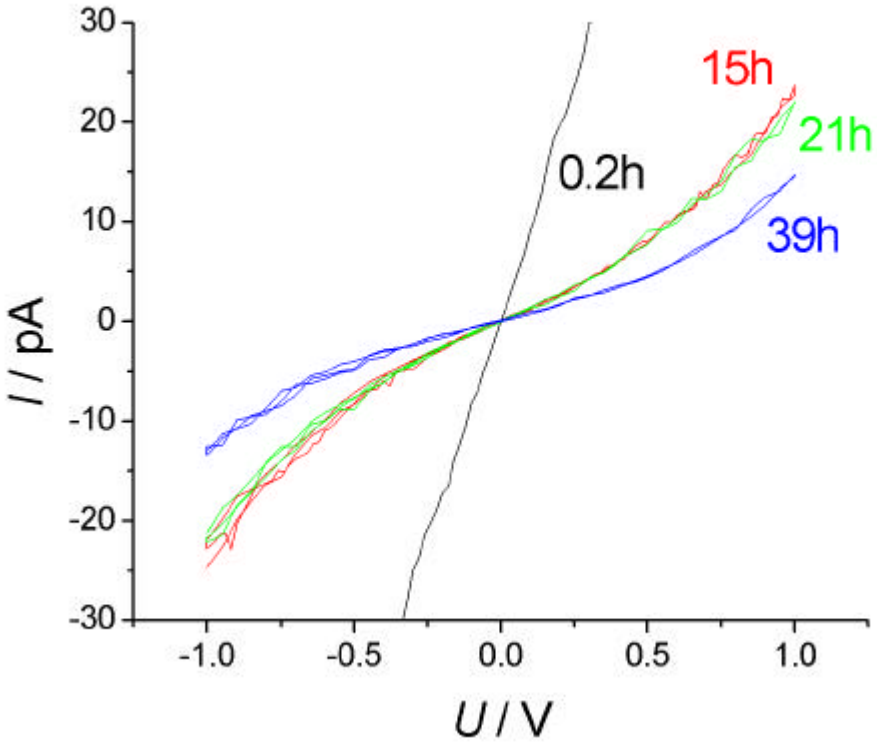

Fig. 6.6: Stability of the activated monolayer: measurements 0.2 (black line), 15 (red line), 21 (green line) and 39 hours (blue line) after the irradiation (E = 10 keV, t = 30 s, D = 80 nm)

6.4 Preparation of asymmetrically activated monolayers

If the "activation" of the Au_{55}-layer is really a similar effect like the doping of a semiconductor, then the generation of a junction inside the layer (between the two electrodes) should mean that an asymmetrical *I*-*V* curve must be measurable. This experiment is easy to realize: only half of the interstice of the two contact tips has to be exposed with the electron beam. In practice it means that the layer is irradiated just around one of the electrodes. Fig. 6.7 presents an *I*-*V* curve measured after exposure with the electron beam for 10 s with an energy of 10 keV. The asymmetry is about 2 V, which is quite big for this type of systems. At E = +2 V the current starts to increase. That shows the break down potential of the "diode", except that it seems to be reproducible, so the same curve is measurable after each other on the same system.

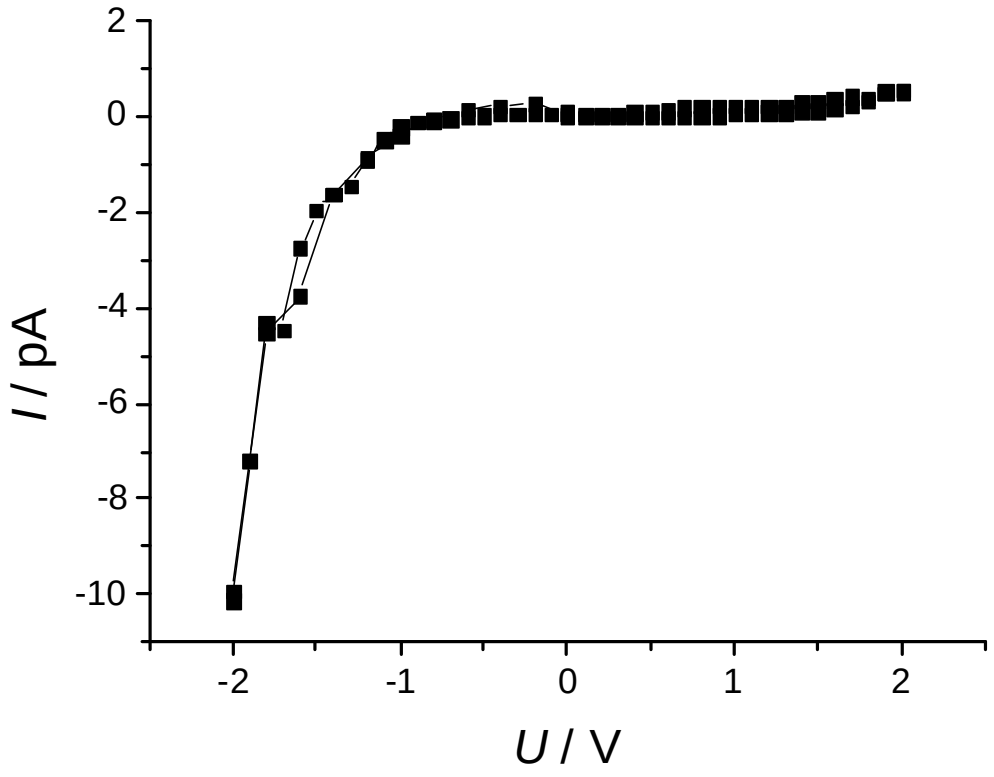

Fig. 6.7: Exposure to an electron beam around the left contact tip. (E = 10 keV, t=10 s, D = 300 nm)

This phenomenon excludes all symmetrical explanations of the activation.

6.5 Properties of asymmetrically activated cluster monolayers

During the characterization of this system, the irradiation parameters were systematically changed, to find out the optimal energy and time of the exposure, as well as the best thickness of the SiO_2 layer. These experiments were also helpful to find out the cause of this behavior. The quantitative comparison of the data is not easy, because the value of the measured current depends strongly on the ratio of the exposed-not exposed area: a too long exposition of the irradiated part involves a better conduction, than the other half. It means that if a larger area is exposed, the resistance of the layer in one direction will be smaller, and the asymmetry a little higher. Because the electron beam is controlled by hand, and the sample is continuously drifting, these parameters are not easy to monitor. The voltage asymmetry is the only measured value, which can be a characteristic of the "diode", because it is not very sensitive to the geometric parameters.

6.5.1 The effect of the polymer film

A thin (about 1 nm) and a thick (about 100 nm) film of pure polymer were adsorbed to the surface, and one tip was exposed to the beam (Fig. 6.8).

a) b)

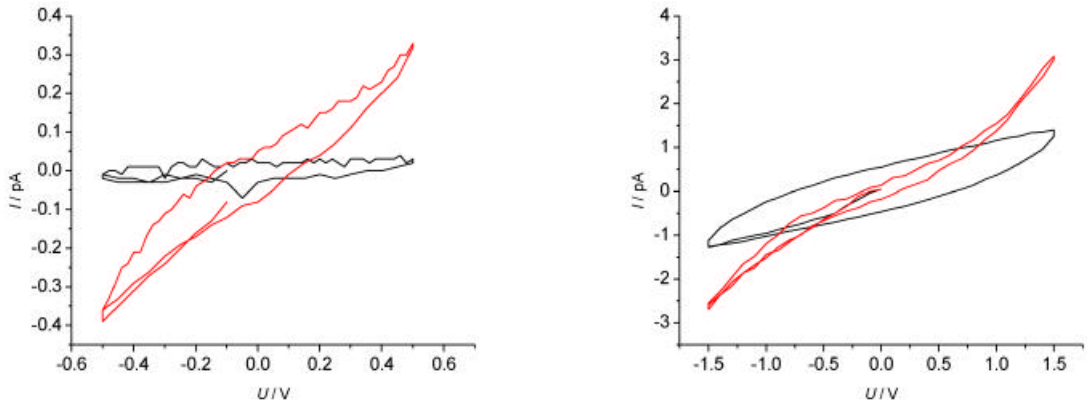

Fig. 6.8: Irradiation of pure polymer film with electron beam. *a*: a 1 nm thick film is exposed around the right tip, *b*: a 100 nm thick film is exposed around the left tip. The black lines shows the *I-V* curve before irradiation, the red lines after the exposure. (E = 10 keV, t=10 s, D = 80 nm in both cases)

A symmetrical activation is easily observable, but it is not big enough to explain the activation process of the cluster layer (noted that the polymer layer under the clusters is about 1

nm thick) (see chapter 8.6.1). The *I-V* curves of the excited state of the PVP film seems to be rather an effect of the smaller distance between the electrodes, caused by the reduction of the polymer film to carbon contaminates, than a doping effect of a semiconductor.

6.5.2 Dependence of the asymmetry on the side of the irradiation

The direction of the asymmetry can easily be changed, because the tungsten structures are equivalent to each other. If the current is allowed to flow from left to right, then the left tip has to be exposed, for the opposite direction the right contact needed to be irradiated (Fig. 6.9). On the other hand, this phenomenon also proves that the observed asymmetry is in connection with the layer and is not an artifact.

a) b)

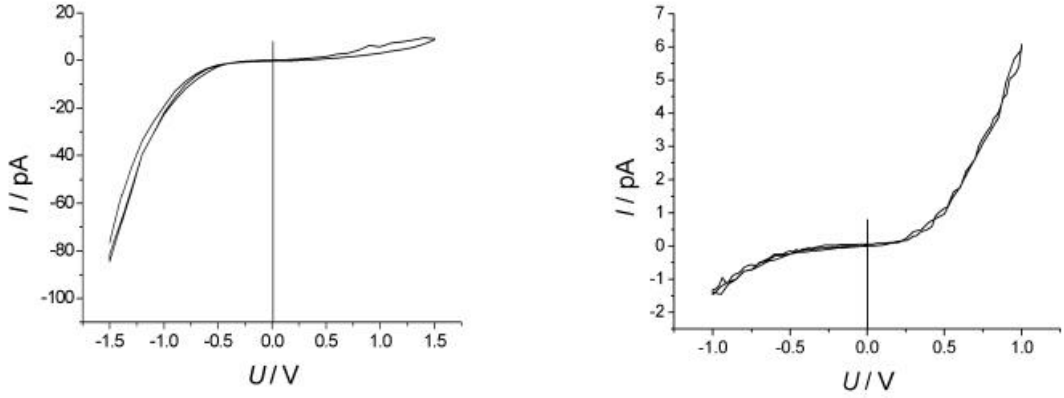

Fig. 6.9: *: I-V* curve of Au_{55} monolayers irradiated around different contacts. *a*: left tip *b*: right tip. (*E* = 10 keV, *t*=10 s, *D* = 80 nm in both cases)

6.5.3 Dependence of the asymmetry on the irradiation energy

Fig. 6.10 presents *I-V* curves of Au_{55} monolayers irradiated around the left tip, with different energies. The hysteresis of the first two curves shows some charging effect, visible, because of the small measured current. This effect can be caused by a very thin water film adsorbed on the surface or some other charges remaining inside the substrate. In Fig. 6.10 it is easily noticeable that the asymmetry increases, when the energy of the electron beam (E) applied is higher: 1 V for E=0.9 keV, 2 V for E = 10 keV, 5 V for E = 16 keV.

a)

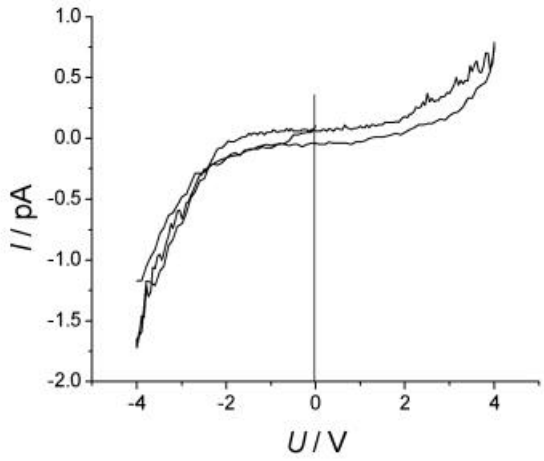

b)

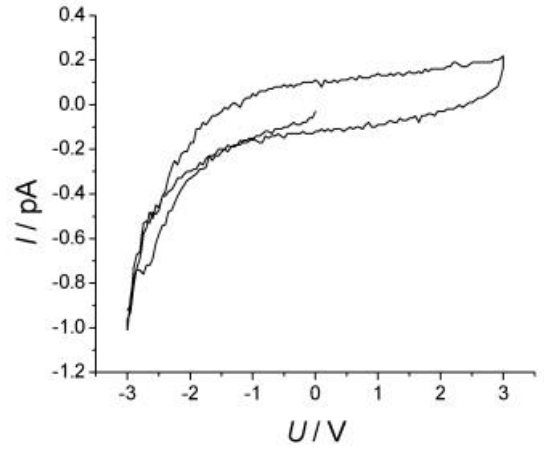

c,)

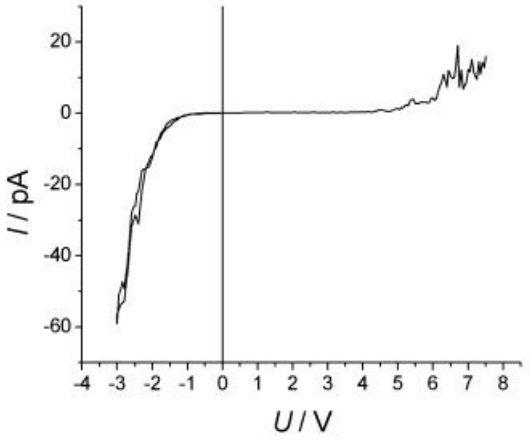

Fig. 6.10*: I-V* curve of Au_{55} monolayers irradiated around the left tip, with different energies of the electron beam. *a*: E = 0.9 keV, *b*: E = 10 keV, *c*: E = 16 keV (*t*=10 s, *D* = 80 nm in all cases)

6.5.4 Dependence of the asymmetry on the irradiation time

a)

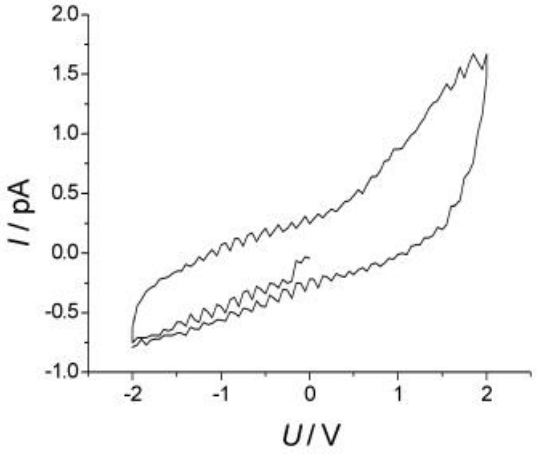

b)

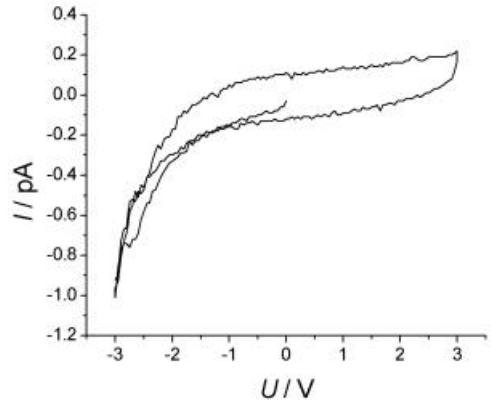

c)

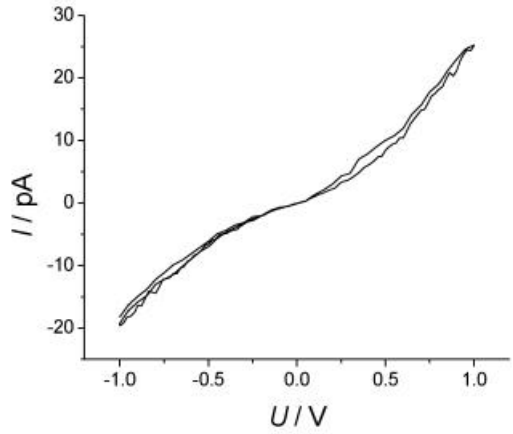

Fig. 6.11*: I-V* curve of Au_{55} monolayers irradiated around one of the tips, for different time with a 10 keV electron beam. *a*: t = 5 s (right tip) , *b*: t = 10 s (left tip), *c*: t = 30 s (right tip) (*D* = 80 nm in all cases.)

As it can be observed in Fig. 6.11, the time of the irradiation also affects the shape of the *I-V* curve. It seems to influence both the height of the gap and the intensity of the active site. The second sign is quite hard to separate from other effects (see the introduction of chapter 6.5), but the comparison between the current of the activated state and the background current give some information. An irradiation of 5s is to too small to get a real effect, and 30s overactivate the system because a small asymmetry is observed almost without any gap (see Fig. 6.11 c). The optimal irradiation time turned out to be 10s.

6.5.5 Dependence of the asymmetry on the thickness of the SiO_2 layer

a)

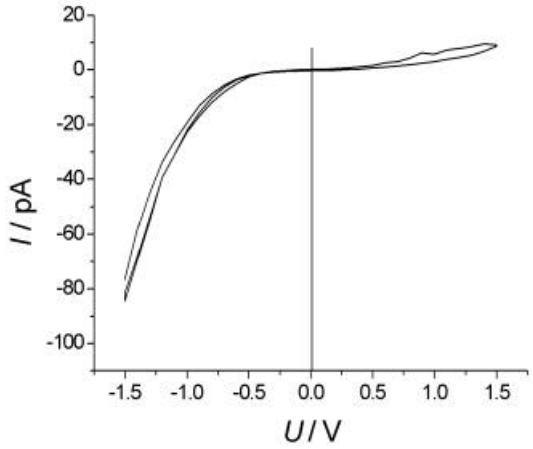

b)

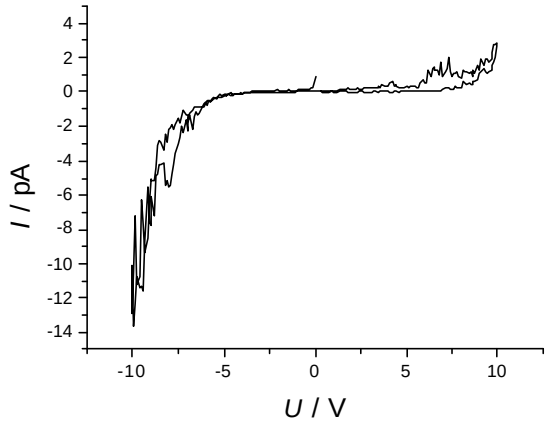

Fig. 6.12*: I-V* curves of Au_{55} monolayers irradiated around the left tip, on substrates with different SiO_2 thicknesses. (a): D = 80 nm, (b): D = 300 nm, (t = 10 s, E = 10 keV in all cases.)

The substrate used consisted of a silicon platelet with an oxidized SiO_2 film on it. The thickness of this layer turned out to influence the behavior of the Au_{55} layer. This influence is dramatic: the usual asymmetry of 1-2 V in the case of the 80 nm thick layer increases to 3-7 V with the increasing of the SiO_2 thickness to 300 nm. This shows that the effect is in connection with the substrate-cluster layer interaction. The difference between the two cases that the conducting Si phase is separated with a thicker isolating gap. This fact makes more difficult the relaxation of the charges trapped in the top films. This effect also can be observed on the SEM images, on the smaller contrast.

6.5.6 Relaxation and reactivation process

The activated samples don't remain activated over one day. They begin to relax. After some time, depending on the sample, they loose their activated state and become non-conducting. As it will be discussed in chapter 6.6 this phenomenon excludes numerous of the imaginable explanations. A sample, deposited on a 80 nm thick layer of SiO_2 and irradiated 10 s with a 10 keV electron beam, relaxes in the course of 15 hours (Fig. 6.13).

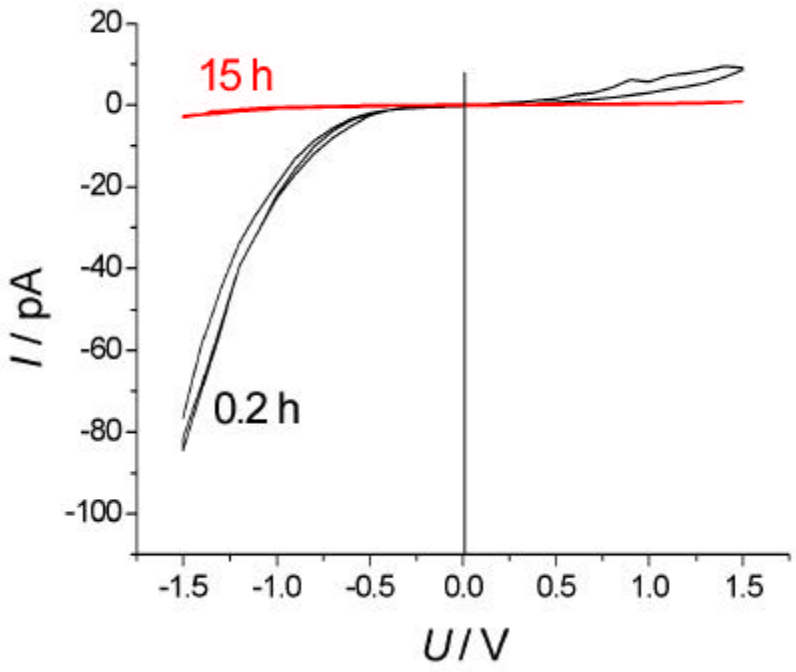

Fig. 6.13*: I-V* curve of the relaxation process of Au_{55} monolayers irradiated around the left tip. |: 0.2 Hours, | 15 hours after the irradiation (D = 80 nm, t = 10 s, E = 10 keV)

For the samples with 300 nm SiO_2 thick films on their surface, the relaxation process is faster and is reproducible: the layer can be reactivated successively (Fig. 6.14). It is assumed that the same might occur in the case of the substrates with 80 nm layer thickness, but it was not measured.

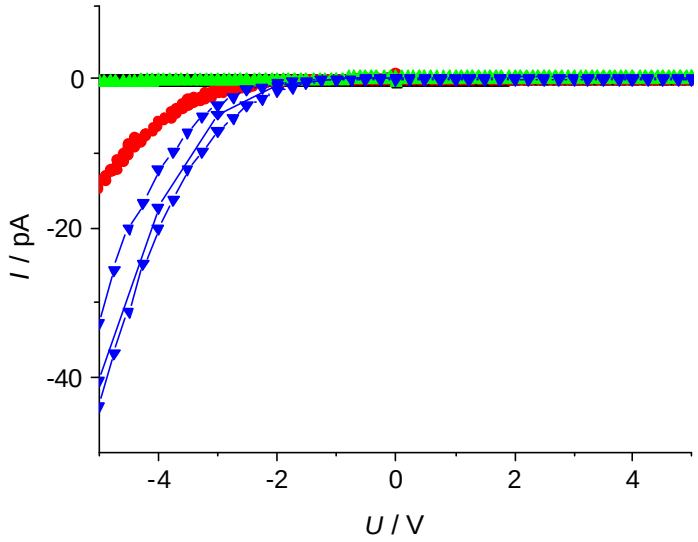

Fig. 6.14*: I-V* curve of the relaxation process of Au_{55} monolayers irradiated around the left tip. : before irradiation, : 0.2 hours, : 7 hours after the irradiation : 0.2 hours after reactivation (D = 300 nm, t = 10 s, E = 10 keV)

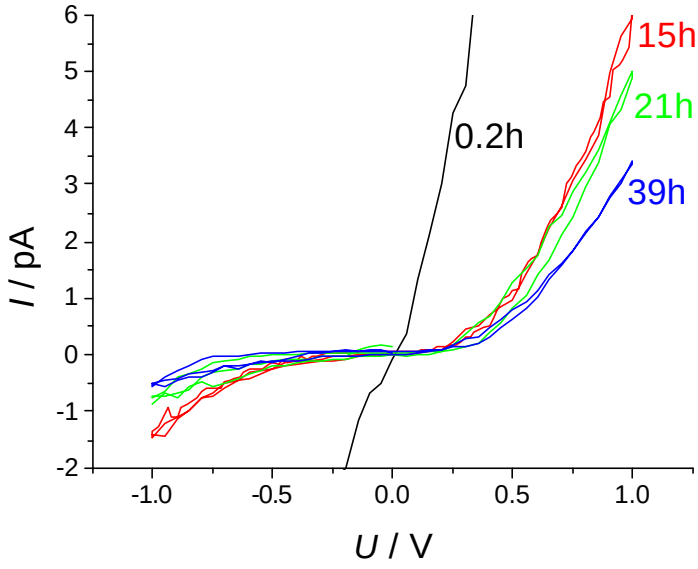

Fig. 6.15*: I-V* curve of the relaxation process of Au_{55} monolayers irradiated around the right tip. : 0.2 hours, : 15 hours, , : 21 hours : 39 hours after the irradiation (D = 80 nm, t = 10 s, E = 10 keV)

The overactivated sample also relaxes (Fig. 6.15) trough a diode effect, but slower than the same sample irradiation with a shorter time.

6.6 Explanations and discussion

Many arguments can be considered to explain the activation effect, as well as the asymmetrical behavior after asymmetrical irradiation:

a) charging effect,
b) aggregation of the clusters and formation of bigger colloids,
c) formation of carbon film contaminate,
d) decomposition of the polymer film, forming a conductor, or semiconductor layer,
e) chemical reaction inside the ligand shell (for example the cross-linking effects assumed in Ref. [140] and [141]),
f) the addition to the LUMO or dispossession from the HOMO of charge-carriers or forming excess of electrons or holes in the material.

Arguments a) – d) would be the "artifactual" explanations, because they are not in connection with the structure of the cluster layer (see the following chapter). e) and f) points assume structural changes in the Au_{55} cluster layer, using the properties of the mentioned nanoparticle.

6.6.1 "Artifactual" effects

In the following paragraphs the artifactual effects will be investigated one by one.

The charging effect can be excluded because the reason of the activation should be a permanent effect.

The decomposition of the clusters with concomitant formation of colloids might happen during the exposition, but this reason is also excluded, because in this case the sample cannot relax because colloids cannot rebuild clusters under these conditions (see chapter 6.5.6).

It can be proved with AFM, and light microscopic images, that carbon film contaminate does form during the exposition. But this reason is also excluded, because it cannot cause asymmetrical *I-V* behavior.

The experiments with the thick and thin polymer layer (see chapter 6.5.1) were necessary to exclude the formation of anisotrop carbon layers. The film in this case was also activated by the electron beam, but no asymmetrical behavior was observed. The activation effect, which can be observed on Fig. 6.8 seemed to be rather the effect of the smaller electrode-distance, than the formation of a carbon film.

Another experiment was done to exclude the carbon film contamination effect: blind sample without any layers was exposed around one of the tips. In this case no activation effect was obtained.

The logical investigation of the "artifactual" effects showed, that none of them is responsible for the asymmetrical *I-V* characteristics of the asymmetrically treated samples.

6.6.2 Structural changes in the Au_{55} cluster layer

The nature of the structural changes in the Au_{55} cluster layer will be discussed assuming e) and f) explanation. The changes of the electron energy levels will be discussed together with the chemical or structural changes inside the layer.

First, the cause of the rectifying behavior of a silicon-based diode is shown in order to give an example to the reason of an asymmetric *I-V* curve.

In Fig. 6.16 the energy diagram of an n-p semiconductor diode is presented. The electrons in the n doped part of the circuit element occupy some of the LUMO states, so they have bigger energy. On the p doped part some of the HOMO states are free, so the electrons occupy smaller energy levels. The Fermi level of the metal contacts are normally situated between the HOMO and the LUMO of the semiconductor. This situation is shown in Fig. 6.16 a. After applying the voltage, the Fermi level of the negative electrode increases, and that of the positive electrode decreases. If the n doped part is negative, then the electrons transit always onto smaller energy levels (Fig. 6.16 b). If the p doped part of the diode is

negative, than between the n and p part the electrons have to flow upwards (Fig. 6.16 b), what is a quite energy consuming step and is allowed just at high potentials.

This model can also be applied, if in the exposed area of the ligand shell of the clusters is cross-linked with each other (Fig. 6.17).

a)

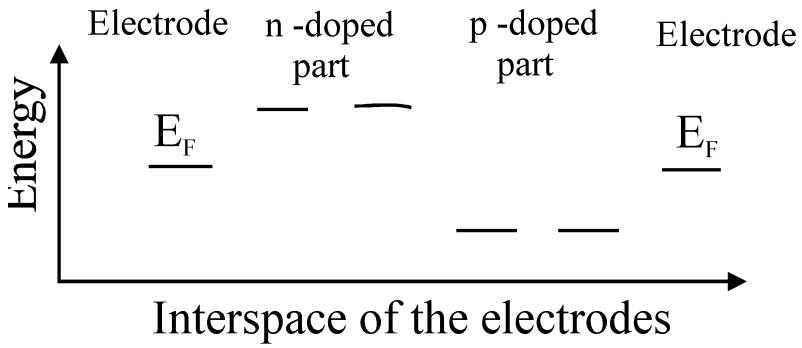

b)

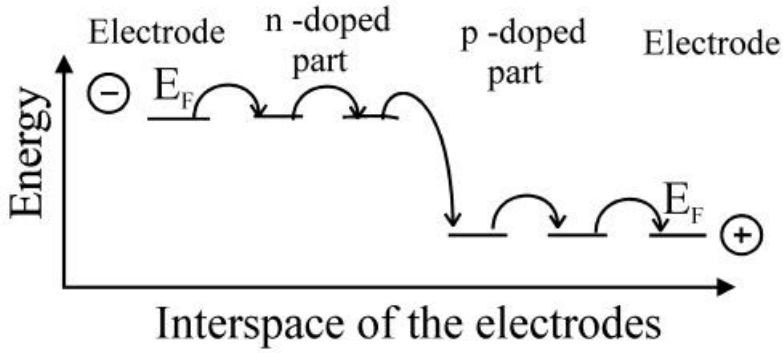

c)

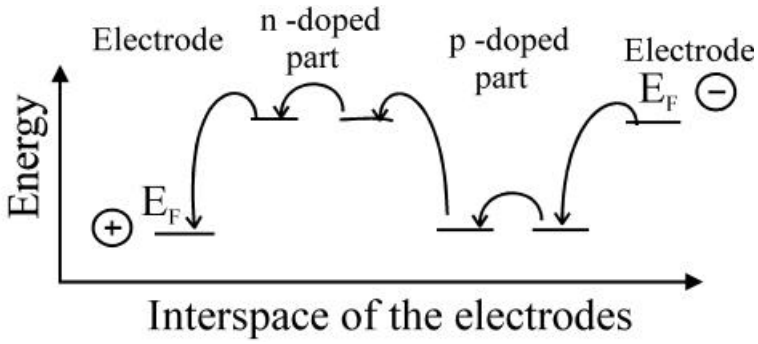

Fig. 6.16*:* Energy diagram of an n-p semiconductor diode: primary state (a), polarized state (b) and the opposite direction polarized states (c). E_F denotes the Fermi level.

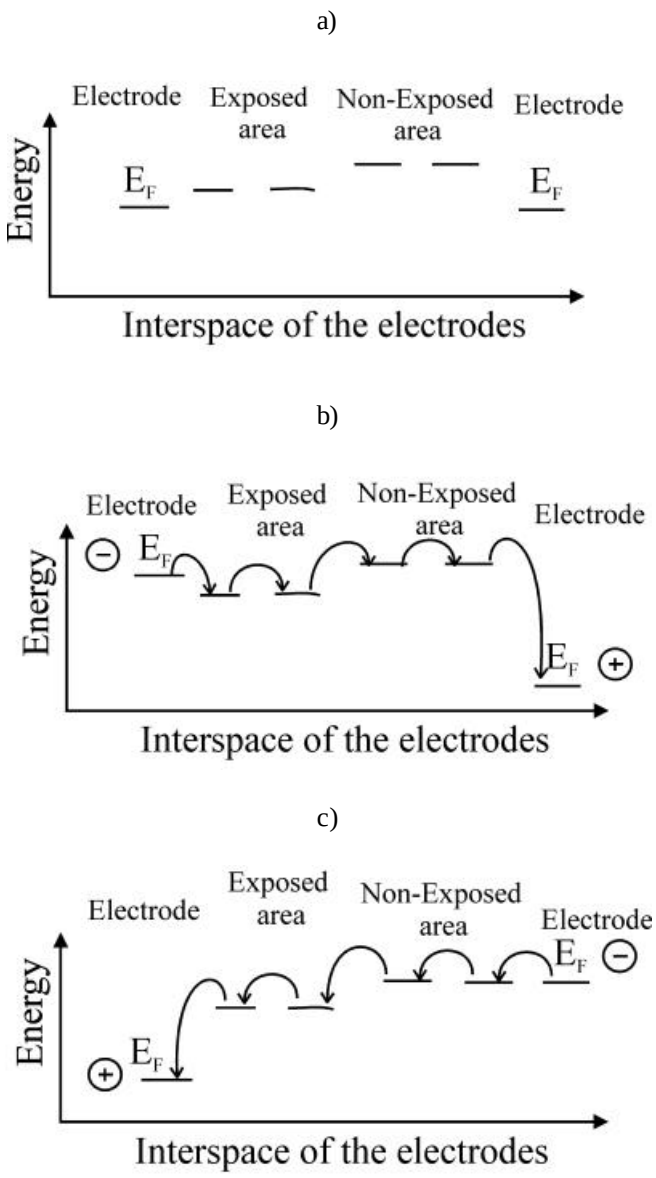

Fig. 6.17*:* Energy diagram of a cluster system exposed around the left tip (with the cross-linked model): primary state (a), polarized state (b) and the opposite direction polarized states (c). E_F denotes the Fermi level.

The cross-linked cluster system can be treated as a cluster polymer, which means that because of the interaction of the electron-orbitals, the HOMO-LUMO gap is smaller. That causes an energy difference between the LUMO's of the exposed and the non-exposed sides. The conductance in this case happens through the LUMO. If the irradiated side is negative, (Fig. 6.17 b) then on the border of the non irradiated and irradiated side the electrons have to tunnel "upwards". If an opposite voltage is applied, this gap is avoided, so the rectifying effect can be expected. If the interaction of the electron orbitals is not assumed, the difference in the activation energy in the two directions can lead to the rectification.

Electrons can be added to the system during the exposition with the electron beam, if somehow electrons are trapped inside the layer. This phenomenon can also be a reason for the rectifying behavior.

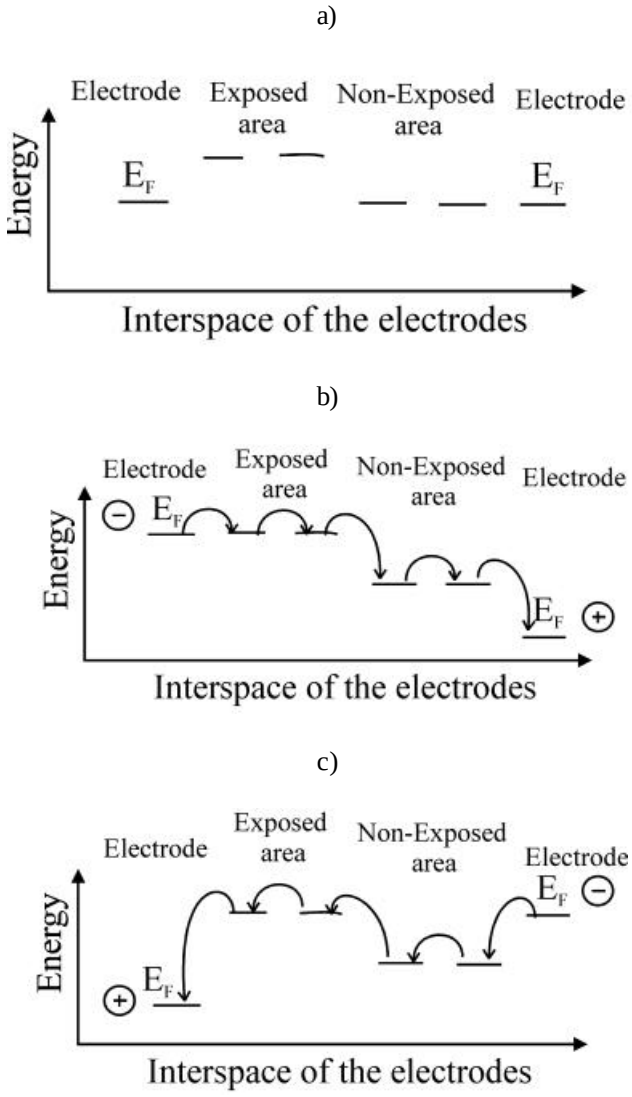

Fig. 6.18*:* Energy diagram of a cluster system exposed around the left tip (with the trapped charges in the cluster layer model): primary state (a), polarized state (b) and the opposite direction polarized states (c). E_F denotes the Fermi level.

If charges are trapped inside the cluster layer, these electrons occupy a part of the LUMO states, similar to n doped semiconductors (Fig. 6.18 a). If a voltage is applied to this system, with the negative part on the exposed area, the electrons have free way (Fig. 6.18 b). If the voltage is applied in the opposite direction (Fig. 6.18 c), on the exposed-not exposed border a gap is formed. The main difference between the expected rectifying behavior of

the cross-linked and this model, that this model assumes the opposite rectifying behavior, than the one discussed before.

Dispossession of charges can be generated by the exposition to an electron beam, if the electrons are trapped inside the SiO_2 layer. This happens quite easily inside silicon-oxides and these additional electrons create so-called image charges of opposite charge inside the cluster layer. This model predicts a rectifying behavior with the opposite direction as the above discussed model (Fig. 6.19).

a)

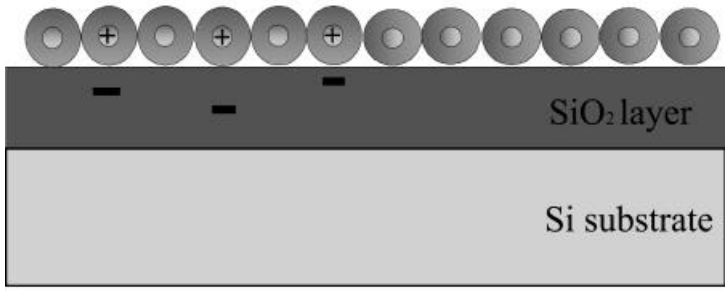

b)

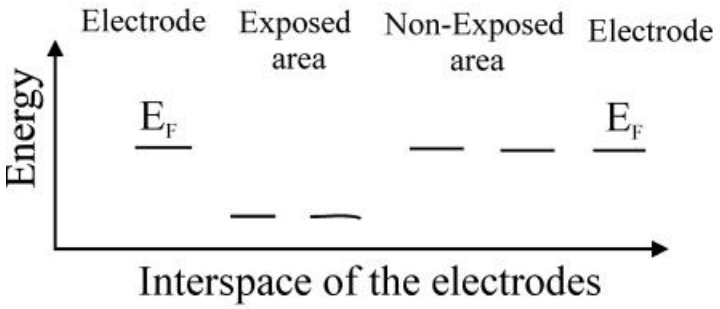

c)

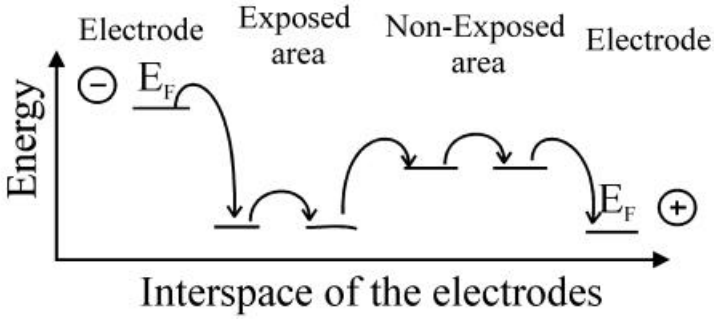

d)

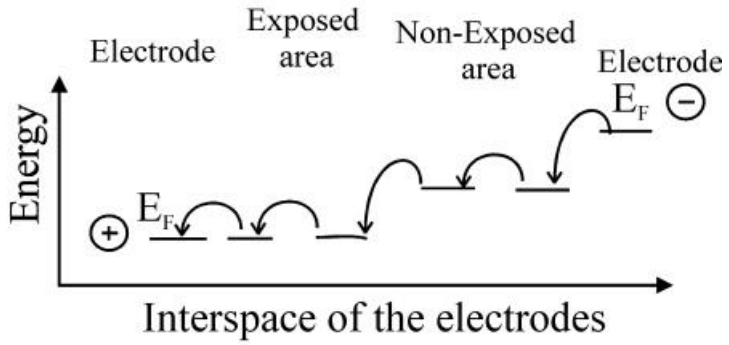

Fig. 6.19*:* Energy diagram of a cluster system exposed around the left tip (with the trapped charges in the SiO_2 layer model): primary state (a), polarized state (b) and the opposite direction polarized states (c). E_F denotes the Fermi level.

The image charges are positive, since the trapped electrons are negative (Fig. 6.19 a). That means that electrons are missing from the HOMO states, so the conducting electrons have smaller energy than those in non-exposed parts of the layer (Fig. 6.19 b). The electrons have thus free way if the exposed area is positive (Fig. 6.19 c), and there is a gap by the application of the opposite voltage (Fig. 6.19 d).

If the sample has not the possibility to relax electrically (as it might be in the case of these substrates) they do not loose they charge after the exposition. So it might happen, that the top layers of the used platelet remain negatively charged. In this case a charge distribution may occur, which leads to the formation of negatively charged cluster centers. This small islands act as a gate for the electron transfer (Fig. 6.20). Speaking in the language of the energy levels we get the same situation as it was shown on Fig. 6.18, but the cause of the increase of the energy levels in this case is the higher energy of the negatively charged clusters in the layer.

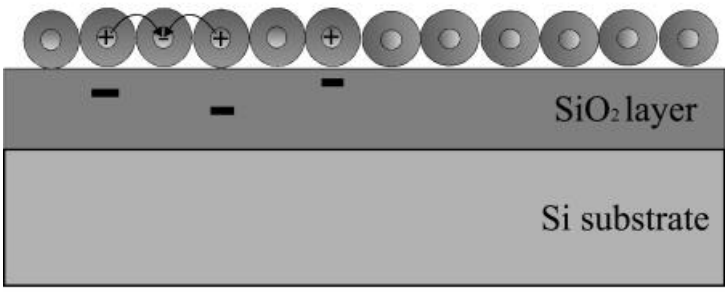

Fig. 6.20*:* Cause of the charge distribution in the case of negatively charged sample.

Addition or dispossession of electrons inside the Au_{55} layer means additional negative or positive charges in the film. This phenomenon might lead to a rearrangement of the particles, because the additional charges tend to be delocalized. This delocalization is more effective, if the entities in a lattice are arranged in a square lattice with a fraction of charge on every second particle (Fig. 6.21). A very much idealized picture of this situation can be observed on Fig. 6.21.

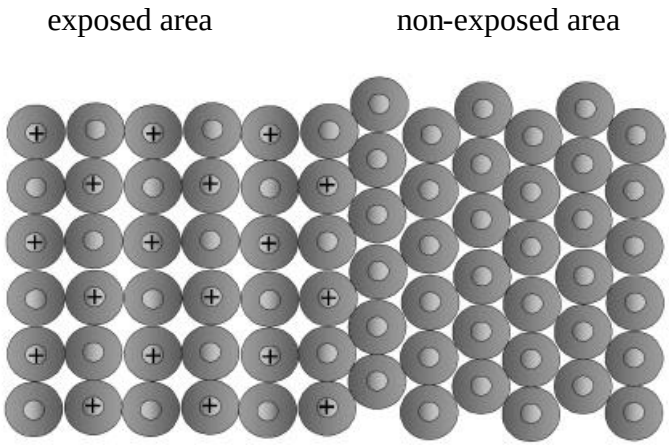

Fig. 6.21*:* Rearrangement of the particles in the cluster layer with the delocalization of the charges in the case of the dispossession of the electrons (trapped charges in the SiO_2 layer).

The detailed investigation of these three cases shows, that each of them be used to explain the rectifying behavior, however not in the same direction. In all three cases the change of the electron configuration might lead to a rearrangement of the particles in the cluster layer.

6.6.3 Conclusion

Finally the possibility of the above explanations will be discussed in the light of the properties of the asymmetrical behavior.

The asymmetry in the *I-V* curve can be discussed in terms of the "cross-linking model". A higher energy of bombarding electrons increases the probability of cross-linking reactions in the sample. An energy threshold can be assumed for the first cross-linking reaction, but it might be smaller than the smallest energy used for the exposition. Increasing he irradiation energy in terms of the "formation of image charges model" leads also to increasing *I-V* asymmetry, since with the increasing energy of the bombarding electrons deeper regions of the SiO_2 layer are available, thus increasing the number of trapped electrons.

With increasing of the exposition time both the number of the trapped electrons and the number of the cross-linker bonds can increase.

The dependence of the *I-V* asymmetry from the SiO_2 layer thickness is a strong argument for the formation of trapped charges, since the cross-linking reaction is not in connection with the reactions happening in the SiO_2 layer.

The decision after the above discussion might be that electrons are trapped inside the SiO_2 layer, which inducing image charges of opposite charge in the cluster film. This image charges might cause dispossession of charges, so forming holes in the layer, or barriers for the electron movement. This phenomenon might lead to a structural rearrangement in the cluster layer, accompanied by the delocalization of the charges. This rearrangement and the change of the electron configuration may lead to the experimentally observed asymmetrical "diode" behavior.

7 Summary

In this study, the electrical properties of Au_{55} cluster systems were investigated. Two main topics were addressed:

- the difference between the charge transfer mechanism of physically and chemically cross-linked Au_{55} systems,
- and the conducting properties of dense packed cluster monolayers.

The electrical conductivity measurements were carried out separately for two-, *quasi*-two, and three-dimensional arrays of Au_{55} clusters.

The following problems had to be solved during the work:

- For two-dimensional samples:
  - A monolayer was prepared with the silanization of a substrate surface, followed by the deposition of the clusters. These layers consist of large (10 µm) dense-packed islands. These films do not contain any movable ions like H^+ or traces of conducting solutions (see chapter 8.6.2.1 and 5.1.1).
  - A Langmuir-Blodgett monolayer of $Au_{55}(PPh_3)_{12}Cl_6$ has been created on a suitable substrate. This monolayer contains traces of conducting solution (water) of a small concentration. It has been proved that keeping the sample in vacuum, this solvent can be evaporated, without a significant change in the structure of the monolayer (see chapter 8.6.1.2 and 5.1.1).
  - Experimental parameters have been optimized for cross-linking the particles on the surface (see chapter 8.6.2.1 and 5.1.1).
  - In a suitable electrode arrangement, the optimal electrode and substrate geometry were developed for the electrical conductivity measurements (see chapter 8.6.1.2, 8.7.1.2 and 5.2.1).
- For *quasi*-two-dimensional samples:
  - Both chemically and physically cross-linked multilayers of gold nanoparticles were synthesized. The physically cross-linked layer one spin-coated onto the substrate (see chapter 8.6.1.1 and 5.1.1), while the chemical layers were prepared with step-by-step self assembly methods (see chapter 8.6.2.2 and 5.1.1).

- A measurement method has been developed for their electrical characterization, with a slight modification of the method by U. Simon [114] for three-dimensional samples (see chapter 5.2.2)

- For three-dimensional samples
  - Conjugated α,ω-dithiols (1,5 NDSH and 2,6 NDSH) were synthesized and used as bridging ligands, which form a conjugated electron system inside the cluster network (see chapter 8.3).
  - The synthetic parameters were optimized for the cross-linkage reaction of the Au_{55} metal cores (see chapter 8.5).

During the work it has been showed that different charge transfer mechanism occurs in physically and chemically cross-linked systems. The nature of this difference is similar to the well-known inner-sphere/outer-sphere charge transfer mechanism in aqueous solution chemistry.

It can also be concluded that the asymmetrical irradiation of the cluster monolayers with an electron beam leads to an asymmetrical charge transfer behavior. This effect might be caused by the image charges, which results from trapped charges in the SiO_2 layer.

8 Experimental

8.1 Chemicals

NAME	FORMULA	ABBR.	PURITY	DESTINATION
	$Au_{55}(PPh_3)_{12}Cl_6$ (see fig Fig. 2.9)	Normal Au_{55}	90-95%	Synth [117]
Dichloromethane	CH_2Cl_2	DCM	99.5%	Applichem
Ethane-dithiol	$HS\text{-}CH_2\text{-}CH_2\text{-}SH$	EDSH	99%	FLUKA
Ethanol	$CH_3\text{-}CH_2\text{-}OH$	EtOH	99.8%	FLUKA
3-mercapto-propyl trimethoxysilane	$(OMe)_3Si\text{-}(CH_2)_3\text{-}SH$	TMSPSH	95%	ABCR
Toluene	$C_6H_5CH_3$	Toluene	99.5	FLUKA distilled
1-hydroxy-3,7 dithio-purine	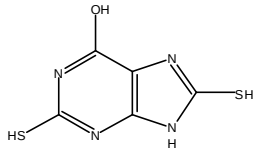	Purine	98%	Avocado
4,4'-thiobis-benzenethiol	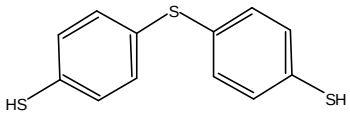	TBBT	98%	Aldrich
Naphtaline-1,5-disulfonic acid sodium salt	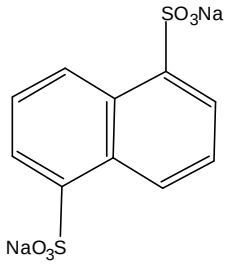	$1,5NSO_3Na$	95%	Aldrich
Naphtaline-2,6-disulfonic acid sodium salt	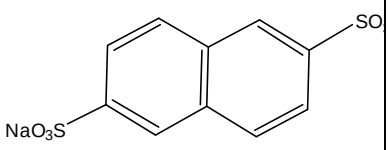	$2,6NSO_3Na$	95%	FLUKA

1,5-Dithio-naphtaline	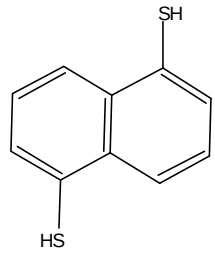	1,5NSH	70%	Synth [146]
2,6-Dithio-naphtaline	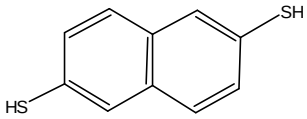	2,6NSH	92%	Synth [147]
Sulfolane	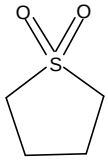	Sulfolane	99.5%	FLUKA
Tetrahydrofurane	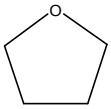	THF	99.5	FLUKA distilled
Dimethyl-formamide	$H(CO)N(Me)_2$	DMF	99%	Acros
Ethyl acetate	CH_3-CH_2-O-(CO)- CH_3	EtAc	99.5%	FLUKA
Poly-vinyl-pyrrolidone	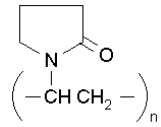	PVP	99.5	FLUKA
3-Chloroprpyl-dimethylchlorosilane	$Cl(Me)_2Si$-$(CH_2)_3$-Cl	CDMSPCl	95%	ABCR
N,*N*-dimethyl-*O*-(3-chloropropyl-dimethylsilyl)-carbamate	$(Me_2N)O(CO)O(Me)_2Si$-$(CH_2)_3$-Cl	KDMSPCl	70%	Synth
pentane	$CH_3CH_2CH_2CH_2CH_3$	Pentane	99.7	FLUKA distilled
Potassium-hydrogen sulfide	KSH	KSH	98%	Synth
Phosphorus	$POCl_3$	$POCl_3$	99%	FLUKA

oxychloride				
Mercury-chloride	$HgCl_2$	$HgCl_2$	99%	Rieder de Häen
Zinc	Zn	Zn	98%	Roth
Concentrated Sulfuric acid	cc. H_2SO_4	cc. H_2SO_4	98%	Baker Analysed
Diethyl ether	Et_2O	Et_2O	99.5%	Roth
Acetonitrile	CH_3CN	MeCN	99.5%	FLUKA
Hydrochloric acid	HCl	HCl	36%	FLUKA
Sodium-hydroxide	NaOH	NaOH	99.9%	FLUKA
Tin-chloride	$SnCl_2 \cdot 2H_2O$	$SnCl_2$	95%	FLUKA
Ammonium chloride	NH_4Cl	NH_4Cl	95%	FLUKA
Glacial acetic acid	CH_3-COOH	Acetic acid	99-100%	FLUKA
	$(Au_{55}Purine_x)_n$	Au_{55}(Purine)		Synth
	$(Au_{55}Purine_yPurine_y)_n$	Ox. Au_{55}(Purine)		Synth
	$(Au_{55}TBBT_x)_n$	Au_{55}(TBBT)		Synth
	$(Au_{55}TBBT_y\text{-}TBBT_y)_n$	Ox. Au_{55}(TBBT)		Synth
	$(Au_{55}(1,5NSH)_x)_n$	Au_{55}(1,5NSH)		Synth
	$(Au_{55}(1,5NSH)_y(1,5NSH)_y)_n$	Ox. Au_{55}(1,5NSH)		Synth
	$(Au_{55}(2,6NSH)_x)_n$	Au_{55}(2,6NSH)		Synth
	$(Au_{55}(2,6NSH)_y(2,6NSH)_y)_n$	Ox. Au_{55}(2,6NSH)		Synth

Tab. 8.1: Names, conformations, abbreviations, purity and source of the chemicals

All the solvents and chemicals were used as received, except THF and toluene, which were distillated on Na/benzophenone and pentane on CaH_2. All reactions were carried out in nitrogen atmosphere and the solvents were carefully degassed before used.

8.2 Synthesis of the $Au_{55}(PPh_3)_{12}Cl_6$ cluster

The $Au_{55}(PPh_3)_{12}Cl_6$ cluster was synthesized by the method developed in our working group in 1981 [116][117]. The main idea of the reaction is that the used gold salt $[Au(PPh_3)Cl]$ is reduced by diborane (see chapter 2.4.1). During the reaction $Au_{55}(PPh_3)_{12}Cl_6$ is formed under certain experimental conditions. For the synthesis first the apparatus shown on Fig. 8.1 has to be built up.

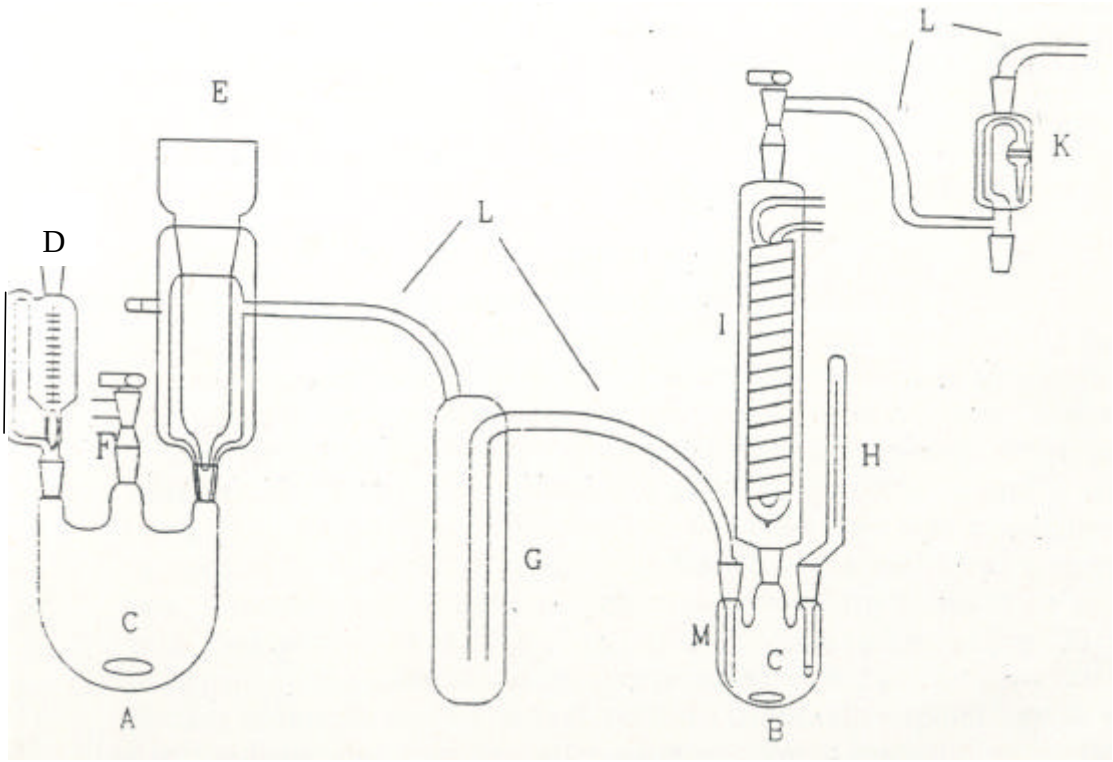

Fig. 8.1: Apparatus for synthesizing $Au_{55}(PPh_3)_{12}Cl_6$ cluster. Figure is adapted from [117].

A 500 ml three-necked, round-bottomed flask [A], containing 20 g of $NaBH_4$ (0.53 mol) and 100 mL of 1,2-dimethoxyethane, is equipped with a Teflon coated magnetic stirrer, a dry-ice cooler [E] and a dropping funnel filled with 100 ml BF_3-ether [F]. This flask is connected to a second one [M] via a flexible polyethylene tube [L] and a cooled trap [G]. The second flask, equipped by a magnetic stirrer [C] and a reflux condenser [L] itself con-

nected to a mercury safety valve [K], is filled with 3,96 g of $Au(PPh_3)Cl$ (0.008 mol) and 150 mL of benzene. The trap as well as the dry ice cooler are cooled with a mixture dry-ice-ethanol. Dropping BF_3-ether onto the $NaBH_4$ solution (flask A) induce the formation of the gas diborane, which via the tube bubble trough the benzene solution heated at 50°C. The color of the solution changes to brown after few minute and become darker. After 45 min, the production of diborane is stopped and the brown suspension is allowed to cool back to room temperature. The suspension obtained is then filtered using a sintered funnel. The precipitate isolated is cleaned with benzene twice and dried two hours under reduce pressure. The product in then dissolved in CH_2Cl_2 and filtered through an Anatop filter to get rid of the bigger colloids, or recrystalising from a CH_2Cl_2 solution with the slow addition of pentane to avoid the presence of smaller particles. The clusters should never remain in solution more than two or three hours! After two filtration, the clusters are isolated by evaporation under reduce pressure of the solvent and characterized by TEM.

8.3 Synthesis of the ligands with two terminal –SH groups

Five different ligands with two terminal –SH ligands were used, EDSH, Purine, TBBT, 1,5NDSH and 2,6NDSH (for chemical names see Tab. 8.1). The first three were commercially available. 1,5-Naphtalene-dithiol (1,5NDSH), 2,6-Naphthalene-dithiol (2,6NDSH) were obtained by reduction of the sodium salts of the corresponding sulfonic acids. Both syntheses contained two steps: the preparation of sulfonyl chlorides (1) and their reduction (2).

8.3.1 Synthesis of 1,5-naphtalene-dithiol

1,5-NDSH was synthesized in a two-step synthesis (Eq 3.1).

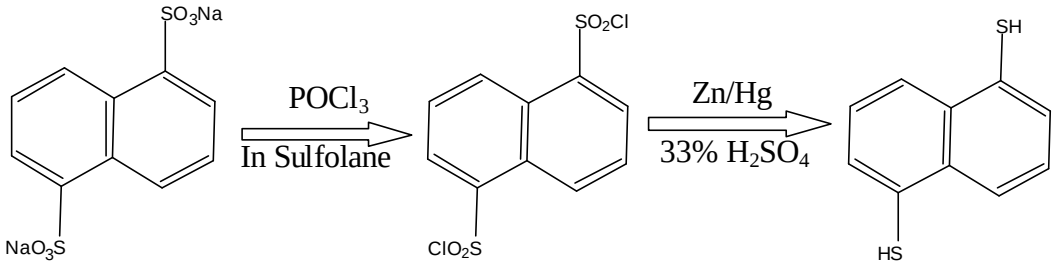

3.1

First the sulfonyl chloride was prepared with Fujita's method [145]:

3 g of 1,5NDSO$_3$Na (or 2,6NDSO$_3$Na) (0.009 mol) was added into the mixture of 5.8 mL acetonitrile (0.11 5.8 mL of sulfolane (0.061 mol) and 4.2 mL of $POCl_3$ (0.045 mol). After stirring the suspension at 72 °C for 3 hours, it was cooled down to 5 °C. 50 mL of water were added into the reaction mixture carefully, then the suspension was stirred another 10 minutes at 10 °C. The white precipitate obtained was isolated by filtration and dried in air overnight.

Reduction of 1,5NDSO$_2$Cl is accomplished with a zinc-amalgam in sulfuric acid [146].

1,25 g $HgCl_2$ (0.0046 mol) was dissolved in 30 mL 0.2M HCl solution and 6,25g Zn (0.095 mol) was added into it. After 10-15 min of stirring , the amalgam was filtered through a Büchner funnel and washed with water containing a trace of HCl, ethanol and Et_2O.

7,5 g of the still wet amalgam was added to the mixture of 45 mL 33% H_2SO_4 and 1.5 g sulfonyl chloride (0.0046 mol). The suspension was stirred and refluxed for 6 hours at 110 °C. After cooling the obtained suspension was let overnight without stirring at room temperature. The next day, the mixture was filtered and the precipitate extracted with 200 mL of hot ether. After concentration of the solution, the product was crystallized at low temperature. The white crystals were isolated by filtration and dried under reduce pressure.(Anal. Calc: C: 62.5; H: 4.16; S: 33.33. Found C: 62; H: 4.18; S: 32.8 %.).

8.3.2 Synthesis of 2,6-naphtalene-dithiol

2,6-NDSH was synthesized in a two-step synthesis. The first step, which resulted in sulfonyl chloride, was prepared with Fujita's method [145], as by the 1,5-NDSH (see chapter 8.3.1).

The reduction of 2,6-NDSO$_2$Cl by $SnCl_2$was realized using Caesar's method [147].

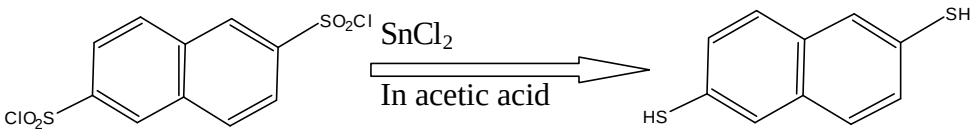

3.2

For the preparation the following apparatus is needed (Fig. 8.2).

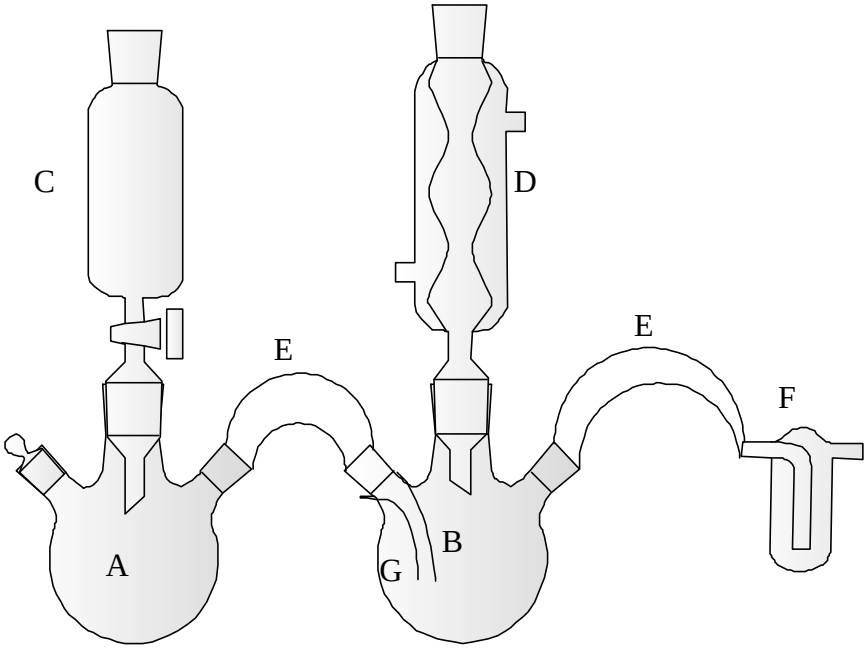

Fig. 8.2: Apparatus for synthesizing 2,6NDSH.

A mixture of 12,5 g (0.066 mol) of stannous chloride dihydrate and 50 mL of glacial acetic acid (flask [B]) was saturated with anhydrous hydrogen chloride produced by dropping conc. H_2SO_4 [A] on NH_4Cl [C]. When all the stannous chloride had dissolved, the solution was heated to 90 °C and 1g (0.003 mol) of 2,6NDSO$_2$Cl added quickly with shaking. The temperature was kept for 30 min and then allowed to cool to room temperature. The suspension was poured into 30 mL of concentrated HCl and filtered. The white precipitate was extracted with 25 ml of NaOH 5% and the solution was filtrated trough a sintered glass funnel in 30 mL of HCl concentrated. This procedure was repeated twice and the solid product dried on air. (elem. anal theoretical C: 62.5%, H: 4.16%, S:33.33%; found C: 61.78%, H: 4.07%, S:32.77%)

8.4 Synthesis of the spacer molecules for the two-dimensional layers

Two different spacer molecule were used: 3-mercapto-propyl trimethoxysilane (TMSPSH) and *N*,*N*-dimethyl-*O*-(3-chloropropyl-dimethylsilyl)-carbamate (KDMSPCl). The first was commercially available, but the second had to be synthesized.

8.4.1 Synthesis of *N,N*-dimethyl-*O*-(3-chloropropyl-dimethylsilyl)-carbamate

KDMSPCl was synthesized by Knausz method [156]. All manipulations were carried out under moisture free conditions. The synthesis involves two steps: first, 2.63 g N,N-dimethyl-amine (0.116 mol) were treated with carbon dioxide in a dichloromethane solution. The reaction mixture was cooled with ice. This reaction gives the corresponding alkylammonium salt of the alkylcarbamic acid:

$$2\ Me_2NH + CO_2 \rightarrow [Me_2NC(O)O]^- Me_2NH_2^+ \qquad 3.3$$

In the second step the carbamate is silylated with a stoichiometric amount (10 g, 0.058 mol) of 3-chloroprpyl-dimethylchlorosilane.

$$[Me_2NC(O)O]^- Me_2NH_2^+ + Cl\text{-}SiMe_2\text{-}C_3H_6Cl \rightarrow Me_2NC(O)O\text{-}SiMe_2\text{-}C_3H_6Cl + Me_2NH_2^+Cl^- \qquad 3.3$$

The silylation of ammonium carbamate salt took 8 hours at room temperature. The *N,N*-dimethyl-*O*-(3-chloropropyl-dimethylsilyl)-carbamate was distilled off in vacuum (B. p. 80-82 °C/1 mmHg). The products were identified by IR and NMR spectroscopy.

8.5 Ligand exchange reactions

Two types of ligand exchange were carried out. The first one was the ligand exchange trough a solid-liquid interface, this will be presented in chapter 8.6.2. The other, the cross-linking and precipitation method will be discussed in the following.

A round bottomed flask with nitrogen inlet was charged with 300 ml of dichloromethane, and 100 mg of $Au_{55}(PPh_3)_{12}Cl_6$. The flask was equipped with a dropping funnel which was filled with 100 ml solutions of the other ligand (Tab. 8.2). The ligands were in 40 times excess to the cluster. The ligand solution was added dropwise into the flask and mixed vigorously. The ligand exchange reactions were performed under two different conditions: in the presence and absence of air. The reactions with air turned out to be faster (1-2 hours) than those without air (3-5 weeks).

The product was purified by washing with CH_2Cl_2, and the solvent of the ligands. The elementary analysis results are presented in Tab. 8.2.

LIGAND	ATMOSPHERE / S_{ligand}	YIELD %	C M%	H M%	N M%	S M%	AU M%	NEAREST STOICHIOMETRY
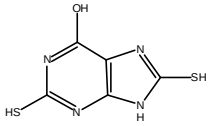	N_2 / DMF	38	13.67	1.34	8.5	6.72	56.9	$(Au_{55}(purine)_{20})_n$
	Air / DMF	66	11.6	0.88	7.18	6.17	63.6	$(Au_{55}(purine)_{16}$--$(purine)_{16})_n$
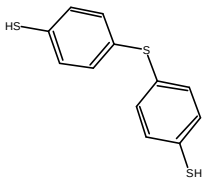	N_2 / CH_2Cl_2	52	19.52	1.32	0	11.2	58.7	$(Au_{55}(TBBT)_{22})_n$
	Air / CH_2Cl_2	78	16.29	1.1	0	8.18	65,7	$(Au_{55}(TBBT)_{14}$--$(TBBT)_{14})_n$
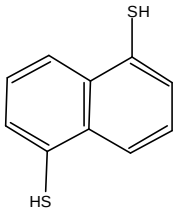	N_2 / THF	59	10.47	0.68	0	3.61	81.21	$(Au_{55}(1,5NDSH)_8)_n$
	Air / THF	53	18.23	1.14	0	6.76	65.0	$(Au_{55}(1,5NDSH)_{18}$--$(1,5NDSH)_{18})_n$
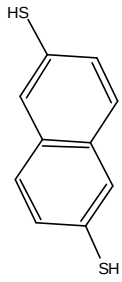	N_2 / THF	47	19.18	1.65	0	6.21	60.7	$(Au_{55}(2,6NDSH)_{17})_n$
	Air / THF	60	18.32	1.47	0	6.22	64.5	$(Au_{55}(2,6NDSH)_{16}$--$(2,6NDSH)_{16})_n$

Tab. 8.2: Solvents of the ligands, and elemental analysis results of the prepared cluster systems.

8.6 Preparations of Au_{55} layers

8.6.1 Physical layers

8.6.1.1 Dropping and evaporation methods

Quasi-two and *quasi*-one dimensional samples were prepared with this technique.

*Quas*i-two-dimensional samples were fabricated by means of spin-coating technique, which is discussed in chapter 2.4.5.4 and depicted in Fig. 5.24. 1 mg $Au_{55}(PPh_3)_{12}Cl_6$ was dissolved in 1 mL dichloromethane. This solvent was slowly spin-coated onto a 1x1 cm quartz plate, with an original roughness of 2 nm. The thickness of the layers (300 and 500 nm) was determinated by AFM.

Quasi-one-dimensional structures were prepared by using a very diluted cluster solution. A 1 mg/100 mL aqueous solution of 15 nm gold colloids was dropped (0.05 mL) onto a quartz plate. The drying process forms so-called dropping circles arose from the colloids. The thickness of the ring can be influenced by modification of the concentration of the solution. With this technique microwires were prepared, with cross sections of 1 and 10 μm^2. These structures were contacted with conducting silver spots at different distances (50 and 75 μm).

8.6.1.2 Modified Langmuir-Blodgett techniques

With this technique $Au_{55}(PPh_3)_{12}Cl_6$ layers and chemically cross-linked monolayers were prepared.

For the preparation of $Au_{55}(PPh_3)_{12}Cl_6$ monolayers a dichloromethane solution of normal Au_{55} (5.5 mg/10 ml) was dropped onto aqueous PVP solution (1,1 mg/l) containing already a substrate dipped inside. After evaporation of dichloromethane, the layer was transferred to the substrate, (cover-glass(8x8 mm), or any other sample), with pulling it out from the liquid with a speed of about 1cm/3s. With this technique islands of closed Au_{55} monolayers could be obtained (Fig. 5.10).

For the preparation of covalently cross-linked Au_{55} system, 40 μl of a normal Au_{55} solution (0.55 mg in 10 ml CH_2Cl_2) was dropped onto a pure water surface, and the solvent was let evaporate. As a second step a TBBT solution (5.4 mg in 100 ml EtAc) was dropped onto the water. (the molar ratio of the TBBT/ $Au_{55}(PPh_3)_{12}Cl_6$ was 30). After waiting for 30 seconds the sample was pulled out with a speed of 0.8 cm/s (see Fig. 5.11).

8.6.2 Chemical layers

Chemical methods for the layer preparation start with the modification of the substrate surface, followed by the chemisorption of the clusters. In this work both mono- and multilayers were prepared using this technique.

8.6.2.1 Preparation of a monolayer

The experiment was divided in 4 steps: a glass substrate was first dipped into a 0.2 M HCl solution (30 min) and then into 3-chloropropyl-dimethylsilan-carbamate for 2 hours under N_2 atmosphere. After washing the sample carefully with pentane to remove the excess of the silane, it was heated for 30 minutes to 120°C into a drying box. The thickness of the layer measured by AFM was smaller than 0.5 nm. Thereafter, the sample was successively dipped in an ethanol solution of KSH for 30 min, washed with ethanol, to remove the excess of the KSH, dipped into a $Au_{55}(PPh_3)_{12}Cl_6$ dichloromethane solution for 30 min, and finally washed with CH_2Cl_2. With this method a monolayer was obtained with relative big closed islands of clusters (up to 10 µm). To cross-link the deposited particles, the sample was dipped into a dithiol solution for 30 min and washed with the solvent selected to solubilize the linker used (the solvents list is presented in Tab. 8.2).

8.6.2.2 Preparation of a multilayer

For these experiments 3-chloropropyl-trimethoxisilane was used [148]. The glass sample was first dipped into HCl solution to increase the concentration of the surface –OH groups. Then, the substrate was refluxed for 24 hours in a toluene solution of TMSPSH (5 mL TMSPSH into 100 ml toluene). The 16 nm thick silane layer obtained (AFM measurement) was washed with toluene, and thereafter dipped into a cluster solution (0.1 g/mL). To prepare multilayers, this substrate was dipped into an ethanol solution of ethane dithiol (the volume ratio was 80:1), and back to the cluster solution. These last two steps were repeated several times. The as-prepared samples were connected with conducting silver spots with a diameter of approximately 1 mm.

8.7 Instrumental

8.7.1 Preparations

8.7.1.1 Langmuir-Blodgett instruments

Two different modified Langmuir-Blodgett (LB) instruments were used. The first and easiest one was prepared from an old microscope stand. The table was fixed in a certain position, and tweezers were attached to the movable focus adjuster screw, so that the angle and its position could be changed. A Petri cup was placed onto the microscope table. The substrate was fixed between the tweezers and moved inside the cup. The used liquid was filled into the Petri cup so that the substrate was fully dipped into it and the other liquid was dropped on top of it. After evaporation of the second solvent, the sample was pulled out slowly.

The other instrument was a self-built modified LB-instrument. It consisted of a motor (Newport 850 F) and a Controller (Newport Motion Control MM4000), regulated by a PC. The substrate was fixed on the motor-arm, to draw it into and to pull it out of the solvent. With changing the position of the motor, the angle of immersion can be controlled between 15° and 90°. Another motor (Actuator 850 F) moved Teflon barrier, which compressed the surface of the liquid in the trough. The trough was made of Teflon. Unfortunately, there was no instrument for measuring the surface pressure in this case.

The sample was fixed at the motor-arm and moved into the liquid that filling the trough. Another solution was dropped onto the surface, and let the solvent evaporate. The barrier compressed the surface and at least the sample was pulled out from the trough.

8.7.1.2 Sample preparation for the two-dimensional measurements

The samples for the two-dimensional measurements were prepared by Prof. Dr. C. Radehaus and M. Schumann in the Technical University of Chemnitz by electron beam lithography. A Si wafer was oxidized on its surface during the formation of an 80 nm SiO_2 layer. It was covered with a tungsten film, then with an electron beam sensitive lack. The

as-prepared sample was exposed to an electron beam. As a result, of this the exposed part of the lack will be water soluble, so it can be easily removed without disturbing the other part of the substrate. The tungsten on the lack-free parts is dissolved by an acid. As a last step the lack is removed with some organic solvent (Fig. 8.3).

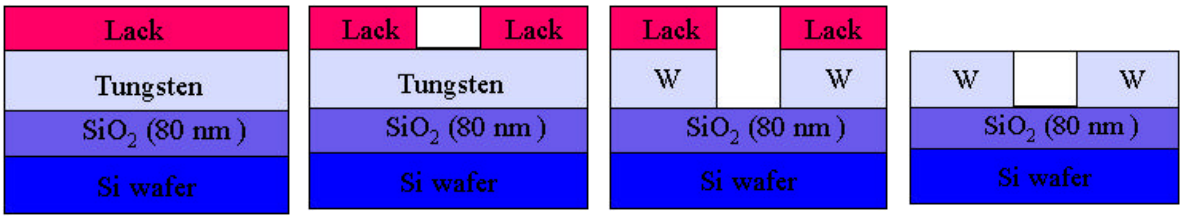

Fig. 8.3: Sample preparation with electron beam lithography. A Si wafer is oxidized on its surface, and covered with a Tungsten film, and an electron beam sensitive lack. After the exposure to an electron beam, the exposed part of the lack will be water soluble, so it can be washed. The tungsten on the wished parts are dissolved and at least the lack is removed.

The substrates obtained with this technique is shown in Fig. 8.4. The relative big squares are the contact pads. For the measurements they will be contacted with sharp tips. The long wires are contacts leading to tips on the surface. The two wires coming from left and right are the source and the drain, with a distance of 20 to 100 nm, the third one is a little farther used as the gate electrode. Many images of the contact structures can be found in chapter 6.

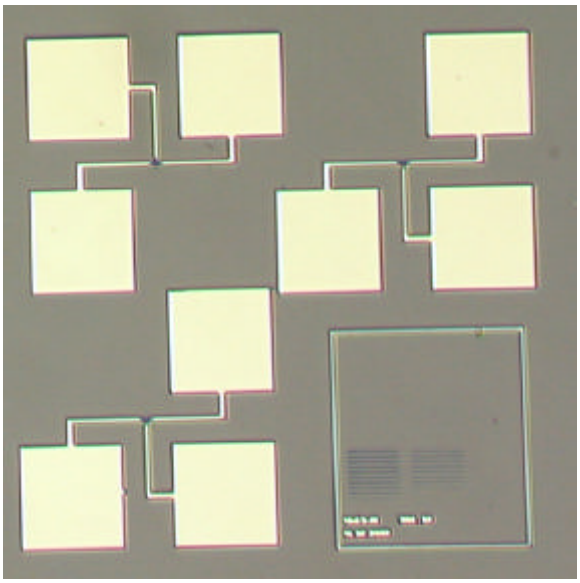

Fig. 8.4: A light microscopic image of the contact pads prepared by electron beam lithography.

Another type of electron beam lithographically prepared samples are the comb structures. This means that the two electrodes are like two combs opposite to each other (Fig. 8.5.)

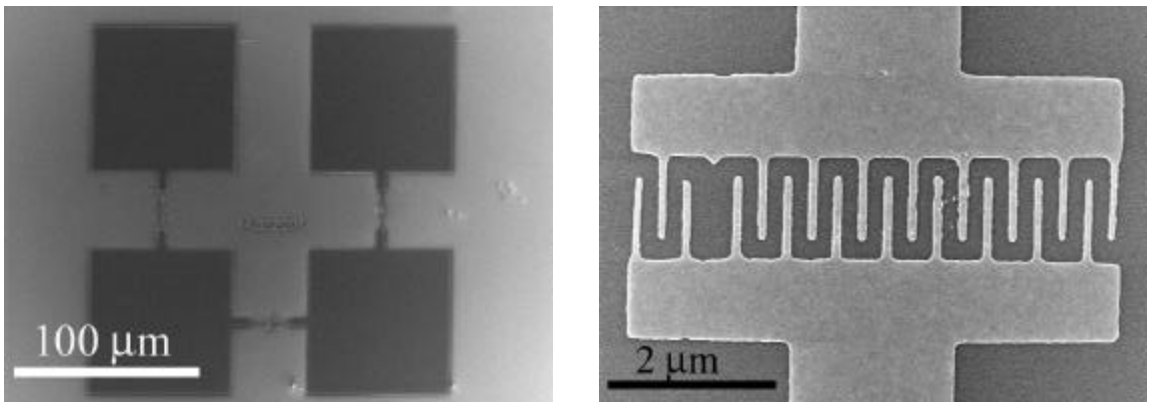

Fig. 8.5: SEM image of the comb structures prepared by electron beam lithography. The right picture is a zoom of the left one.

The sizes of the combs are 1x6 (A), 1x10 (B) and 3x10 (C) µm. The distances of the electrodes vary between 100-200 nm, the breadths of them are between 100 and 200 nm.

8.7.2 Preparation of the three-dimensional samples

For the electrical measurements the samples were pressed into pellets with a pressure of $4 \cdot 10^7$ Pa for 5 min, and then let relax for another 5 min. The shape of the pellets was cylindricwith approximately 0.2 mm of thickness, and 0.5 cm diameter. They were connected from the bottom and the top with conducting silver spots

8.7.3 Equipments

The characterisation of the samples were carried out by a Nanoscope II Atomic Force Microscope.

TEM measurements was performed using a Philips CM 200 FEG transmission electron microscope at 200 kV.

The activation energy measurements was performed on a Keithley 2400 instrument.

The measurements on the electron beam lithography fabricated samples was carried out by a Keithley 236 SMU.

The impedance measurements was performed on a Zahner IM6e instrument with a SIM software.

9 Literatur

[1] G. Schmid, *Custers and Colloids: from theory to applications*, WCH Publishers, New York, (1994)

[2] J. Bardeen and W. H. Brattain, *Phys. Rev*. **74**, 230 (1948)

[3] B. E. Deal, *Interface* **6**, 18 (1997)

[4] D. L. Feldheim and C. D. Keating, *Chem. Soc. Rev.* **37** 1, (1998)

[5] A. O. Orlov, I. Amlani, G. H. Berstein, C. S. Lent, and G. L. Snider, *Science*, **277**, 928 (1997)

[6] J.R. Heath, P.J. Kuekes, G. Snider, R.S. Williams, Science, **280**, 1716 (1998)

[7] C. J. Gorter, *Physica* **17** 777 (1951)

[8] I. Giaver and H. R. Zeller, *Phys. Rev.* **20**, 1504 (1968)

[9] I. Giaver and H. R. Zeller, *Phys. Rev. Lett*. **181**, 789 (1969)

[10] P. Braunstein, L. A. Oro, P. R. Raithby, *Metal clusters in chemistry* Wiley-WCH, New York (1999)

[11] F. E. Kruis, H. Fissan, A. Peled, *J. Aerosol. Sci***. 29**, 511, (1998)

[12] R. P. Andres, T. Bein, M. Dorogi, S. Feng J. I. Henderson, C. P. Kubiak, W. Mahoney, R. D. Osifchin, R. Reifenberger, *Science*, **272**, 1323 (1996)

[13] M. Dorogi, J. Gomez, R. D. Osifchin, R. P. Andres, R. Reifenberger, *Phys. Rev. B*, **52**, 9071, (1995)

[14] B. Wang, X. Xiao, P. Sheng, *J. Vac. Sci. Technol. B.*, **18**, 2351 (2000)

[15] C. P. Vinod, G. U. Kulkani, C. N. R. Rao, *Chem. Phys. Lett*. **289**, 329, (1998)

[16] M.N. Vargaftik, V.P. Zargorodnikov, I.P. Stolarov, I.I. Moiseev, V.A. Likholobov, D.I. Kochubey, A.L. Chuvilin, V.I. Zaikosvsky,_ . K.I. Zamaraev, G.I. Timofeeva, J. *Chem. Soc., Chem. Commun*. 937–939 (1985)

[17] H. Hirai, *J. Macromol. Sci. – Chem.* **A13**, 633, (1979)

[18] M. Faraday, *Phil. Trans. Roy. Soc.* **147**, 145 (1857)

[19] H. B0nnemann, W. Brijoux, R. Brinkmann, E. Dinjous, R. Fretzen, T. Joussen, B. Korall, *J. Mol. Catal*. **74**, 323, (1992)

[20] J. Turkevitch, P. C. Stevenson, J. Hillier, *Disc. Faraday Soc.* **11** 55 (1951)

[21] J. Turkevitch, R. S. J. Miner, I. Okura, S. Namba, *Proc Swedish. Symp. Catal*. 111 (1981)

[22] D. N. Furlong, A. Launikonis, W. H. F. Sasse, J. V. Saunders, *J. Chem. Soc. Faraday Trans*. **80**. 571 (1984)

[23] A. Harriman, G. R. Millward, P. Neta, M. C. Richoux, J. M. Thomas, *J. Phys. Chem.* **92**, 1286, (1988)

[24] J. Turkevitch, G. Kim, *Science* **169**, 873, (1970)

[25] M. Brust, M. Walker, D. Bethell, D. J. Schiffrin, R. Whymann, *Chem. Commun.* 801 (1994)

[26] M. Brust, D. Bethel, D. J. Schiffrin, C. J. Kiely, *Adv. Mater***. 7**. 795, (1995)

[27] A. C. Templrton, S. Chen, S. M. Gross, R. W. Murray, *Langmuir*, **15** 66 (1999)

[28] P. H. Hess, P. H. Parker, *J. Appl. Polym. Sci*. **10**, 1915, (1966)

[29] J. R. Thomas, *J. Appl. Phys*. **37**, 2914 (1966)

[30] B. G. Esrshov, e. Janata, M. Michaelis, A. Henglein, *J. Phys. Chem.* **95**, 8996, (1991)

[31] G. B. Khomutov, A. Yu Obydenov, S. A. Yakovenko, E. S. Soldatov, A. S. Trifonov, V. V. Khanin, S. P. Gubin, *Mat. Sci. Eng*, **C8-9**, 309, (1999)

[32] Suslick, K. S.; Choe, S.-B.; Cichowlas, A. A.; Grinstaff, M. W. *Nature*, **353**, 414 (1991)

[33] Grinstaff, M. W.; Cichowlas, A. A.; Choe, S.-B.; Suslick, K. S. *Ultrasonics*, **30**, 168. **(**1992)

[34] F. Dassenoy, K. Philippot, T. O. Ely,C. Amiens, P. Lecante,E. Snoeck, A. Mosset, M. J. Casanove, B. Chaudret, *New J. Chem.* **703** (1998)

[35] A. Rodriguez, C. Amiens, B. Chaudret, M. J. Casanove, P. Lecante J. S. Bradley, *Chem. Mater*.**, 8**, 1978 (1996)

[36] S. Roginsky, A. Schalnikoff, *Kolloid Z*. **43**, 67, (1927)

[37] J. S. Bradley, E. W. Hill, M. E. Leonowitz, H. Witzke, *J. Mol. Catal*. **41**, 59 (1987)

[38] M. T. Reetz, W. Helbig, S. A. Quaiser, in A. Fürstner (ED.), *Active metals: Preparation, Characterisation, Application*, VCH, New York (1996)

[39] N. Toshima, T. Takahashi, *Bull. Chem. Soc. Japan*, **65**, 400 (1992)

[40] P. A. Jacobs, N. I. Jaeger, P. Jiru, G. Schulzeklo (eds) *Metal microstructures in zeolites*. Elsevier, Amsterdam (1982)

[41] R. Pelster, U. Simon, *Colloid Polym. Sci*. **277,** 2 (1999)

[42] R. S. Bowles, J. J. Kolstad, J. M. Calo, R. P. Andres, *Surf. Sci*. **106**, 117, (1981)

[43] A. N. Patil, D. Z. Paithankar, N. Otsuka, R. P. Andres, *Z. Phys*, **D26,** 135 (1993)

[44] R. P. Andres, J. D. Bielefeld, J. I. Henderson, D. B. Janes, V. R. Kolagunts, C. P. Kubiak, W. J. Mahoney, R. G. Osifchin, *Science*, **273**, 1690 (1996)

[45] T. T. Yau, P. Mulvaney, W. Xu, G. M. Spinks, *Phys. Rev. B*, **57,** R124 (1998)

[46] K. V. Sarathy, G. Raina, R, T. Yadav, G. U. Kulkarni, C. N. R. Rao, *J. Phys. Chem B*, **101**, 9876, (1997)

[47] S. J. Green, J. J. Pietron, J. J. Stokes, M. J. Hostetler, H. Vu, W. P. Wuelfing, R. W. Murray, *Langmuir*, **14**, 5612, (1998)

[48] K. S. Mayya, V. Patil, M. Sastry, *Bull. Chem. Soc. Jpn*. **73**, 1757, (2000)

[49] M. Rolandi, K. Scott, E. G. Wilson, F. C. Meldrum, *J. Appl. Phys.* **89**, 1588, (2001)

[50] M. Brust, D. Bethell, D. J. Schiffrin, C. J. Kiely *Adv. Mater*. **7**, 795,(1995)

[51] S. Chen, *J. Phys. Chem B*, **104**, 663, (2000)

[52] L. Han, M. M. Maye, F. L. Leibowitz, N. K. Ly, C. J. Zhong, *J. Mater. Chem.* **11**, 1258 (2001)

[53] F. L. Leibowitz, W. X. Zheng, M. M. Maye, C. J. Zhong, *Anal. Chem.* **71**, 5076 (1999)

[54] J. R. MacDonald, *Impedance Spectroscopy*, Wiley, New York, **(**1987)

[55] D. L. Klein, P. L. McEuen, J. E. Bowen Katari, R. Roth, A. P. Alivisatos, *Appl. Phys. Lett.* **68**, 2574, (1996)

[56] M. Brust, D. Bethell, C. J. Kiely, D. J. Schiffrin, *Langmuir*, **14**, 5425, (1998)

[57] T. Sato, H. Ahmed, D. Brown, B. F. G. Johnson, *J. Appl. Phys*. **82**, 696, (1996)

[58] T. Vossmeyer, E. DeIonno, J. R. Heath, *Angew.Chem.* **109**, 1123, (1997)

[59] S. Chen, R. W. Murray, *J. Phys. Chem. B*, **103**, 9996, (1999)

[60] S. Chen, R. W. Murray, *Langmuir*, **15**, 682, (1999)

[61] S. Chen, *Adv. Matter*. **12**, 186, (2000)

[62] S. Chen, *Langmuir* **17** 2878, (2001)

[63] M. J. Hostetler, A. C. Templeton, R. W. Murray, *Langmuir***, 15**, 3782 (1999**)**

[64] L. C. Brousseau, S. M. Marinakos, J. P. Novak, D. L. Feldheim, *Mater. Res. Bull***.** 129 (1998)

[65] T.-A. Hanaoka, A. Heilmann, M. Kröll, H.-P. Kormann, T. Sawitowski, G. Schmid, P. Jutzi, A. Klipp, U. Kreibig, R. Neuendorf, *Appl. Organomet. Chem.* **12,** 367, (1998)

[66] S. T. Yau, P. Mulvanez, W. Xu, G. M. Spinks, *Phys. Rew. B*, **57**, R15 124, (1998)

[67] M. Y. Han, L. Zhou, C. H. Quek, S. F. Y. Li, W. Huang, *Chem. Phys. Lett*. **287**, 47, (1998)

[68] M. Dorogi, J. Gomez, R. Oschifchin, R. P. Andres, R. Reifenberger, *Phys. Rew. B*, **52**, 9071 (1995)

[69] R. P. Andres, T. Bein, M. Dorogi, S. Feng, J. I. Henderson, C. P. Kubiak, W. Mahoney, R. Oschifchin, , R. Reifenberger, *Science*, **272**, 1323 (1996)

[70] T. Junno, M. H. Magnusson, S. B. Carlsson, K. Deppert , J. O. Malm, L. Montelius, L. Samuelson *Microelectronic Eng***. 47** 179 (1999)

[71] S. H. M. Persson, L. Olofsson L. Gunnarsson, *Appl. Phys. Lett*. **74,** 2546 (1999)

[72] A. Bezryadin, C. Dekker, G. Schmid, *Appl. Phys. Lett***. 71** 1273 (1997)

[73] T. Junno, S. B. Carlsson , H. Q. Xu, L. Montelius, L. Samuelson, *Appl. Pys. Lett***. 72** 548 (1998)

[74] S. W. Chung, G. Markovich, J. R. Heath, J. Phys. Chem. B, 102, 6685, (1998) S. M. Marinakos, L. C. Brousseau, A. Jones, D. L. Feldheim**,** *Chem Mater***. 10** 1214 (1998)

[75] M. Gleiche, Li F. Chi, H. Fuchs, *Nature*, **403** 173, (2000)

[76] L. C. Brousseau, S. M. Marinakos, J. P. Novak, D. L. Feldheim, *Mater. Res. Bull*. **Suppl. S** 129, (1998)

[77] C. A. Berven, M. N. Wybourne, L. Clarke, J. E. Hutchison, L. O. Brown, J. L. Mooster, M. E. Schmidt, *Supelattices and Microstructures***, 27** 489 (2000)

[78] J Richter, M Mertig, W Pompe, I. Mönch, H. K. Schackert, *Appl. Phys. Lett*. **78**, 536 (2001)

[79] C. Gutierrez-Wing, P. Santiago, J. A. Ascencio, A. Camacho, M. Jose-Yacaman, *Appl. Phys. A***, 71** 237 (2000)

[80] J. Zheng, Z. Zhu, H. Chen, Z. Liu, *Langmuir*, **16**, 4409, (2000**)**

[81] L. Motte, E. Lacaze, M. Maillard, M. P. Pileni, *Langmuir*, **16**, 3803, (2000)

[82] L. Motte, F. Billoudet, E. Lacaze, J. Douin,⊥ M. P. Pileni *J. Phys. Chem. B*, **101**, 138 (1997)

[83] M. J. Hostetler, J. E. Wingate, C. J. Zhong, J. E. Harris, R. W. Vachet, M. R. Clark, J. D. Londono, S. J. Green, J. J. Stokes, G. D. Wignall, G. L. Glish, M. D. Porter, N. D. Evans, R. W. Murray, *Langmuir*, **14**, 17, (1998)

[84] J. Fink, C. J. Kiely, D. Bethell, D. J. Schiffrin, *Chem. Mater*. **10**, 922 (1998**)**

[85] J. R. Heath, C. M. Knobler, D. V. Leff, *J. Phys. Chem. B*, **101**, 189 (1997)

[86] C. P. Collier, R. J. Saykally, J. J. Shiang, S. E. Henrichs, J. R. Heath, *Science*, **277**, 1978 (1997)

[87] J. P. Bourgoin, C. Kergueris, E. Lefevre, S. Palacin, *Thin Solid Films***,** *329* 515 (1998)

[88] K. S. Mayya, M. Sastry, *Langmuir*, **15**, 1902, (1999)

[89] T. Zhu, X. Zhang, J. Wang, X. Fu, Z. Liu, *Thin Solid Films*, **327**, 595, (1998)

[90] D. Bethell, M. Brust, D. J. Schiffrin, C. Kiely, *J. Electroanal. Chem***. 409**, 137, (1996)

[91] K. C. Grabar, P. C. Smith, M. D. Musick, J. A. Davis, D. G. Walter, M. A. Jackson, A. P. Guthrie, M. J. Natan**,** *J. Am. Chem. Soc.* **118**, 1148, (1996**)**

[92] T. Sato, D. Brown, B. F. G. Johnson, *Chem. Commu*n., 1007 (1997)

[93] D. M. Schaefer, R. Reifenberger, A. Patil, R. P. Andres, *Appl. Phys. Lett.* **66**, 1012, (1995)

[94] J. P. Spatz, S. Mössmer, C. Hartmann, M. Möller, T. Herzog, M. Krieger, H.-G. Boyen, P. B. Kabius, *Langmuir***, 16**, 407 (2000**)**

[95] D. L. Feldheim, K. C. Grabar, M. J. Natan, T. E. Malluk, J. Am. Chem. Soc. 118, 7640, (1996)

[96] Y. J. Liu, Y. X. Wang, R. O. Claus, *Chem. Phys. Lett***. 298**, 315 (1998)

[97] E. Hao, T. Lian, *Chem. Mater.* **12,** 3392 (2000)

[98] A. N. Shipway, M. Lahav, I. Willner, *Adv. Mater.* **12**, 993 (2000)

[99] F. Auer, M. Scotti, A. Ulman, R. Jordan, B. Sellergren, J. Garno, G.-Y. Liu, *Langmuir,* **16**, 7554 (2000)

[100] A. Kumar, A. B. Mandale, M. Sastry, *Langmuir*, **16**, 6921, (2000)

[101] M. D. Musick, C. D. Keating, L. A. Lyon, S. L. Botsko, D. J. Pena, W. D. Holliway, T. M. McEvoy, J. N. Richardson, M. J. Natan, *Chem. Mater.* **12**, 2869, (2000)

[102] K. V. Sarathy, P. J. Thomas, g. u. Kulkarni, C. N. R. Rao, *J. Phys. Chem. B*, **103**, 399, (1999)

[103] D. B. Janes, M. Batistuta, S. Datta, M. R. Melloch, R. P. Andres, J. Liu, N. P. Chen, T. Lee, R. Reifenberger, E. H. Chen, J. M. Woodall, *Superlattices and Microstructures*, **27**, 555, (2000)

[104] W. P. McConnell, J. P. Novak, L. C. Brousseau, R. R. Fuierer, R. C. Tenent, D. L. Feldheim, *J. Phys. Chem. B***, 104**, 8925 (2000)

[105] P. J. Thomas, G. U. Kulkarni, C. N. R. Rao, *Chem. Phys. Lett*. **321** 163–168 (2000)

[106] T. Sato, H. Ahmed, *Appl. Phys. Lett*. **70** 2759 (1997)

[107] A. N. Korotkov, *Molecular Electronics*, (1996)

[108] U. Simon, V. Gasparian, *Phys. Stat. Sol. B***, 205**, 223 (1998)

[109] R. P. Andres, S. Datta, S. Dorogi, J. Gomez, J. I. Henderson, D. B. Janes, V. R. Kolagunta, C. P. Kubiak, W. Mahoney, R. F. Osifchin, R. Reifenberger, M. P. Samanta, W. Tian, *J. Vac. Sci. Technol***. A 14,** 1178, (1996)

[110] H. Perez, R. M. Lisboa, de Sousa, J-P. Pradeau, P-A. Albouy, *Chem. Mater*.**, 13**, 1512 2001)

[111] Y. J. Liu , Y. W. Wang , R. O. Claus, *Chem. Phys Lett*. **298** 315 (1998)

[112] R. H. Terril, T. A. Postlethwaite, C. Chen, C.-D. Poon, A. Terzis, A. Chen, J. E. Hutchinson, M. R. Clark, G. Wignall, J. D. Londono, R. Superfine, M. Falvo, C. S. Johnson, E. T. Samulski, R. W. Murray, *J. Am. Chem. Soc*. **117,** 12537 (1995)

[113] W. P. Wuelfing, S. J. Green, J. J. Pietron, D. E. Cliffel, R. W. Murray, J. Am. Chem. Soc**. 122** 11465 (2000)

[114] U. Simon, *Habilitationsschrift Universität Essen* (1998)

[115] N. Sandhyarani, M. R. Resmi, R. Unnikrishnan, K. Vidyasagar, Shuguang Ma, M. P. Antony, G. Panneer Selvam, V. Visalakshi, N. Chandrakumar,⊥ Kannaiyan Pandian, Yu-Tai Tao, T. Pradeep, *Chem. Mater***, 12**, 104.(2000)

[116] G. Schmid, R. Pfeil, R. Boese, F. Bandermann, S. Meyer, G. H. M. Calis, J. A. van der Velden, *Chem. Ber*. **114**, 3634, (1981)

[117] G. Schmid, *Inorg. Synth*. **7**, 214, (1990)

[118] J. D. Aiken, R. G. Finke, *J. Mol. Cat. A*, **145** 1 (1999)

[119] F. M. Mulder, R. C. Thiel, L. J. de Jongh, P. C. M. Gubbens, *Nanostruct. Mater***. 7**, 269 (1996)

[120] G. Schmid, *Tetrahedron*, **7**, 2321 (1988)

[121] G. Schmid, R. Pugin, J.-O. Malm, J.-O. Bovin, *Eur. J. Inorg. Chem.* 813 (1998)

[122] G. Schmid, R. Pugin, W. Meyer-Zaika U. Simon**,** *Eur. J. Inorg. Chem.* 2051 (1999)

[123] R. Flesch, *Dissertation, Universität Essen*, (1997)

[124] G. Schmid, *J. Chem.Soc., Dalton Trans*. 1077, (1998)

[125] S. Peschel, *Dissertation, Universität Essen*, (1997)

[126] M. Baumle, *Dissertation, Universität Essen*, (1999)

[127] M. A. Marcus, M. P. Andrews, J. Zegenhagen, A. S. Bommannavar, P. Montano, *Phys. Rev. B*, **42**, 3312, (1990)

[128] L.F. Chi, M. Hartig, T. Drechsler, Th. Schwaack, C. Seidel, H. Fuchs, G.Schmid *Appl. Phys*. **A 66**, S187 (1998)

[129] G. Schön, U. Simon, *Colloid Polym. Sci*. **273**: 101, (1995)

[130] G. Schön, U. Simon, *Colloid Polym. Sci*. **273**: 202, (1995)

[131] S.-T. Yau, P. Mulvaney, W. Xu, G. M. Spinks *Phys. Rev. B* **57**, R124-127, (1998)

[132] W. H. Richardson, *Appl. Phys. Lett*. **71** , 1113, (1997)

[133] G. Schmid L. F. Chi, *Adv. Mater*. **10** 515, (1998)

[134] G. Horhyak, M. Kröll, R. Pugin, T. Sawitowski, G. Schmid, J.-O. Bovin, G. Karsson, H. Hofmeister, S. Hopfe, *Chem. Eur. J*. **3**, 1951, (1997)

[135] O. Vidoni, T. Reuter, V. Torma, W. Mayer-Zaika, G. Schmid, *Chem. Mater.* Submitted.

[136] S. Peschel, G. Schmid, *Angew. Chem. Int. Ed. Engl*. **34**, 1442, (1995)

[137] G. L. Hornyak, S. Peschel, T. Sawitowski, G. Schmid, *Micron*, **29**, 183, (1998)

[138] H. P. Kormann, *Dissertation, Universität Essen*, (2001)

[139] G. Schmid, N. Beyer, *Eur. J. Inorg. Chem.* 835 (2000)

[140] L. Clarke, M. N. Wybourne, M. Yan, S. X. Cai, J. F. W. Keana, *Appl. Phys. Lett*. **71**, 617, (1997)

[141] L. Clarke, M. N. Wybourne, L. O. Brown, J. E. HutchinsonM. Yan, S. X. Cai, J. F. W. Keana, *Semicond. Sci. Technol*. **13**, A111, (1998)

[142] M. P. J. van Staveren, H. B. Brom, L. J. De Jongh, *Phys. Rep*. **208**, 1, (1991)

[143] G. Schmid, *Bull. Pol. Acad. Sci. Chem.* **46**, 229, (1998)

[144] U. Simon, G. Schön, G. Schmid, *Angew. Chem.* **105**, 264, (1993)

[145] S. Fujita, *Synthesis*, 423, (1982)

[146] P. D. Caesar, *Org. Synth*. 693, (1953)

[147] P. D. Caesar, *J. Am. Chem. Soc*. **73**, 1097, (1951)

[148] G. Schmid, N. Klein, L. Korste, U. Kreibig, D. Schönauer, *Polyhedron*, **7**, 605 (1988)

[149] N. F. Mott, *Phil. Mag*. **19**, 835, (1969)

[150] N. F. Mott, E. A. Davis, *Electronic Processes in Non-Crystalline Materials*, Oxford University Press, Oxford, (1971)

[151] N. F. Mott, *Conduction in Non-Crystalline Materials*, Clarendon Press, Oxford, (1993)

[152] Hong S, Reifenberger R, w. Tian, S. Datta, J. Henderson, C. P. Kubiak**,** *Superlattices and Microstructures***, 28,** 289, (2000)

[153] J. R. MacDonald, *Impedance Spectroscopy*, Wiley New York, (1987).

[154] A. L. Efros, B. I. Shklowskii, *Phys. Stat. Solidi***, B76**, 475. (1976)

[155] M. Schumann, Y. Liu, T. Raschke, C. Radehaus, G. Schmid, *Nanoletters*, (2001)

[156] D. Knausz, A. Meszticzky, L. Szakács, B. Csákvári, K. Újszászi, *J. Organomet. Chem.*, **256,** 11, (1983)

[157] J. E. Morris, T. J. Coutts, *Thin Solid films*, **47**, 3, (1977)

[158] H. Taube, *Science*, **226**, 1028 (1984)

[159] H. Taube, *Electron Transfer reactions of Complex Ions in Solution*, Academic Press, New York 1970

List of the used abbreviations

AFM	Atomic Force Microscope
EBL	Electron Beam Lithograpy
LB technique	Langmuir-Blodgett technique
SEM	Scanning Electron Microscope
SET	Single Electron Tunneling
	Single Electron Transistor
STM	Scanning Tunneling Microscope
STS	Scanning Tunneling Spectroscopy
TEM	Transmission Electron Microscope

Zusammenfassung

Einen interessanten Bereich der heutigen Nanotechnologie stellen Untersuchungen an Clustermaterialen dar, die spezielle elektrische Quanteneffekte („quantum size effect“) zeigen. Deren potentielle künftige Anwendungen liegen in der „single electron”-Elektronik. Der Au_{55} Cluster, beschützt mit unterschiedlichen Ligandhüllen aus phosphor- und schwefelorganischen Molekülen, ist ein der am besten geeigneten Modellsysteme für diese Messungen [1].

In der vorliegenden Arbeit wurde auf folgende zwei Schwerpunkte konzentriert. Einerseits sollten die Einflüsse kovalenter Brücken zwischen den Clustern auf den Ladungstransfer-Mechanismus der Nanopartikel Systemen, andererseits die Elektronentransport in geschlossenen Clustermonolagen untersucht werden.

Die heutige Ansicht in der Literatur, ob die Liganden zwischen zwei Clustern den Ladungstransfer-Mechanismus beeinflussen oder nicht, ist umstritten. Reifenberger und Mitarbeiter [69] haben es gefunden, dass die chemische Natur der Liganden, insbesondere deren Endgruppen üben einen Effekt auf die Leitfähigkeit einer Probe aus. Die Untersuchungen von Simon [114] führten dagegen zum Schluss, dass die Aktivierungsenergie der Nanopartikel Systeme nur vom Abstand der Nanopartikel, nicht aber von der chemischen Natur der Liganden abhängt.

Um diesem scheinbaren Widerspruch nachzugehen, wurden die elektrischen Eigenschaften von zwei-, quasi-zwei-, und dreidimensionalen Au_{55}-Clustersystemen untersucht. Es stellte sich heraus, dass das Modell von Simon nur für physikalisch verbrückte Systeme gültig ist. Für kovalent (chemisch) verbrückte Nanopartikel-Systemen ist die Aktivierungsenergie kleiner als die nach dem erwähnten Modell gewartet und hängt stark von der chemischen Natur der verbrückenden Liganden ab. Die Aktivierungsenergie zeigt keinen Trend als Funktion der Interpartikel-Abstand in diesem Fall.

Im letzten Teil der Arbeit wird über elektrische Eigenschaften der Clustermonolagen berichtet. In den Messungen wurden Si-Plättchen als Trägersubstanz verwendet, mit durch Elektronenstrahllithographie gebildeten Wolfram Kontakt Strukturen auf der Oberfläche versehen. Um die Leitfähigkeit der Clustermonolage beobachten zu können, muss die

Oberfläche der Probe zu SiO_2 oxidiert werden. Es wurde gezeigt, dass das Nanopartikel System durch Bestrahlung mit Elektronenstrahl aktiviert werden kann. Wir erklären dieses Phänomen mit dem Überschuss von gefangenen Elektronen in der SiO_2 Lage, der durch positive Bildladungen in die Clusterlage induziert wird. Dieser Effekt bildet die Elektronenkonfiguration und vielleicht auch die Struktur des Arrangement um. Asymmetrische Bestrahlung der Lage führt zu eine asymmetrische *I-V* Charakteristik. Dieser Befund kann ähnlich erläutert werden, wie das Gleichrichtensverhalten einer Halbleiterdiode, wobei die Bildladungen in der Clusterlage mit Elektronenlöchern der Halbleiter in Analogie stehen.

Curriculum vitae

NAME:	Viktoria Torma
ADRESS:	Templomsor u. 38 9081 Gyõrújbarát, Ungarn Tel: +0036 30 2439125 E-mail: t_vikkancs@hotmail.com
DATE AND PLACE OF BIRTH:	02.03.1975, Gyõr
PARENTS:	Attila Torma, teacher in Gyõr Gizella Szelid, teacher in Gyõr
NATIONALITY:	Hungarian
FAMILY CONDITION:	Married
LANGUAGES:	German, English, Hungarian

Studies

1989 – 1993 Miklós Révai High School in Gyõr
High school graduation: Excellent.

1993 – 1998 Eötvös Loránd University, Budapest
Chemistry studies
Final Exam: very good
Title of the diploma work: Investigation of the Oxygen-Reduction with Impedance Spectroscopy
Supervisor: Dr. Gyõzõ Láng, Assistant Professor at the Eötvös-University of Sciences, Budapest.
Diploma: very good

Undergraduate research:

1994 – 1996 Investigation of the graphite-water interface with Scanning Tunnelling Spectroscopy
Supervisor: Dr. Gabor Nagy, Central Research Institute for Physics, Budapest

1996 – 1998 Investigation of the Oxygen-Reduction on Gold Electrode with Impedance Spectroscopy
Supervisor: Dr. Gyõzõ Láng Assistant Professor at the Eötvös-University, Budapest.

1997 Undergraduate Research Conference, I. Pries

1998 – 2002 Ph. D. work in the working group of Prof. Dr. Günter Schmid
Institute for Inorganic Chemistry, University of Essen

Lebenslauf

NAME:	Viktoria Torma
ADRESSE:	Templomsor u. 38 9081 Gyõrújbarát, Ungarn Tel: +0036 30 2439125 E-mail: t_vikkancs@hotmail.com
GEBURTSDATUM und ORT:	02.03.1975, Gyõr
ELTERN:	Attila Torma, Lehrer in Gyõr Gizella Szelid, Lehrerin in Gyõr
STAATSANGEHÖRIGKEIT:	Ungarisch
FAMILIENSTAND:	Verheiratet
SPRACHKENNTNISSE:	Deutsch, Englisch, Ungarisch

Studien

1989 – 1993 Miklós Révai Gymnasium in Gyõr
Abitur mit ausgezeichnetem Ergebnis bestanden.

1993 – 1998 Eötvös Loránd Universität, Budapest
Fachrichtung: Chemie
Abschlussprüfung: sehr gut
Titel der Diplomarbeit: Untersuchung der Sauerstoffreduktion auf Goldelektrode mit Impedanzspektroskopie
Betreuer: Gyõzõ Láng, Dozent an der Eötvös-Universität, Budapest.
Diplom: sehr gut
Qualifikation: Diplom – Chemiker
Undergraduate research:

1994 – 1996 Untersuchung der Graphit – Wasser Grenzfläche mit Rastertunnelmikroskopie
Betreuer: Gabor Nagy, Zentrales Forschungsinstitut für Physik, Budapest

1996 – 1998 Untersuchung der Sauerstoffreduktion auf Goldelektroden mit Impedanzspektroskopie
Betreuer: Gyõzõ Láng, Dozent an der Eötvös-Universität, Budapest.

1997 Konferenz des Nationalen Studentenkreises: I. Preis

1998 – 2002 Doktorarbeit bei Prof. Dr. Günter Schmid in Essen,
Institut für Anorganische Chemie

Publikationen

Structure/Property – Relations in Au_{55} Cluster Layers Studied by Temperature Dependent Impedance Measurements
Viktoria Torma, Günter Schmid Ulrich Simon, *ChemPhysChem*, 2001 321-325

The Diode Behavior of Asymmetrically Ordered Au_{55} Clusters
Viktoria Torma, Matthias Schumann, Christian Radehaus, Günter Schmid,
ChemPhysChem, 2001 546-548.

Quasi One-Dimensional Gold Cluster Arrangements
Olivia Vidoni, Torsten Reuter, Viktoria Torma, Wolfgang Meyer-Zaika, Günter Schmid, *J. Mater. Chem.* 2001 **11** .

Die Ergebnisse wurde auch in den folgenden Postern veröffentlicht:

Investigation of Cluster layers by impedance and activation energy measurements
V. Torma, Priv. Doz. U. Simon, Prof. Dr. G. Schmid
7th International Symposium on Electrochemical Methods in Corrosion Research Budapest, 2000

Investigation of Au_{55} cluster monolayers with electronic measurements
V. Torma, M. Schumann, Dr. Raschke, Prof. Dr. Radehaus, Prof. Dr. G. Schmid
SFB 452, Kollective molekulare Ordnungsprozesse in der Chemie. Entstehung, Struktur, Dynamik und Eigenschaften von höher organisierten Systemen, Nov, 2000

Elektrische Eigenschaften von ligandenstabilisierten Au_{55} Cluster Monolagen
V. Torma, M. Schumann, Olivia Vidoni, Torsten Reuter, Yungping Liu, Dr. Raschke, Prof. Dr. Radehaus, Prof. Dr. G. Schmid*SFB 452: Begutachtung*, März, 2001

Herstellung von neuartigen ein-, zwei- und dreidimensionalen Anordnungen von Au_{55}-Clustern
V. Torma O. Vidoni, T. Reuter, Y. Liu, M. Schumann, Prof. Dr. G. Schmid
SFB 452: Begutachtung, März, 2001